POLITECNICO DI TORINO

Master of Science in Biomedical Engineering

Master's degree thesis

Finite element analysis of child head impact in Judo

Supervisors:

Prof.ssa Laura Gastaldi

Prof. Stefano Pastorelli

Ing. Valeria Rosso

Prof. Alessandro Scattina

Candidate:

Carmela Cioffi

Academic Year 2019/2020

Table of Contents

Abstract

In sports impacts, the evaluation of brain injuries can be performed by analyzing the kinematics entities of the head. However, determining the stress and strain on the brain is a more comprehensive and appropriate approach: for this purpose, finite element modeling (FEM) is a tool that has found wide application. The aim of this thesis is to evaluate the stress on the brain of children during projections usually used in judo practice. Two six-year-old children performed four types of projections (o-soto-gari, o-uchi-gari, ippon-seoi-nage and tai-otoshi) during which the linear acceleration and angular velocity of the head were measured with an inertial sensor applied to the forehead. The projections were simulated using the children finite element (FE) model PIPER and the software LS-Dyna. The experimental data were used as input parameter for the FE model. The stresses on the brain were evaluated in terms of the Von Mises Stress. The data were analysed using the HyperView software. The evaluation was carried out both in space, to highlight the most stressed portions of the brain, and in time to correlate these stresses with the linear acceleration and angular velocity to which the subject's head was exposed. Results obtained show that there are considerable differences in the maximum values of Von Mises between repetitions of the same technique. It could be attributed, as the variability of field of motion in terms of shape and magnitude, to the inexperience of the child in practicing the technique and to the greater attention in planning the movement to fall correctly avoiding trauma. In any case, it seems that the higher Von Mises values were reached when higher accelerations and velocity were prescribed. In all techniques the most stressed region was placed near the interfaces between different brain materials.

List of figures

List of tables

1. Introduction on Judo

Judo is a sport originating in Japan and is increasingly widespread, in fact it is commonly practiced in schools and gyms. Judo competitions include two participants (same age group, same weight category) wearing the typical judo uniform, the *judogi*, fighting each other on *tatami*. The objective of a Judo match is to project the rival on his back, immobilise him on the ground or to force him to surrender by suffocation, strangulation or joint lever. In this way, the match victory is given. Before practicing throwing techniques, it is necessary to handle the right way of falling without injury risk, so falling safely, *ukemi*, when judoka receives a throw, in order to not touch head with the floor, for preserving health and life. In judo and some other martial arts, *tori* is the person who completes the technique against *uke,* who receives a thrown.

Four types of breakfalls were trained by Judo founder:

- Rear breakfall (ushiro ukemi): *uke* brings his arms to shoulder height and takes a step backwards by flexing his neck forward to avoid touching his head on the floor. At this point, he bends his back letting himself roll, and when his back touches the floor he places the palm of his hands on the *tatami* to cushion the fall.
- Side breakfall (yoko ukemi): *uke*, from a standing position, brings the body to rotate in the frontal plane while falling on the tatami with his right buttock while simultaneously tapping the palm of his right hand always on the tatami.
- Rolling breakfall (zempo kaiten ukemi): forward breakfall similar to a somersault starting from a standing position.
- Front breakfall (mae ukemi): carried out by falling forward with the body in an stretched position like a "board" and at the moment of contact with the tatami, the hands and forearms are placed to form a single point of support that is used to spring by bending the arms.

The study of ukemi represents the most important phase in the training of a new pupil, as learning to fall serves to be able to practice Judo without danger, to avoid suffering damage as a result of the numerous projections that one undergoes daily.

Official techniques are 68, even if variations and personal modifications to get a more efficient throw are permitted in competition. Traditionally, *nage-waza* are categorised into five groups depending on which part of tori body is used for throwing uke:

- Tachi-waza, tori projects uke maintaining an upright or semi-erect posture:
    - Te-waza: performed with the primary assistance of the arms;
    - Koshi-waza: performed with the primary assistance of the hip;
    - Ashi-waza: performed with the primary assistance of legs.
- Sutemi-waza, tori sacrifices his balance in order to project uke:
    - Ma-sutemi-waza: performed by falling on back;
    - Yoko-sutemi-waza: performed by falling on hip.

Each technique, *nage-waza*, is composed of four phases subsequent in time:

- Kumi kata, establishing firm grip or grips;
- Kuzushi, breaking opponent's balance;
- Tsukuri, turning in and fitting the throw;
- Kake, completing the throw.

In this study, several techniques, considered to be among the most dangerous, were analysed:

1. O-soto-gari, which causes a backward fall that can cause head trauma;

2. O-uchi-gari, which involves a movement similar to whiplashing the head of a falling person;

3. Ippon-seoi-nage, one of the most common techniques in Judo competitions;

4. Tai-otoshi, one of the fastest and most powerful techniques used.

This sport is becoming very popular, but there are some techniques that can be risky. Therefore, particular interest has been directed to injuries resulting from this sport.
Being thrown is the most common injury mechanism, but sprains, strains and contusions, usually of the knee, shoulder and fingers, are the most frequently reported injuries.[1] Also, head injuries could happens, although less frequently; when both head and neck are involved the consequence could often be serious. [1] Kamitani[2] reported that being thrown is the principal injury mechanism of severe head injuries (70%) among judo practitioners, who were mainly younger than 20 years (90%) and practicing judo for less than 3 years (60%). The comparison between novice group and experienced group settings was chiefly studied in literature: for example, Koshida[3] observed a significantly higher peak neck

extension momentum in the experienced group, that is associated with the risk of head injuries during judo. In addition, the novice judokas demonstrated a significantly greater flexed pattern in the trunk and hip movement than the experienced judokas. Another interesting research area is the one concerning the comparison between elite and collegiate athletes: Ishii[4] measured the speed of the two classes of athletes during the execution of the seoi-nage Judo technique, showing that elite players move faster, avoiding the counterattack.

In that study, the authors assumed lack of falling skills as the prominent cause for severe head injuries among inexperienced judokas.[2]

In Table 2.7, all the studies conducted and used to explore the topic of this paragraph have been reported.

An in-depth literature research was carried out focusing on the concept of Traumatic Brain Injury, trying to understand how it is evaluated and quantified in sport, in particular for Judo, taking a particular interest in children as the practice of this sport is widespread even among the youngest.

2. Literature review

A literature review was carried out to understand the methods applied for studying traumatic brain injury in children and during sporting activities in quantitative manner. This review was focused on the analysis of linear and rotational accelerations and, then, on the analysis of stress and strain.

The research was conducted on PICO, PubMed and Google Scholar looking for articles including words as "Judo", "combat sports", "acceleration", "injuries", "head", "concussion", "hematoma", "TBI", "children", "finite element method" and their combinations.

2.1 Traumatic brain injury

According to Oregon Healthcare[5,6], a head injury is a term that describes a huge collection of injuries that occur to the scalp, skull, brain and underlying tissue and blood vessels in the head. Head injuries are also commonly referred to as brain injury, or traumatic brain injury (TBI), depending on the extent of the head trauma[5]. According to Dawodu[5,7], Traumatic brain injury is a non-degenerative, non-congenital insult to the brain from an external mechanical force, possibly leading to permanent or temporary impairments of cognitive, physical and psychosocial functions with an associated diminished or altered state of consciousness.

The most used method to determine TBI severity is the Glasgow Coma Scale (GCS): it tests the consciousness of the subject, by giving eye opening, verbalization and motor response stimuli and marking his/her responsiveness with a number from 3 (the patient does not produce an answer) to 15 (the subject is fully responsive). Usually GCS values from 13 to 15 correspond to mild TBI, from 9 to 12 to moderate TBI and lower values represent a subject with severe TBI. Factors like drug use, alcohol intoxication, shock, or low blood oxygen can alter a patient's level of consciousness. These factors could lead to an inaccurate score on the GCS. Furthermore, the GCS is usually not used with children, especially those too young to have reliable language skills. The Pediatric Glasgow Coma Scale, or PGCS, a modification of the scale used on adults, is used instead. The PGCS still uses the three tests – eye, verbal, and motor responses; the three values are considered separately as well as together.

2.1.1 Traumatic brain injury in sport

Benefits of regular physical activities and sports participation on cardiovascular system and brain health are incontestable. Physical exercise lowers the danger of cardiovascular diseases, type 2 diabetes, hypertension, obesity, and stroke, and leads positive effects on cholesterol levels, antioxidant systems, inflammation, and vascular function.[8] Training similarly improves psychological health, reduces age related loss of brain volume, increases cognition, decreases the risk of developing dementia, and delays neurodegeneration.[8] Nevertheless, playing sports, almost all sports comprehending agonism, is linked with dangers, involving a risk for mild or severe Traumatic Brain Injuries (TBI) and, rarely, catastrophic traumatic injuries and death.[8] TBI can generally be classified as acute or chronic. Acute TBI is used to describe injuries that occur immediately at the time of impact, with subsequent signs and symptoms of TBI, whereas chronic TBI refers to the long-term consequences of single or multiple brain traumas.[5] Both in sport represents an important public health concern in modern day society. Although brain injuries are not the most common type of sport-related injury, they can be associated with substantial morbidity and, potentially, mortality.[9]

2.1.2 Traumatic brain injury in children

Nowadays, according to epidemiologic studies, traumatic brain injury (TBI) is the main cause of death and disability among children.[10] With young pediatric population, many concussive injuries can be due not only to vehicle traffic accidents and falls, but also to sports impacts.[11] Practising sport leads to great physical and psychological benefits; however, if agonism (high level) and children (individuals with poor movement skills) are considered the risk of TBI and, rarely, catastrophic trauma and death increased. Children are often treated as small adults and sure enough sports products are produced in a certain size and then resized according to the proportions of the child. This line, essentially, can be followed for some products, such as sportswear, but with head injuries the same hypothesis is inappropriate.[12]

Therefore, it was necessary to understand how children brain have been different from adults one. Brain of 6 year old is 90% of an adult's brain size; in addition, there are differences in the relative volumes of grey and white matter, in the development of the neural pathways[13] and in mechanical properties.

Indeed, remarkable advances in the field of pediatric neuroimaging have opened new beginnings into understanding of the living growing human brain. It emerges that with increasing age, there are changes in remodeling of the pathways in the brain, which causes variations in the organization of grey and white matter (figure 2.1).[14]
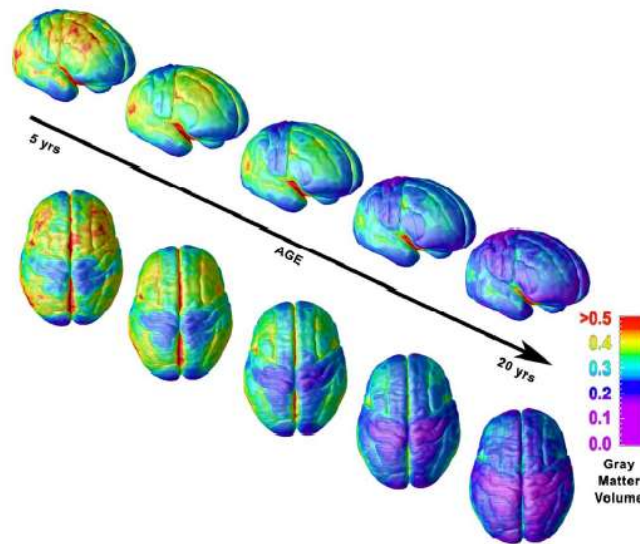
Figure 2.1 - *Right lateral and top views of the dynamic sequence of grey matter maturation over the cortical surface.*

2.2 Kinematics predictors of concussion

In sport, after an impact head motion is often quantified by linear and rotational acceleration; with linear acceleration associated with severe brain injury and rotational acceleration associated with concussion[15], because brain tissue has a high bulk modulus and low shear modulus.[16] Therefore, both linear and rotational acceleration are significant to understand the brain response after an impact and identify TBI risk.

Many studies can be found in the literature about the biomechanical analysis of concussions in sports[17-24]: almost always, sports related to TBI include contact and collision sports, such as American football, boxing, ice hockey, rugby and martial arts, but involvement in any sport activities brings a risk of suffering from head injuries. On the basis of these studies, it was possible to find a relationship between the magnitude of linear and rotational acceleration and duration of acceleration for a concussive event. In particular, figure 2.2 suggested a change in the injury mechanism based on linear acceleration and impact duration and figure 2.3 a relationship between rotational acceleration and impact duration. For short duration events, the main mechanism of injury was the relative motion between the skull and brain; while, for long duration events, the brain moves with the skull inducing intracerebral stresses and strains in the central parts of the brain.[25]
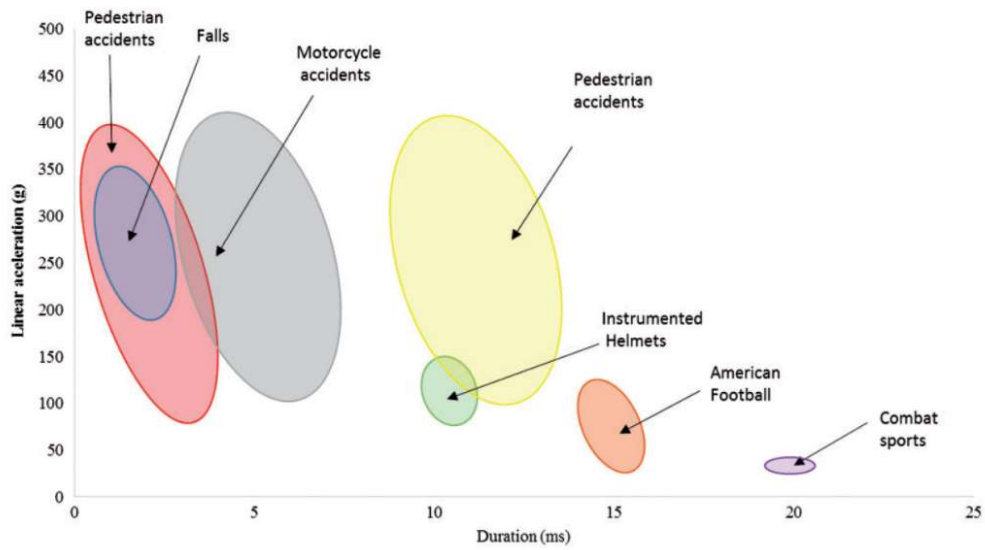
Figure 2.2 *- Linear acceleration magnitude vs duration in different sporting events and environments*[26]
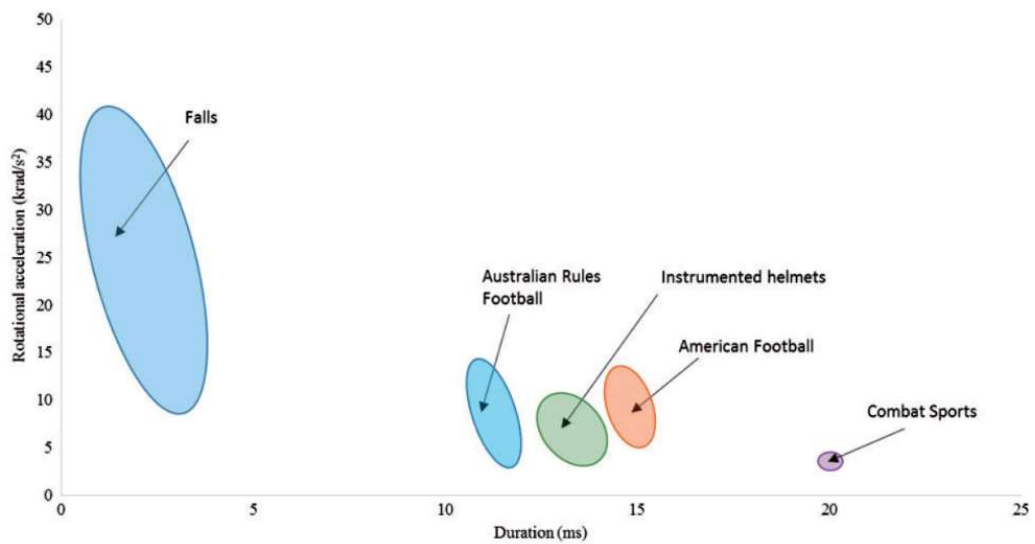
Figure 2.3 *- Rotation acceleration magnitude vs duration in different sporting events and environments*[26]

The relationship between impact magnitude and duration is a characteristic defined by the Wayne State Tolerance Curve (WSTC) and Brain Injury Curve Leuven (BICLE), as can be seen from graphs 2.4 and 2.5.
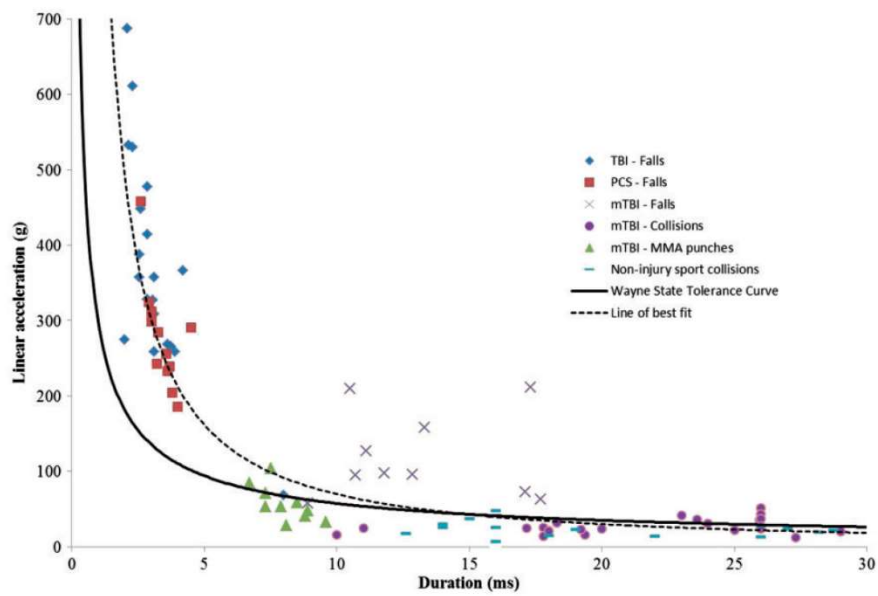
Figure 2.4 - *Linear acceleration magnitude/duration relationships classified by WSTC[26]*
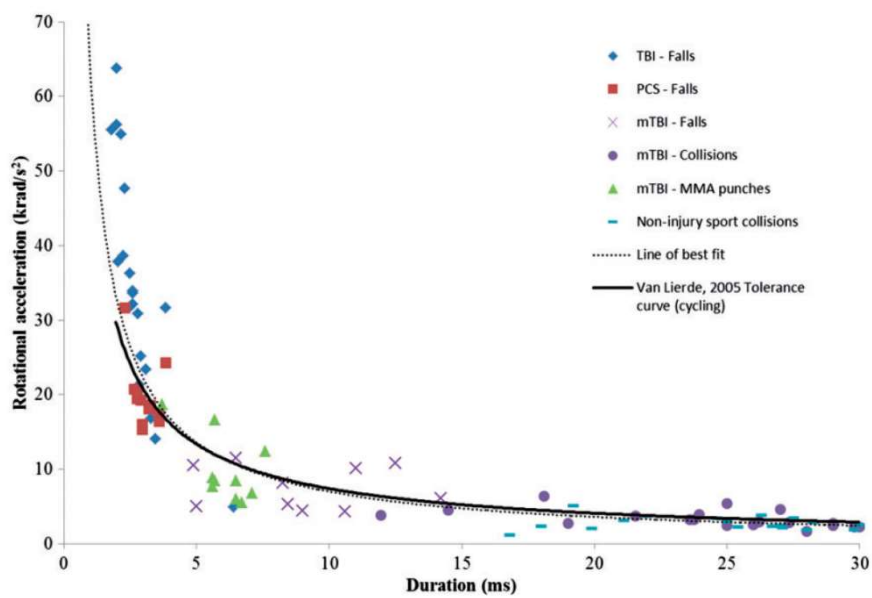
Figure 2.5 - *Rotational acceleration magnitude/duration relationships classified by CICLE[26]*

Considering rotational acceleration, the WSTC would not identify these impacts as an injury risk, probably because of padding was worn on the body and helmets for protection. Furthermore, considering rotational acceleration, the BICLE seems to reliability approximate injury values.[26]

Moreover, it can be found a relationship, between peak linear and rotational accelerations and maximal principal strain in the corpus callosum[25], which shows that strain response may be represented almost entirely by the rotational acceleration inputs and less by linear acceleration inputs (figure 2.6 and 2.7).
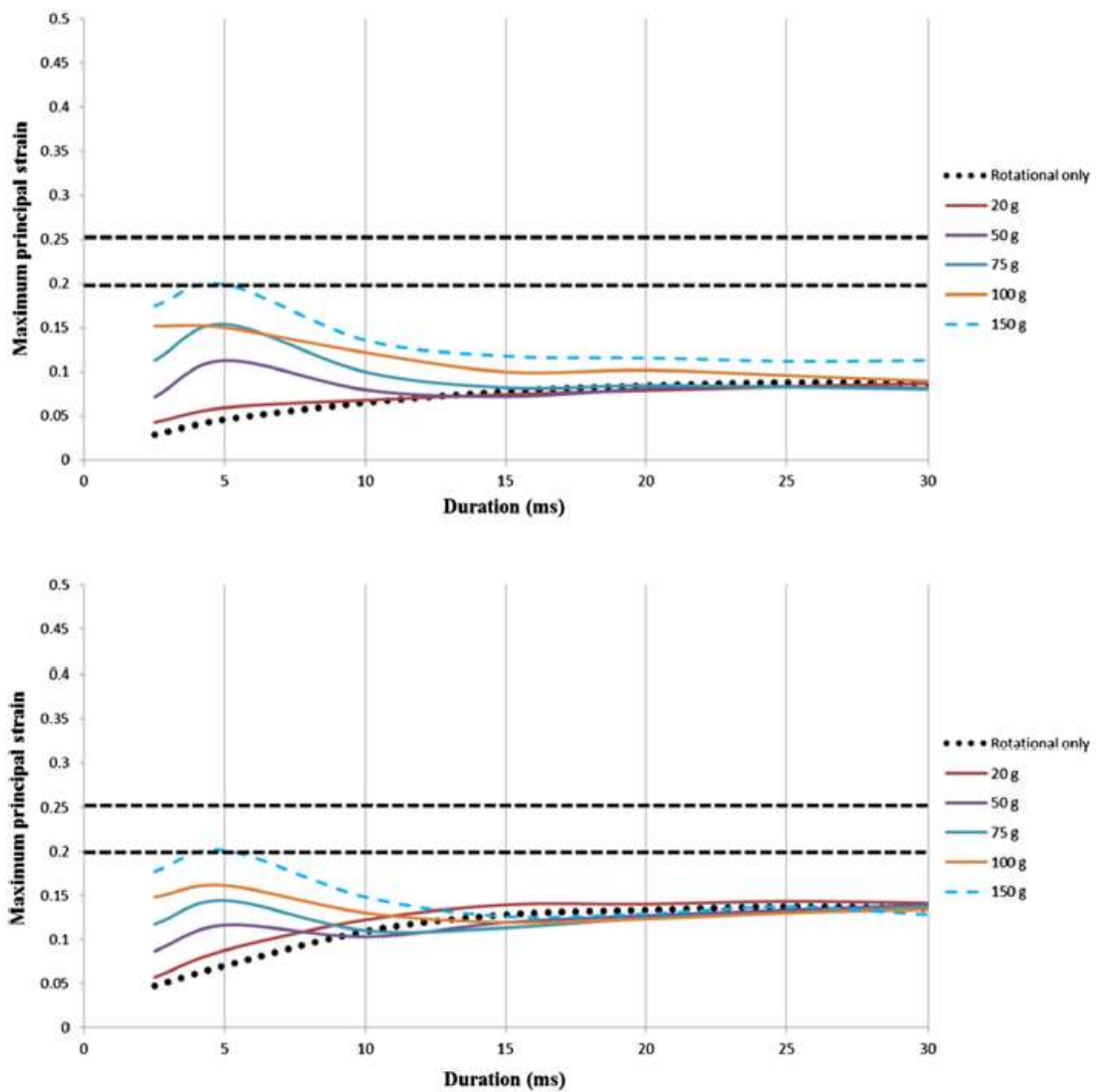
Figure 2.6 - *Maximum principal strain in the corpus callosum for different rotational acceleration input interacting with varying magnitudes of linear acceleration for different durations.[25]*
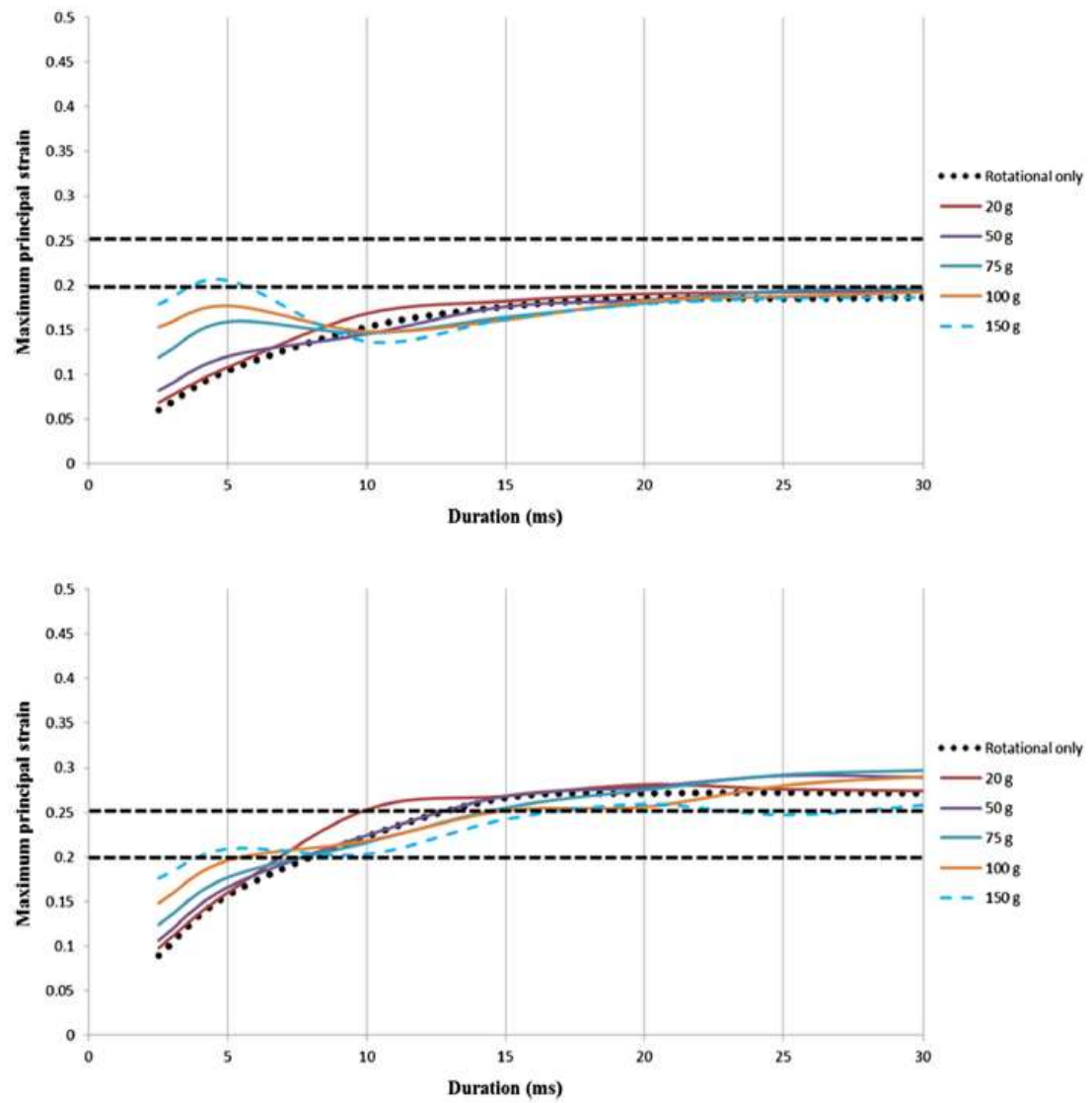
Figure 2.7 *- Maximum principal strain in the corpus callosum for different rotational acceleration input interacting with varying magnitudes of linear acceleration for different durations.*[25]

2.2.1 Experimental test

During impact, linear and rotational accelerations and velocities can be achieved using gyroscopic rate sensor and accelerometers. In Table 2.6, all the studies conducted and used to explore the topic of this paragraph have been reported. Studies specific for testing helmets[17,19,20,27] have utilized commercially available helmet-mounted accelerometer arrays and head kinematics resulting from head impact in real-time during live play was measured using the Head Impact Telemetry (HIT), which is a device capable of recording the acceleration-time history of an impact usually from 6 linear accelerometers. Other than sensorized helmet, instrumented mouthguard, which contained a low-power, high-g triaxial accelerometer with 200g maximum per axis and a triaxial angular rate gyroscope, was used by King[21]. In King[20] and Le[23] studies, instead, athletes wore the XPatch, which measures the magnitude with linear and rotational acceleration, as well as the frequency and location of head impacts and was placed, respectively, on the skin covering their mastoid and behind the player's right ear just before participation in match activities and was removed immediately after completion of the match. Researchers have found that xPatch sensors are appropriate for making frequency and magnitude comparisons between groups when all participants are wearing the xPatch sensor.[28] Supplementary, head-mounted sensors, such as the xPatch, deliver an accurate recognition of the peak angular acceleration of head impacts compared with other helmet mounted systems.[29]

Many studies[11,15,30,31] instead of collecting data in filed, involved a physical reconstructions test, which includes a monorail drop rig (Figure 2.8) to conduct physical reconstructions of falls. These tests use a test-setup that consist of an instrumented Hybrid III head, equipped with accelerometers arranged on a mount in a 3 x 2 x 2 x 2 array to capture linear and angular acceleration, which is attached to a drop carriage, is elevated to the prescribed height (0.02 m[30]), and then released on top of the anvils.
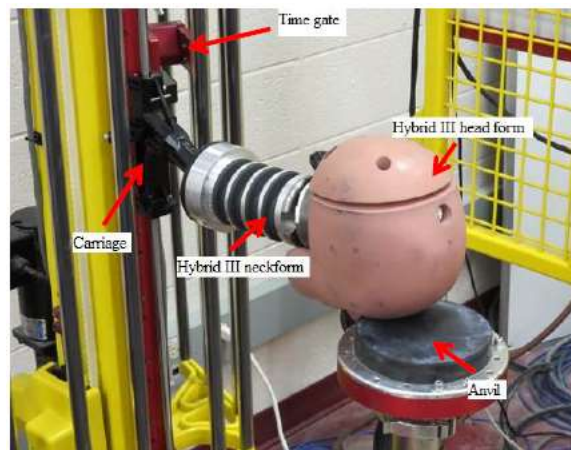
Figure 2.8 - Example of a monorail drop test set-up using a Hybrid III headform

Bussone[18] used a head sensor package that was designed and constructed with micro-electromechanical (MEMs) gyroscopic rate sensors and linear accelerometers that were mounted to an adjustable lightweight headband on head of a 50th percentile male Hybrid-III ATD.

It is important to note that in many studies not only the raw data are evaluated, i.e. acceleration and speed, but also other parameters, which are useful to better define the impact.

Crisco[28] plotted the data as cumulative histograms enables the reporting of values for individual players normalized for the total number of players on each team. Hanlon,[19] in order to determine the type of impact, header or nonheader, in addition to linear and angular accelerations, the head injury criterion (HIC) was analysed in order to determine differences in severity by location. The HIC is the most commonly acknowledged and widely applied head injury criterion, which assumes that head linear acceleration alone is a valid indicator.[32] It was proposed to focus the severity index on that part of the impact that was likely to be relevant to the risk of injury to the brain. Besides, more commonly the Head Impact Telemetry Severity Profile (HIT$_{SP}$) was used, and is a weighted composite score including linear and rotational accelerations, impact duration, as well as impact location.[22]

The reconstruction protocols use headforms and modelling methods that are representative of general human anthropometrics and tissue characteristics for the respective age ranges but are not biofidelic to each individual that was injured.[15] Furthermore, headforms neckforms have a directional stiffness built into them that were designed for cervical flexion and extension in car crash environments, that are different from sports one.[31]

Finally, there are researches[11,15,33] that have used the software Madymo to predict the motion of systems of bodies connected by kinematic joints and estimate the head velocity on impact for each impact location.

In order to simulate falls and pedestrian accident, impact velocity can be evaluated from literature[15,30,31] (0.5-6 m/s)or using the following equation[34,35]:

$$v = \sqrt{2hg}$$

where h is the height of fall, and g is the gravity acceleration. Furthermore, Roth[34] conduced, in order to investigate the influence of high of fall on the model response, a parametric study has been performed varying the high of fall from $h - 30\%$ to $h + 30\%$, which established that if h have been increased, there was a rise of shearing stress.

2.3 Finite element modelling of head injuries

Injury criteria that induced head injuries can be divided into three categories, as planned by van den Bosch:[36]

- Injury criteria based on translational accelerations of the head's centre of gravity;
- Injury criteria based on translational and rotational accelerations of the head's centre of gravity;
- Injury criteria based on stresses and strains in the brain tissue, through finite element modelling (FEM).

Injury criteria based on measures head kinematics, explained in the first two points and described in the paragraph 2.2.1, are widely employed in sporting brain injury research. However, in order to determine strain in brain tissue, the finite element modelling (FEM), is probably a more complete and appropriate approach.[37] Recently, there is a tendency among researchers to use head injury predictors that are based on the head tissue level response, rather than on its kinematics.

Finite element modelling can be considered as an important computational tool for study the dynamic response of the head when in is subjected to external accelerations. Using a finite element model of the human brain, it may be clear that brain strain has been attributed to head rotation and brain pressure has been attributed to head translation[38] and that as duration of rotational acceleration increased, the magnitudes of strain increased, even if these results were consistent for impacts at very high speeds and consequently high energy, which are not typical of sports impacts.[25]

Brain injury is reported to correlate well with stress, strain and strain rate.[39] However, strains and strain rates inside the brain (during impact) are difficult to measure. This can be achieved using FEM, where stresses and strains are used to compute injury parameters in the skull and intracranial contents. Therefore, these models bring an injury evaluation closer to reality.[32]

The most common metrics used for calculating risk are the maximum principal strain[40,46,50] (MPS), and the cumulative strain damage measure[40] (CSDM), even if in some studies are presented strain rate[41], the product of strain and strain rate[41], pressure and Von Mises Stress[34,41,42,48]. The MPS has been used to calculate risk of concussive injury[40] and Diffusion Axonal Injury (DAI).[43] The CSDM is a cumulative (not decreasing) measure that depends on time and has been used to calculate a measurement of the total volume of the brain that exceeded a certain strain threshold (e.g. 0.05, 0.10, 0.15, and 0.20) during the impact

simulation; it has been used at differing levels for predicting risk of head injuries such as CSDM10 for concussion[40], CSDM15 and CSDM25 for DAI.[43]

2.3.1 FEM in sport activities

Different type of FE models for the adult brain have been widely used recently. They differ on the mesh densities, on the different mechanical characteristics, and on the different medical imaging. Using FE models, a lot of studies have reconstructed and examined impact in different sports: Taekwondo, Ice Hockey, Lacrosse, American Football, Judo. [33,37,50,41,42,44–49] In Table 2.8, all the studies conducted and used to explore the topic of this paragraph have been reported.

Some suggested values for brain injury threshold strains and stresses are given from literature and reported in table 2.1 by Koncan:

Brain Region	Value	Strain variable	Author(s)
Grey matter	0.26 (50% risk)	MPS	Kleiven (2007)
Grey matter	0.48 (average)	MPS	Post et al. (2013)
White matter	0.26 (50% risk)	MPS	Patton et al. (2015)
White matter	0.38 (average)	MPS	Post et al. (2013)
Corpus callosum	0.15 (50% risk)	MPS	Patton et al. (2015)
Corpus callosum	0.21 (50% risk)	MPS	Kleiven (2007)
Corpus callosum	0.28 (average)	MPS	McAllister et al. (2012)
Midbrain	0.15 (50% risk)	MPS	Patton et al. (2015)
Midbrain	0.34 (average)	MPS	Viano et al. (2005)
Cerebrum	0.32 (average)	MPS	Viano et al. (2005)
-	0.44 (average)	MPS	Oeur et al. (2015)
-	0.32 (50% risk)	MPS	Kimpara and Iwamoto (2012)
-	0.31 (50% risk mild DAI)	MPS	Deck and Willinger (2008)
Midbrain	0.19 (50% risk)	Shear strain	Zhang et al. (2004)
-	0.32 (50% risk)	Shear strain	Kimpara and Iwamoto (2012)
-	0.60 (50% risk)	CSDM10	Kleiven (2007)
-	0.18 (50% risk)	CSDM10	Kimpara and Iwamoto (2012)
-	0.55 (50% risk of DAI)	CSDM15	Takhounts et al. (2003)

MPS: Maximum principal strain
CSDM: Cumulative strain damage measure

Table 2.1 - Summary of finite element model metrics associated with risk of concussive injury[12]

Bar-Koshba[42] used two head model to study contact sport: bonded, in which the nodes that are shared between the skull and Cerebrospinal Fluid (CSF) are always connected so that the skull and the CSF are constrained and not able to separate during deformation, and free, in which the meshes are allowed to freely disconnect during deformation, as it is clear in the figure 2.9.
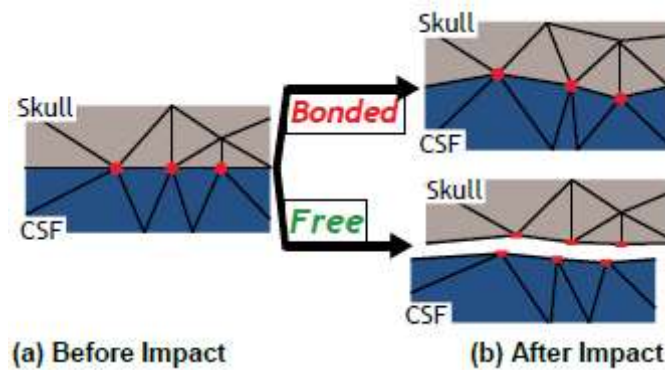
Figure 2.9 - *A comparison of the mesh connectivity between the bonded and free model for the interface between the skull and the CSF*

In both models, the normal stresses or the pressure terms are significantly larger (on the order of 10^4 Pa) then the shear stresses. For the bonded model, the pressure magnitude starts at 1.7 MPa and ends at minimum of -1 MPa at the posterior of the brain, while in the free model, the maximum pressure is 2.7 MPa and approaches zero as a function of distance from the anterior of the brain.

Patton[41] has focused his study on sporting impacts to the unprotected head, using a Royal Institute of Technology (KTH) FE Human Head Model. Von Mises stress was the most effective out of the tissue-level brain injury predictors and it was also found that the thalamus and corpus callosum were brain regions with strong associations with concussion. For the thalamus, tentative tolerance limits were proposed for a 50% likelihood of concussion: 2.24 kPa, 24.0 s^{-1}, and 2.49 s^{-1} for von Mises stress, strain rate, and the product of strain and strain rate, respectively. For the corpus callosum, tentative tolerance limits were proposed for a 50% likelihood of concussion: 3.51 kPa, 25.1 s^{-1}, and 2.76 s^{-1} for Von Mises stress, strain rate, and the product of strain and strain rate, respectively.

American football was studied by Elkin[45], using SIMon and GHBMC model, and established that peak kinematics, injury metrics and brain strain varied significantly with impact location and impact speed. Both FE models generated similar ranges, distributions and time histories for the brain strain parameters: the 95th percentile MPS for the whole brain varied from 0.10 to 0.50 for the SIMon model and 0.11 to 0.54 for the GHBMC model, whereas

CSDM25 varied from 0.00 to 0.48 for the SIMon model and from 0.00 to 0.43 for the GHBMC model. Furthermore, impact location and speed had a significant effect on 95th percentile MPS for the whole brain and all the anatomical regions, whereas the effect of model (SIMon vs. GHBMC) was only significant for the left and right cerebellum. Also, Post[49] using Wayne State University Brain Injury Model (WSUBIM), have studied MPS, which assumes slightly higher values than the previous study, in fact its maximum value is equal to 0.767.

Ito[46] using SIMon model has focused attention on Judo, valuating distribution of MPS, assessing that brain injury risk is high in the lateral region and callosum (0.667). CSDM was examined in order to evaluate injury risk of diffuse axonal injury (0.229).

Morse[47] has computed the von Mises stresses and principal strains for each of impact trials in lacrosse simulation: the highest Von Mises stress and principal strain magnitudes in lacrosse simulations were 46 Pa and 0.06%. These values were compared with the peak values to reported TBI injury threshold numbers found in the literature: the thresholds of Von Mises stress and principal strain typically range from 14.8 to 33 kPa and 26–40%, respectively.

The determination of such tolerance value is difficult and is one of the main difficulties in research, since the various parameters can assume different values depending on the type of sport, the type of impact, the location of the impact; in addition to differences in loading conditions, as well as material properties and boundary conditions. Furthermore, since measurements of brain tissue deformation and responses cannot be calculated in vivo, they have to be estimated later, using finite element models, as in these studies, which may not properly represent reality.

2.3.2 FEM in children

The head is made up of distinct anatomical sections of tissue, bone, and cerebrospinal fluid. Therefore, in order to obtain a careful representation of the stresses and strains in the brain, its model have to be endowed with well-defined geometries and meshes, precise constitutive models and correct boundary conditions.[42]

In children, FE modelling is developing topic and limited, even if children are at higher risk for concussion, prolonged recovery, and repeat concussive injury when compared to adults.[51] In Table 2.9, all the studies conducted and used to explore the topic of this paragraph have been reported.

Scaling adult models has been used to study concussive impacts in children.[11,12,30] While the using of scaled adult FE models to study youth has its disadvantages and limitations, it was one method to most commonly used study concussion in young children. The Scaled University College Dublin Brain Trauma Model (Scaled UCDBTM, figure 2.10)[52] uses a contact surface between the brain and CSF; while models submitted subsequently have continuous mesh connecting the brain to CSF. Its geometry is based on medical imaging on an adult male cadaver.
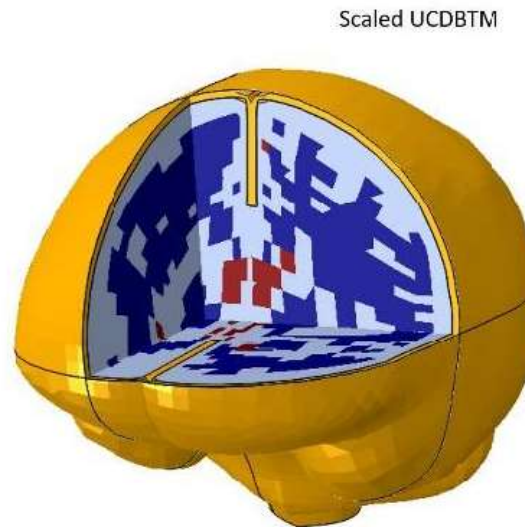
Figure 2.10 - Finite element model of scaled UCDBTM

Mechanical properties have been summarized for Scaled UCDBTM (table 2.2):

Material	Young's Modulus [MPa]	Poisson's ratio	Density [kg/m³]
Scalp	16.7	0.42	1000
Cortical Bone	15000	0.22	2000
Trabecular Bone	1000	0.24	1300
Dura	31.5	0.45	1130
Pia	11.5	0.45	1130
Falx and Tentorium	31.5	0.45	1130
Brain	Hyper Elastic	0.50	1040
Facial Bone	5000	0.23	2100

Table 2.2 - Mechanical properties of the scaled UCDBTM model

Roth[34] proposed a 3-year-old subject model, which is based on the geometrical 3D reconstruction of slices obtained by CT scanner (figure 2.11). This model includes the scalp, the skull and sutures, the face, the cerebrospinal fluid, the tentorium and falx membranes and the brain; fontanels are closed.
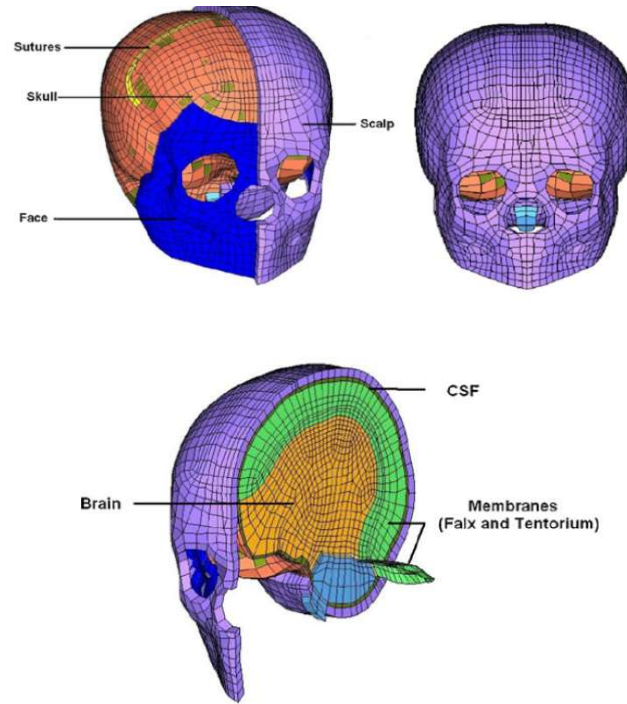
Figure 2.11 - *Finite element model of the 3-year-old child head by Roth*

Mechanical properties have been summarized in table 2.3, whose data has been extracted from literature and Young's modulus of the skull was chosen according to the interpolation curve:

Material	Young's Modulus [MPa]	Poisson's ratio	Density [kg/m³]
Membranes	31.5	0.45	1140
CSF	0.012	0.49	2040
Scalp	16.7	0.42	1200
Sutures	10-1500-3000-4700	0.22	2150
Skull	4700	0.22	2150

Table 2.3 - *Mechanical properties of the Roth head FE model*

Later, within the PIPER project, a new child model (PIPER Child model), a scalable model between at least 1.5 and 6 years of age was developed. It was presented in 2016 in Munich for the 14th International Conference Protection of Children in Cars. In particular, the development of the PIPER head model described in Giordano and Kleiven[53] was continued. Significant updates were made to the mesh of the brain and meninges with the purpose to improve the quality and stability of the model. The head PIPER Model (figure 2.12) include skull, cerebellum, falx, tentorium, facial bones, suture.

Figure 2.12 - *The 1.5 y.o (left) and 6 y.o models (right) obtained by scaling using the PIPER tool*
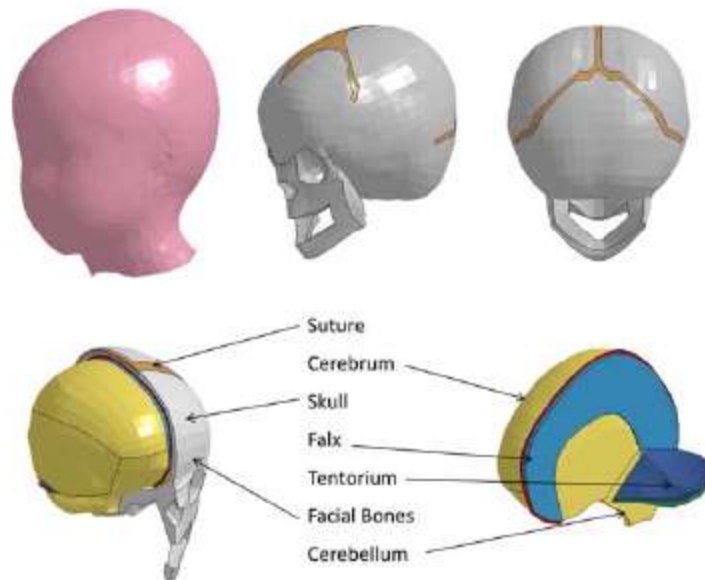
Figure 2.13 - *Finite element model of PIPER Model*

The model was based on computer tomography and medical imaging of one child provided by the Hospices Civils de Lyon (HCL, France). Model validation was conducted using the normalized integral square error (NISE) method, to evaluate the biofidelity of the model.

Mechanical properties have been summarized in table 2.4, whose data has based on experimental evidence:

Material	Young's Modulus [MPa]	Poisson's ratio	Density [kg/m³]
Scalp	Hyperelastic	0.49	1.14
Outer Compact Bone	9000	0.22	2
Inner Compact Bone	9000	0.22	2
Porous Bone	1000	0.24	1.3
Brain tissue	Hyperelastic	0.5	1.04
CSF	2100	0.5	1
Dura Mater	Mooney – Rivlin[54]	0.45	1.13
Pia Mater	11.5	0.45	1.13
Falx	31.5	0.45	1.13
Tentorium	31.5	0.45	1.13

Table 2.4 - *Mechanical properties of the PIPER model*

In closing, Koncan[30] introduced a FE model of a 6-year-old child for use in sporting impact research of young children. The model (figure 2.14) was based on MRIs; but using a single individual, as in previous cases, to reconstruct child head model established a limitation, since the model may not be an accurate representation of all individuals in this age group. The model assessment was conducted using the NISE method, employed before by Giordano and Kleiven, to evaluate the biofidelity of the model.
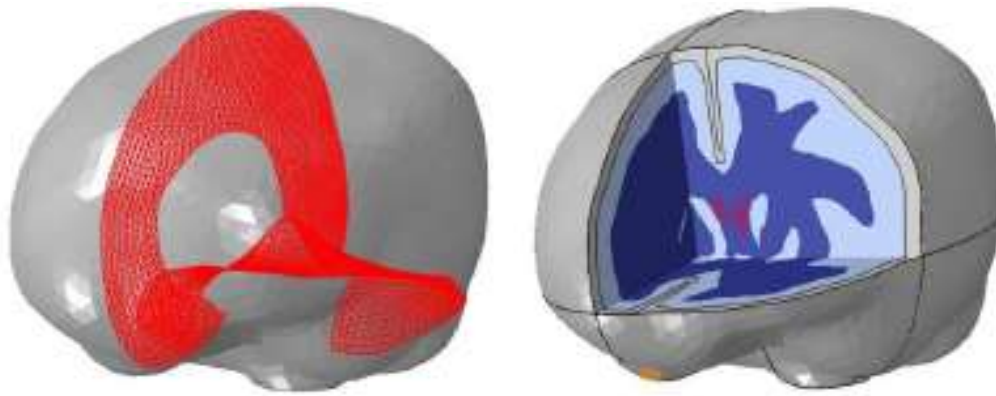
Mechanical properties have been summarized:

Material	Young's Modulus [MPa]	Poisson's ratio	Density [kg/m³]
Skull	Rigid	-	2000
Pia	11.5	0.45	1130
Falx and Tentorium	21.5	0.45	1130
Brain	Hyperelastic	0.5	1060
CSF	0.0015	0.5	1000

Table 2.5 - Mechanical properties of Koncan head FE model

The UCDBTM is one of the most widely used models in the literature, even in its scaled version, so there is more data that can be used to analyse the results. The lack of validation data is still the most evident limitation for FE models, with a minimum number of published data on adults and no intracranial data for children and adolescents. Nevertheless, it can be considered a fairly precise way to study brain injury, using the appropriate metrics.

Authors	Title	Publication	Aim	Material and Methods	Results
Bryan R. Cobb, Jillian E. Urban, Elizabeth M. Davenport, Steven Rowson, Stefan M. Duma, Joseph A. Maldjian, Christopher T. Whitlow, Alexander K. Powers, Joel D. Stitzel	Head Impact Exposure in Youth Football: Elementary School Ages 9–12 Years and the Effect of Practice Structure[17]	2013	Quantify the head impact exposure of youth football players for all practices and games over the course of single season.	- 50 players, age 9–12 - HIT system: six single-axis accelerometers on the head	- Improve the safety of youth football through rule changes, coach training, and equipment design. - Head impact can be reduced significantly by limiting contact in practices to levels below those experienced in games. - Head impact exposure at the youth level may effectively be reduced by limiting contact in practices.
Joseph J. Crisco, PhD; Russell Fiore, MEd, ATC; Jonathan G. Beckwith, MS`; Jeffrey J. Chu, MS`; Per Gunnar Brolinso; Stefan Duma, PhDI; Thomas W. McAllister; Ann-Christine Duhaime;	Frequency and Location of Head Impact Exposures in Individual Collegiate Football Players[28]	2010	Quantify the frequency and location of head impacts that individual players received, between practice and game sessions, and among player positions.	- Players from 3 NCAA football programs. - Helmet instrumented with the HIT system. - 6 linear accelerometers at 1000 Hz.	The frequency of head impacts and the location on the helmet where the impacts occur are functions of player position and session type. These data provide a basis for quantifying specific head impact exposure for studies related to understanding the biomechanics and

Richard M. Greenwald					clinical aspects of concussion injury, as well as the possible effects of repeated subconcussive impacts in football.
William R. Bussone, Tara L. A. Moore, Darrin Richards, Robert T. Bove, Jr., Irving Scher and Michael T. Prange	Measurements of Non-Injurious Head Accelerations of a Pediatric Population[18]	2009	Increases the upper limit of known non-injurious activities and closes the gap between the lower limit of injurious loading and the upper limit of non-injurious loading.	- Micro-electromechanical (MEMs) gyroscopic rate sensors and linear accelerometers. - ATD. - 6 male and 6 female pediatric have to do 8 activities. - Filter.	- Children generate non-injurious linear and rotational accelerations at least as high as those previously published in studies involving adults.
Erin M. Hanlon, Cynthia A. Bir	Real-Time Head Acceleration Measurement in Girls' Youth Soccer[19]	2012	Collect real-time linear and angular head acceleration data for soccer impacts during girls' youth (U14) soccer play.	- Wireless head acceleration measurement device (the Head Impact Telemetry System). - The head injury criterion and resultant linear and angular accelerations are analyzed and compared with current injury tolerance values for all impacts.	- Head accelerations exceed the majority previous study. - None of the impacts exceeded linear acceleration tolerance values for concussion, but angular accelerations exceed the limits.
Doug King, Patria Hume, Conor Gissane and Trevor Clark	Head impacts in a junior rugby league team measured with a wireless head impact sensor: an exploratory analysis[20]	2017	Investigate the frequency, magnitude, and distribution of head impacts of players in a junior rugby league.	- 19 players - XPatch sensor: triaxial accelerometer and a triaxial angular rate gyroscope - X2Biosystem	The magnitude of impacts for linear and rotational accelerations in this study is similar to the impacts in studies of

					youth football and ice hockey players. But the rugby players are younger, have less body mass and play at a slower speed than the american players. Junior rugby players have to tackle the player to the ground and use a different tackle technique than that used in american football, probably increasing the rotational accelerations recorded at the head.
Fidel Hernandez, Lyndia C. Wu, Michael C. Yip, Kaveh Laksari, Andrew R. Hoffman, Jaime R. Lopez, Gerald A. Grant, Svein Kleiven, Daviv B. Camarillo	Six Degree-of-Freedom Measurements of Human Mild Traumatic Brain Injury[38]	2014	Investigate whether direct measurement of head rotation improves prediction of mTBI.	- Instrumented mouthguards, that measure 6DOF (tri-axial accelerometer, tri-axis gyroscope). - Capture high-definition video. - 18 kinematic and brain finite element criteria are calculated.	- Brain strain has been attributed to head rotation. - Brain pressure has been attributed to head translation.
Doug King, Patria A. Hume, Matt Brughelli and Conor Gissane	Instrumented Mouthguard Acceleration Analyses for Head Impacts in	2015	Quantify head impacts via instrumented mouthguard acceleration	- 38 senior rugby players - Instrumented mouth – guard (X2Biosystems)	- The acceleration magnitudes and number of head impacts in rugby

	Amateur Rugby Union Players Over a Season of Matches[21]		analyses for rugby union players over a season of matches.	- Triaxial accelerometer and triaxial angular rate gyroscope. - All impacts are evaluated through the IMS using a "declacking algorithm".	players is higher than other sport. - Mean linear acceleration measured is similar to the mean linear accelerations for youth, high school, and collegiate american football players but lower than that for female youth soccer players. - Mean rotational acceleration is similar to mean rotational accelerations for youth, high school, and collegiate american football players but less than those for female youth soccer players, concussed american collegiate players, collegiate american football players and professional american football players.
D. King, P. Hume, Gissane, M. Brughelli, T. Clark	The Influence of Head Impact Threshold for Reporting Data in Contact and Collision	2015	- Methods for reporting head impact acceleration data in sport.		

	Sports: Systematic Review and Original Data Analysis[22]		- The effect of the acceleration thresholds on the number of impacts reported.		
Rachel K. Le, MS, ATC, Tabitha D. Saunders, ATC, Katherine M. Breedlove, PhD, ATC, Debbie A. Bradney, DPE, ATC, Jill M. Lucas,* PhD, and Thomas G. Bowman, PhD, ATC	Differences in the Mechanism of Head Impacts Measured Between Men's and Women's Intercollegiate Lacrosse Athletes[23]	2018	Compare sex-specific differences in the magnitude and frequency of head impact mechanisms in lacrosse athletes.	- 31 lacrosse players (16 men and 15 women)4. - Instrumented mouth – guard (X2Biosystems). - Calculate incidence rates (IRs) and incidence rate ratios (IRRs)	The impact mechanisms of head to body in men's lacrosse and stick to head in women's lacrosse are penalties but happens frequently, suggesting that a focus on rule application is necessary.
Jason P. Mihalik, David R. Bell, Stephen W. Marshall, Kevin M. Guskiewicz	Measurement of Head Impacts in collegiate football players: an investigation of positional and event – type differences[27]	2007	Investigate if there are differences in head accelerations between different player positions and different event types in collegiate football. Identify if there is an association between high-magnitude impacts and location of head impacts.	- 72 collegiate football players. - Accelerometers in football helmets. - Position, event type, and location of head impact differences are evaluated by using analyses of variance and χ^2.	- Less than 0.35% of impacts exceeding theoretical injury thresholds resulted in concussion. - More injury data are required before any theoretical thresholds for injury can be confirmed.
Tyler J. Young, Ray W. Daniel, Steven Rowson, and Stefan M. Duma	Head Impact Exposure in Youth Football: Elementary School Ages 7-8 Years and the Effect of Returning Players[24]	2013	Provide data describing the head impact exposure of 7- to 8-year-old football players.	- 19 players. - Helmets are instrumented with 1 of 2 accelerometer arrays that were used in parallel: the commercially	Head impact frequency, acceleration magnitude, and impact location obtained are a further step toward developing effective

				available Head Impact Telemetry (HIT) System or a custom 6 degree of freedom (6DOF) head acceleration measurement device.	strategies to reduce the incidence of concussion in youth football and have applications toward youth-specific football helmet designs.

Table 2.6 – Papers regarding head acceleration found in literature

Authors	Title	Publication	Aim	Material and Methods	Results
Sentaro Koshida, Takanori Ishii, Tadamitsu Matsuda and Toshihiko Hashimoto	Biomechanics of judo backward breakfall for different throwing techniques in novice judokas[3]	2017	Investigate the kinematics and possible risk factors of judorelated head injury when being thrown by comparing the breakfall motion for osoto-gari with that for ouchi-gari in novice judokas	- 12 novice male judokas are recruited - 41 reflective markers are placed on landmarks of the participants - A 20-camera Mac3D motion analysis system (200 Hz).	The significant differences with large effect size in the peak neck extension momentum and the head position with greater neck extension angle between the two techniques suggest that from both epidemiological and biomechanical points of view, being thrown with osoto-gari probably increases the risk head injury to a greater degree than does being thrown with ouchi-gari in novice judokas.
Sentaro Koshida, Takanori Ishii, Tadamitsu Matsuda and Toshihiko Hashimoto	Kinematics of Judo Breakfall for Osoto-Gari: Considerations for Head Injury Prevention[55]	2016	Study the kinematics parameters of the breakfall for osoto-gari to identify the risk of judo-related head injuries by comparing experienced and novice judokas.	- 10 experienced and 12 novice male judokas are recruited - 41 reflective markers to the anatomical landmark of the participants	Kinematic parameters, associated with the incidence of judo-related head injuries, are: - Peak neck extension moment during the breakfall motion: in

				- A 20-camera Mac3D motion analysis system (200 Hz).	the novice group was greater than that of the group of experienced judokas. - Movement patterns of the trunk, left hip and the right knee: indicate that the novice judokas exhibited a significantly greater flexed position during the breakfall motion.
Takeshi Kamitani, Yuji Nimura, Shinji Nagahiro, Seiji Miyazaki and Taisuke Tomatsu	Catastrophic Head and Neck Injuries in Judo Players in Japan from 2003 to 2010[2]	2013	Determine the features of catastrophic head and neck injury in Judo athletes in Japan between 2003 and 2010.	- 72 judo injuries are reported between 2003 and 2010 - Epidemiological study.	The principal reason of head traumas was being thrown: - The contusion area was occipital, caused by osoto-gari technique. - The principal trigger of neck traumas was throwing with uchi-mata technique.
Howard Thomas Hurst, Stephen Atkins and Christopher Kirk	Reliability of a Portable Accelerometer for Measuring Workload During Mixed Martial Arts[56]	2014	Determine the reliability of a portable accelerometer for measuring workload in Mixed Martial Arts.	- 8 male MMA trained partecipants - Equipment: standard MMA competition shorts, a groin protector, gum shield, t-shirt or rash guard, and competition standard 5-ounce MMA	- The accelerometer can provide a useful tool for following and examining workloads in training and competition circumstances.

				gloves. - Minimax X3 tri-axial accelerometers (100 Hz) - Each unit was placed in a neoprene harness worn on the participant's torso, ensuring the accelerometer was positioned at the T3-T4 vertebrae	- Results also suggest that the accelerometer could also be used to determine the efficiency and variability in skills amongst MMA competitors of differing ability levels and could be used to determine benchmark values for workloads in different weight categories in the future.
Masahito Hitosugi, Haruo Murayama, Yasuki Motozawa, Kanto Ishii, Masahiro Ogino, and Katsuhiro Koyama	Biomechanical Analysis of Acute Subdural Hematoma Resulting from Judo[57]	2014	Investigate the biomechanical mechanism of acute subdural hematoma caused by judo and search precautionary methods to decrease injury rate.	- Tri-axial accelerometer placed on the centre of gravity of the ATD's head - High-speed data acquisition system (up to 20 kHz) - High-speed digital video camera (1000 Hz)	Severe contact of the occipital part of the head to the mat and high values for linear and angular accelerations could led to the occurrence of ASDH. Therefore, to reduce severe head injuries in judo, youth participants should master Ukemi.
Haruo Murayama, Masahito Hitosugi, Yasuki Motozawa, Masahiro Ogino,	Simple Strategy to Prevent Severe Head Trauma in Judo[58]	2013	Determine whether the use of an under-mat may diminish impact to the head in judo.	- Japanase male judo expert recruited POLAR anthropomorphic test device (ATD)	- Without an under-mat, peak acceleration ranged from 51.6 to 79.9 g (o-soto-gari)

				- Tri-axial accelerometer onto ATD head's - High-speed acquisition system (20 kHz) - High-speed digital video camera for kinematics (1000 fps)	and 124.9 to 143.2 g (o-uchigari). - With the undermat mounted, duration of the acceleration was Extended and values were reduced and peak acceleration fluctuated from 36.1 to 45.7 g (o-soto-gari) and 73.7 to 92.4 g (o-uchigari). - The HIC values calculated without an under-mat forecast a risk of head traumas (HIC > 250).
and Katsuhiro Koyama					
Haruo Murayama, Masahito Hitosugi, Yasuki Motozawa, Masahiro Ogino and Katsuhiro Koyama	Rotational Acceleration during Head Impact Resulting from Different Judo Throwing Techniques[59]	2014	Determine translational and rotational head acceleration in Judo which are responsible for head Injuries, using two throwing techniques.	- The ATD used is a POLAR dummy with high bio-fidelity - Tri-axial accelerometer on the COG at dummy head, sampled at 20 kHz - High speed digital video camera (1 kHz)	Not only linear acceleration, but also rotational may be sufficient to cause injury.
Declan A. Patton	A Review of Instrumented Equipment to Investigate Head Impacts in Sport[60]	2016	Review the development, validity and potential of instrumented equipment: helmets, headgear, headbands, skullcaps, skin patches, andmouthguards.		

Yoshihisa Ishikawa, Kenji Anata, Hironori Hayashi, Takayuki Yokoyama, Takashi Ono and Shuichi Okada	Effects of Different Throwing Techniques in Judo on Rotational Acceleration of Uke's Head[61]	2018	Clarify the rotational acceleration of the head of an uke during tai-otoshi, seoi-nage, osoto-gari, and ouchi-gari when safe ukemi is performed.	- Rotational velocity sensor measures the rotational acceleration in the sagittal plane of the uke's head - Variance analysis	Osoto-gari generated maximum rotational acceleration of the uke's head, so it is linked to injure the head.
Sentaro Koshida, Takanori Ishii, Tadamitsu Matsuda, Toshihiko Hashimoto	Biomechanics of the judo backward breakfall: Comparison between experienced and novice judokas[3]	2014	Investigate the kinematics and muscle activation patterns during a judo backward breakfall in experienced and novice judokas.	- 11 experienced judokas - 13 novice judokas - 31 3D marker trajectory data for the breakfall on the bony landmarks of the judokas - Documentation of head-, neck-, trunk-, hip and knee-angle time profiles - Documentation of electromyographic activities of the sternocleidmastoid, external oblique and rectus abdominis muscles during breakfalls	- Difference in the knee joint motion during the judo backward breakfall between the experienced and novice judokas. - No significant differences in the activation patterns of any muscles between the experienced and novice judokas. - The time of hand impact coincides with the timing of peak head linear acceleration.
Sentaro Koshida, Takanori Ishii, Tadamitsu Matsuda, Toshihiko Hashimoto	Trunk biomechanics during breakfall for osoto-gari and its association with judo-related head injury risk in novice judokas[62]	2018	Develop effective injury prevention strategies, studying correlation between trunk biomechanics and judorelated head injury risk.	- 31 novice judokas - Markers are placed on bilateral anatomical landmarks	- Trunk biomechanics during the breakfall for osoto-gari may be associated with the judo-related head injury risk. - Correlation between the trunk COM angular

					velocity in all three motion planes and the biomechanical parameter reflects the judo-related head injury risk.

Table 2.7 – Papers regarding Judo injuries found in literature

Authors	Title	Year of publication	Aim	Materials & Methods	Results
Neda Boroushak, Mansour Eslami, Mohsen Kazemi, Hasan Daneshmandy, John A. Johnson	The dynamic response of the taekwondo roundhouse kick to head using computer simulation[44]	2018	Analyze the effect of the taekwondo roundhouse kick to the head in terms of dynamic variables such as linear and rotational acceleration.	It is used the ADAMS software model: - Head; - Neck and body: modelled by clamped-free beam; - Foot.	Only rotational acceleration causes an injury to head: - By comparing the linear acceleration curves with the threshold tolerance curve of the head, it can be specified that the acceleration created will be located below the linear acceleration threshold. - A comparison of the rotational acceleration-time curve to the rotational acceleration threshold values of the head concluded that the values obtained were within the head injury threshold. Especially at high foot speeds, rotational acceleration can lead to cerebral concussion and brain surface shearing.

Eyal Bar-Kochba, Mark Guttag, Subham Sett, Jennifer A. Franck, Kyle McNamara, Joseph J. Crisco, Janet Blume, and Christian Franck	Finite Element Analysis of Head Impact in Contact Sports[42]	2012	Quantify impact location, magnitude, and linear and angular accelerations of the head in order to increase the understanding of TBI and aid in the development of a neuronal injury criterion.	- HIT system; - It is used a realistic FEM model of the brain derived from MRI scans. The FEA mesh also includes neck muscles and vertebrae, which simulates more realistic angular accelerations, and thus provides a more realistic investigation of	- Parameter to extract is the total contact time (2 ms) in comparision HIT system data produces typical contact times of 10 ms. - The head undergoes a rapid acceleration and deceleration suddenly after impact (CAD): major factor in TBI. - In both models: Normal stress is

				the injury-causing mechanisms.	larger than shear stress because the ratio of bulk and shear modulus for the brain is 10^4. Pressure wave dissipate over distance away from impact site. - Difference between models: Maximum intracerebral pressure is larger in the free model, but difference between maximum and minimum is the same. For the bonded model: constrained boundary condition enforces a tensile pressure at the posterior of the brain. For the free model: since the brain is free to move at the boundary, the pressures must be equal to zero.

Declan A. Patton, Andrew S. McIntosh and Svein Kleiven	The Biomechanical Determinants of Concussion: Finite Element Simulations to Investigate Tissue-Level Predictors of Injury During Sporting Impacts to the Unprotected Head[41]	2015	Investigate the effectiveness of tissue-level brain injury predictors and determine the associations with concussion: - Strain rate - Product of strain and strain rate - Cumulative strain damage measure (CSDM) - Von Mises stress - Intracranial pressure	KTH FE Human Head Model in two version: - Hyper – viscoelastic version (include nonlinear elasticity) - Linear viscoelastic version: CSDM can valutated only for this.	- Von Mises stress: the most effective out of the tissue-level brain injury predictors assessed. - Stress x strain rate: the thalamus and corpus callosum were the brain regions with the strongest associations with concussion
Benjamin S. Elkin, Lee F. Gabler, Matthew B. Panzer, Gunter P. Siegmund	Brain tissue strains vary with head impact location: A possible explanation for increased concussion risk in struck versus striking football players[45]	2018	Examine the effect of impact location on regional brain tissue strain when input energy is constant.	- 24 simulation (2 speeds x 12 impact locations). - 2 finite element models of the brain: Simulated Injury Monitor and Global Human Body Model	Both finite element models generated similar strain results, with minor variations for impacts that generated multi axial rotations, larger variations in brainstem strains for some impact locations and a small bias for the cerebellum.

				Consortium brain model. - The calculation of the cumulative strain damage measure and maximum principal strain.	Based on this experimental and computational simulation study: - Impact location on the football helmet has a large effect on regional brain tissue strain. - The lowest strains consistently occurred in impacts to the crown and forehead, helmet locations commonly associated with the striking player.
Andrew Post, Anna Oeur, Evan Walsh, Blaine Hoshizaki and Michael D. Gilchrist	A centric/non-centric impact protocol and finite element model methodology for the evaluation of American football helmets to evaluate risk of concussion[33]	2013	Examine a proposed protocol for the evaluation of American football helmets for concussive injuries.	9 collision impact site and angle conditions are evaluated for the helmeted Hybrid III headform with one impact per condition and helmet for a total of 27 impacts. The finite element model is UCDTBM.	- The influence of impact site on peak linear and rotational acceleration is analysed: the centric conditions produced larger linear accelerations and the non-centric conditions produce larger rotational accelerations; - The largest magnitude peak maximum principal

					strain and von Mises stress are found for site 6 and 8, which is a non-centric impact across the rear areas of the helmet. - Non-centric impacts produce larger brain deformations.
Daisuke Ito, Koji Mizuno, Masahito Hitosugi, Haruo Murayama, Katsuhiro Koyama	Finite Element Analysis for Understanding Trauma Brain Injury in Judo[46]	2016	Study the acute subdural hematoma (ASDH).	- 3 experimental data are obtained by dummy experiments; - Head impact conditions in Judo are reproduced with a Simulated Injury Monitor (SIMon) FE.	Valutation of: - Maximum Principal Strain (MPS): brain injury risk is high in the lateral region and callosum. - Cumulative Strain Damage Measure (CSDM): examined in order to evaluate injury risk of diffuse axonal injury. - Elongation of bridging veins (one of the most common factors in ASDH) → The possibility that injury risks of rupture of the bridging veins is low in judo and the previous criteria cannot predict ASDH because of low rotational acceleration.

					→ The results may support the hypothesis that almost all ASDH's from non-penetrating impacts are due to the rupture of cortical vessels in the dural/arachnoid complex, not including the bridging veins.
Andrew Post, T. Blaine Hoshizaki, Michael D. Gilchrist, Michael D. Cusimano	Peak linear and rotational acceleration magnitude and duration effects on maximum principal strain in the corpus callosum for sport impacts[25]	2017	Examine the interaction between linear and rotational acceleration and duration on maximum principal strain in the corpus callosum for loading conditions in sporting environments.	It is used the University College Dublin Brain Trauma Model (UCDBTM), which geometry is determined from medical imaging of the head of a male cadaver.	The results establish that magnitude and duration have an effect on the strain incurred by the brain tissue. As the duration of the acceleration increases, the magnitude required to achieve strains reflecting a high risk of concussion decreases, with rotational acceleration becoming the dominant contributor. The magnitude required to attain a magnitude of MPS representing risk of brain injury is 2500 rad/s^2 for impacts of 10–15 ms; indicating that interventions to reduce the risk of concussion in sport must consider the duration of the event while reducing the magnitude of

					acceleration the head incurs.
Justin D. Morse, Jennifer A. Franck, Bethany J, Wilcox, Joseph J. Crisco, Christian Franck	An Experimental and Numerical Investigation of Head Dynamics Due to Stick Impacts in Girls' Lacrosse[47]	2014	Experimental and simulation data are compared to characterize the head acceleration caused by stick-head impacts.	It is used the Navy Research Lab (NRL) Simpleware Head Model.	- The peak acceleration at the center of gravity increased linearly with impact force and was generally in agreement with the experimental data. - Von Mises stresses and peak principal strains, two common literature injury indicators, were examined within the finite element model, and peak values were below the previously reported thresholds for mild traumatic brain injury.
Adam J. Bartsch, Edward C. Benzel, Vincent J. Miele, Douglas R. Morr, Vikas Prakash	Boxing and mixed martial arts: preliminary traumatic neuromechanical injury risk	2012	- Quantify preliminary linear and rotational head impact dosage for selected boxing and	An instrumented Hybrid III 50th percentile anthropomorphic test device (ATD) is hit in 54 pendulum impacts replicating hook punches at low and high energy.	All padding conditions reduced linear impact dosage. Other parameters significantly decreased, significantly increased, or were unaffected depending on padding condition.

	analyses from laboratory impact dosage data[48]		MMA padding in response to hook punches; - Compute theoretical skull, brain, and neck injury risk metrics; - Statistically compare the protective effect of various glove and head padding conditions.	5 padding combinations are examined: unpadded (control), MMA glove–unpadded head, boxing glove–unpadded head, unpadded pendulum–boxing headgear, and boxing glove–boxing headgear.	Of real-world conditions (MMA glove–bare head, boxing glove–bare head, and boxing glove–headgear), the boxing glove–headgear condition showed the most meaningful reduction in most of the parameters. In equivalent impacts, the MMA glove–bare head condition induced higher rotational dosage than the boxing glove–bare head condition. Finite element analysis indicated a risk of brain strain injury in spite of significant reduction of linear impact dosage.
Andrew Post, Marshall Kendall, Janie Cournoyer, Clara Karton, R. Anna Oeur, Lauren Dawson & T. Blaine Hoshizaki	Brain tissue analysis of impacts to American football helmets[49]	2018	Examine how impact site on the helmet and type of impact, affects the risk of concussive injury as quantified using finite element modelling of the human head and brain.	- 4 different models of American football helmet are evaluated using a published centre/non-centric impacting protocol. - 9 impact sites, each helmet is impacted 3 times each per impact at velocity of 6.5 m/s.	The results demonstrate that impacts that happen primarily to the side of the head resulted in higher magnitudes of strain in the grey and white matter, as well as the brain stem. Finally, commonly worn American football helmets are used in this research and significant risk of injury is incurred for all impacts: improvements in American football

					- The WSUBIM is used for the simulations.	helmets are necessary, in particular for impacts to the side of the helmet.
David C. Viano, Ira R. Casson, Elliot J. Pellman, Liying Zhang, Albert I. King, King H. Yang	Concussion in professional football: brain responses by finite element analysis[50]	2005		Compare brain responses with physician determined signs and symptoms of concussion to investigate tissue-level injury mechanisms.	It's used Wayne State University Head Injury Model. The cranium of the finite element model is loaded by translational and rotational accelerations measured in Hybrid III dummies from 28 laboratory reconstructions of NFL impacts including 22 concussions.	- Largest brain deformations happen after the primary head acceleration. - Midbrain strain correlated with memory and cognitive problems and removal from play after concussion. - Concussion injuries happen during the rapid displacement and rotation of the cranium, after peak head acceleration and momentum transfer in helmet impacts.
Andrew Posta, T. Blaine Hoshizakia, Clara Kartona, J. Michio Clarkc, Lauren Dawsona, Janie Cournoyera, Karen Taylora, R. Anna Oeura, Michael D. Gilchrista and Michael D. Cusimanob	The biomechanics of concussion for ice hockey head impact events[37]	2019		Conduct reconstructions of concussive and non-concussive impacts in ice hockey to determine the biomechanics and thresholds of concussive injury in ice hockey.	- The impacts are conducted on a helmeted Hybrid III headform, using either the linear impactor (shoulder impacts), high velocity impactor (elbows), pneumatic puck launcher (pucks),	- Magnitudes of 14g, 1.95 krad/s^2, and 3.5% $CSDM_{10\%}$ are found to have a 50% risk of injury for shoulder to head impacts. - Impacts in ice hockey are mostly of longer duration, typically longer than 15 ms, which results

				or monorail (ice, boards, and glass). - The linear and rotational acceleration time histories are recorded and applied to the University College Dublin Brain Trauma Model (UCDBTM) at the centre of gravity for the determination of the strain based measures (MPS and CSDM).	in a unique loading environment of the head and brain that is currently not being accounted for in ice hockey helmet standards and helmet design.

Table 2.8 – Papers regarding injuries in sport using FEM method found in literature

Authors	Title	Publication	Aim	Material and Methods	Results
D. Koncan, R.A. Oeur, M.D. Gilchrist, and T.B. Hoshizaki	Comparison of a 6-year-old child finite element model to a scaled adult model using simulated fall events for three levels of surface compliance[63]	2019	Test the sensitivity of the newly developed FE model of a 6-year-old child falls at three levels of surface compliance: - Compare trends of response; - Evaluate how material property definitions, model geometry and anatomical differences between models affect the peak strain response.	- Impacts on monorail drop rig. - Instrumented Hybrid III 6-year-old head are attached to a drop carriage, which are then elevated to the prescribed height and released on top of the anvils. - 2 F.E. model: the 6-year-old model was compared against the scaled version of the UCDBTM.	The 6-year-old model, compared to the scaled version of the UCDBTM, has: - Lower peak MPS for low impact durations and higher strains for moderate and long duration impacts (because of the highly accurate representation of the white matter that adds structural rigidity); - A continuous mesh connecting the brain to the CSF, while the scaled adult model uses a contact surface between the brain and CSF. →Higher risk of concussive injury even in well-padded conditions.
David Koncan, Michael Gilchrist, Michael Vassilyadi & Thomas B. Hoshizaki	Simulated brain strains resulting from falls differ between concussive events of young children and	2020	Evaluate if brain strains from FE simulations of falls resulting in concussion are different between children and	- 40 cases: 20 adults and 20 young children (ages 5-7). - Impacts on monorail drop rig.	Children between the ages of 5–7, compared to adults: - Tolerate concussive injuries at reasonably

47

	adults[11]		adults, using common biomechanical metrics of maximum principal strain, and cumulative strain damage measure (CSDM).	- For child cases: Hybrid III 6-year-old head. For adults, female cases: Hybrid III 5th percentile female; male cases: Hybrid III 50th percentile male. Head forms are instrumented with nine single-axis accelerometers. - MADYMO: used to estimate the head velocity on impact for each impact location (back, side, front). - 2 FE model: a 6-year-old child model, or the University College Dublin Brain Trauma Model (UCDBTM) for child and adult cases respectively.	lower strains (MPS, CSDM); - Tolerate concussive injuries from falls at lower impact velocities, due to their lower stature.
F.J. Burgos-Flórez, Diego Alexander Garzón-Alvarado	Stress and strain propagation on infant skull from impact loads during falls: a finite element analysis[35]	2020	Simulate neonates skull trauma after low height falls when variable degrees of ossification of the junctions are present.	- FE model of a fourweek-old infant skull. - Assembly made up of bones, sutures, brain, CSF. - It's simulated low height impact from 30 cm and 50 cm falls. - 2 impacts are simulated: an occipito-parietal impact on the lambdoid suture and a lateral impact on the right parietal. - 6 cases considered: unossified and fully ossified sutures, and sagittal,	- Fully ossified skulls: lower deformation and lower Von Mises stress in the brain. - Skulls with unossified sutures and fontanels: increase in strain magnitude. - In occipital impacts: higher deformations and lower Von Mises stress. →Neonate skull impact when falling backward has a higher

				met_ic, right lambdoid and right coronal craniosynostosis.	probability of resulting in permanent damage.
David Koncan, Michael Gilchrist, Michael Vassilyadi and Thomas Blaine Hoshizaki	A three-dimensional finite element model of a 6-year-old child for simulating brain response from physical reconstructions of head impacts[30]	2018	Ideate a new FE model of a 6-year-old child for use in sporting impact research of young children	- 2 FE model: a 6-year-old child model and the scaled UCDBTM. - 3 impacts are used to validate the 6-year-old (average and stiff) model: impacts C064T1 and C064T4, which are occipital impacts aligned with the COG, as well as C241T3, an offset occipital impact.	Average and stiff model: - Have good agreement with experimental intracranial pressure: in both magnitude and phase among the average model, stiff model, and the experimental data for the initial pressure pulse. - Show similar motion and peak excursions to the scaled UCDBTM. - Have the lowest MPS for impacts C064T1 and C064T4, while the scaled UCDBTM has the lowest strains for impact C241T3.
Andrew Post, T. Blaine Hoshizaki, Michael D. Gilchrist, David Koncan, Lauren Dawson, Wesley Chen, Andrée-	A comparison in a youth population between those with and without a history of concussion using biomechanical reconstruction[64]	2017	Compare the biomechanics of impact between a group of youths who had incurred a previous concussion to a group that had no previous history.	- 2 groups: a "history" group that contained those with a previous history of at least 1 previous diagnosed concussion and a "no history" group containing patients with no previously diagnosed	There is no biomechanical variable that could distinguish between the concussion groups with a history of concussion versus no history of concussion.

Anne Ledoux, Roger Zemek and the Pediatric Emergency Research Canada (PERC) 5P Concussion Team				concussions. - Monorail drop rig system - Hybrid III headform equipped with 9 accelerometers. - MADYMOS is used to simulate falls and pedestrian accident. - Finite element model: UCDBTM. - The outputs of the events are measured in force, energy, peak resultant linear and rotational acceleration, maximum principal strain of the gray and white matter, and CSDM.	
Sebastien Roth, Jonathan Vappoua, Jean-Sebastien Raula, Rémy Willinger	Child head injury criteria investigation through numerical simulation of real-world trauma[34]	2009	Propose a 3-year-old child FE model of the head in order to provide a better understanding of child head injury mechanisms using numerical simulation of real accidents.	- Medical files: 25 real accidents are reconstructed. - FE model with consideration of anatomical and morphological specificities, based on CT scanner slices. - Simulations are performed for different brain constitutive relationships: two linear viscoelastic laws.	Mechanical output parameters (HIC, pressure, shearing stress) are calculated from these simulations and Von Mises stress appears to be clearly the most predictive parameters, allowing clear distinction between injured and non-injured cases, with

					a limit of 48 kPa for moderate neurological injuries appearance.
R. Anna Oeur, Michael D. Gilchrist & T. Blaine Hoshizaki	Interaction of impact parameters for simulated falls in sport using three different sized Hybrid III headforms[31]	2018	Clarify the interactions between mechanical impact parameters and the patterns of acceleration and strain response	- Monorail drop tower. - Different sized Hybrid III headforms are used in the tests: a 6-year-old child, a 5th percentile female, and a 50th percentile adult male. - Four impact velocities: 1.5, 3.0, 4.5, and 6.0 m/s are Selected; three surfaces: unprotected, helmeted, and well-padded/mat; four impact locations: frontal, sagittal, combined-plane motions, and a rotationally dominant motion. - 9 linear accelerometers. - FE model: scaled UCDBTM.	- Compliance produces the greatest increases in head acceleration. - Impact velocity produces the greatest increases in strain. - Smaller headforms are associated with higher responses. - Non-uniform trends for impact location are noted. → There is the need for size-appropriate parameters in the design and development of head protection.

Table 2.9 - *Paper regarding injuries in children using FEM method found in literature*

3. Material and methods

When it has been decided to approach a problem through the use of finite element modelling, it is necessary to consider three essential steps that allow to obtain the final solution:

1. Pre-processing: includes all actions of collection of input signals to be prescribed, geometry importation, model realization that precede the simulation;
2. Solving: properly performed by the LS-DYNA software. The computational resources were provided by HPC@POLITO and used to run the simulation;
3. Post-processing: provides the visualization and analysis of the results obtained by simulation.

3.1 Pre – processing

During pre – processing, by LS-PrePost, a software freely released by LSCT, the model is acquired and the boundary conditions to be applied are chosen, in order to model as best as possible, the phenomenon to describe.

3.1.1 Experimental dataset

Six degree-of-freedom kinematic data, specifically linear accelerations along the x, y, z axis and angular velocities around the x, y, z axis, from a previous laboratory study of Judo impacts were used for this study.[65,66]

Briefly, four techniques, (o-soto-gari, o-uchi-gari, ippon-seoi-nage and tai-otoshi), have been tested on a sample of 40 subjects and each technique has been performed 3 times. The subjects have been divided into agonists and no-agonists on the basis of age (12 years is the threshold between the categories) and supplementary divided on the basis of experience in Judo practice (3 years is the threshold between the children categories, 10 years is the threshold between the children categories). Two inertial measurements unit (IMU) Yost Labs mounted on the middle forehead and on the centre of the sternum was used for all tests.

During the execution of all techniques, the thrower (tori), who projects the faller, is the best of the category (in this case, no-agonist and no-experienced athletes).

Both sensors cited were positioned while uke was in the anatomical reference position. The axes of the sensor on the head, the only one considered in this work of thesis, as specified in chapter 3.2.1, were oriented as shown in figure 3.1:
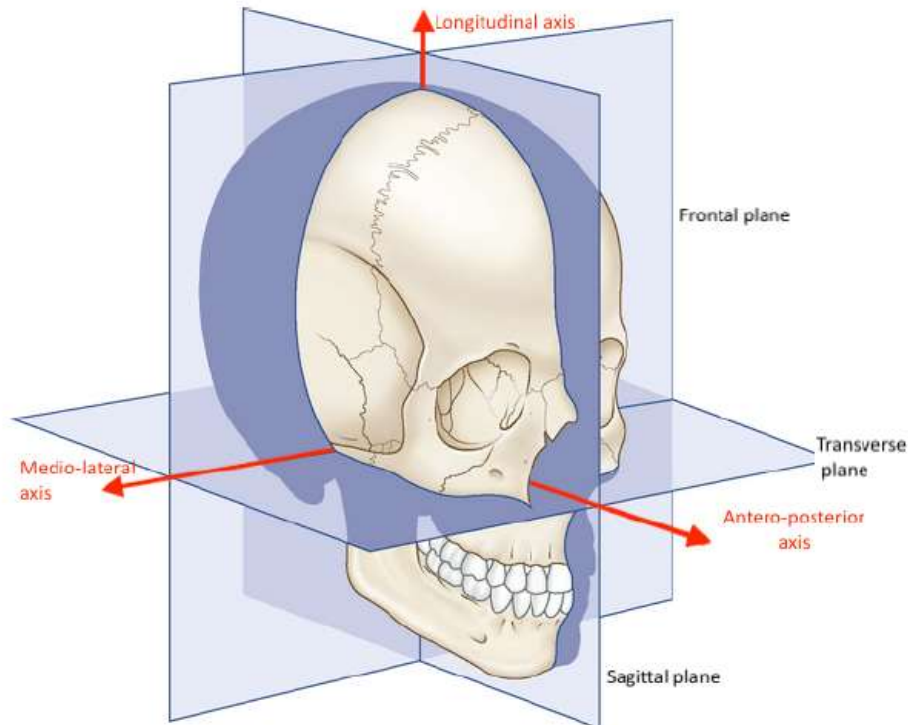
Figure 3.1 - Axis considered in the test

- X axis: along the longitudinal direction (upward positive);
- Y axis: along the medio-lateral direction (right positive);
- Z along: the antero-posterior direction (forward positive).

The data of no-agonist and no-experienced athletes, therefore children younger than 12 years and with less than 3 years of experience, have been made available. Among them, two children aged 6 years were considered, which can be appropriately modelled with the PIPER model, presented in the chapter 3.2.1.

The data of two children, reported in table 3.1, have been used for the current study: for the first child, the data gained from all 4 techniques have been considered; for the second child, the data gained from the first technique (o-soto-gari) have been considered, because of its higher possibility of reaching dangerous levels.[2]

	Height (m)	Weight (kg)	Age at test time (years)	Experience (years)	Belt
First child	1,2	21	6	1	Yellow
Second child	1,15	20	6	2	Yellow

Table 3.1 - Data of two children

All acquired signals last just over 1 second and centred in the peak of head linear acceleration magnitude[66]. Linear accelerations acquired from sensor, before being introduced as input of the model, were post-processed using MATLAB. A low pass filter was used: the cut-off frequency has been set approximately to 45 – 50 Hz. Angular velocity, on the other hand, not need to be filtered.

The trends of the three linear accelerations and the three angular velocity have been reported; in particular, for each technique and for each child, the curves were overlapped, as shown in figures 3.2, 3.3, 3.4, 3.5 and 3.6.
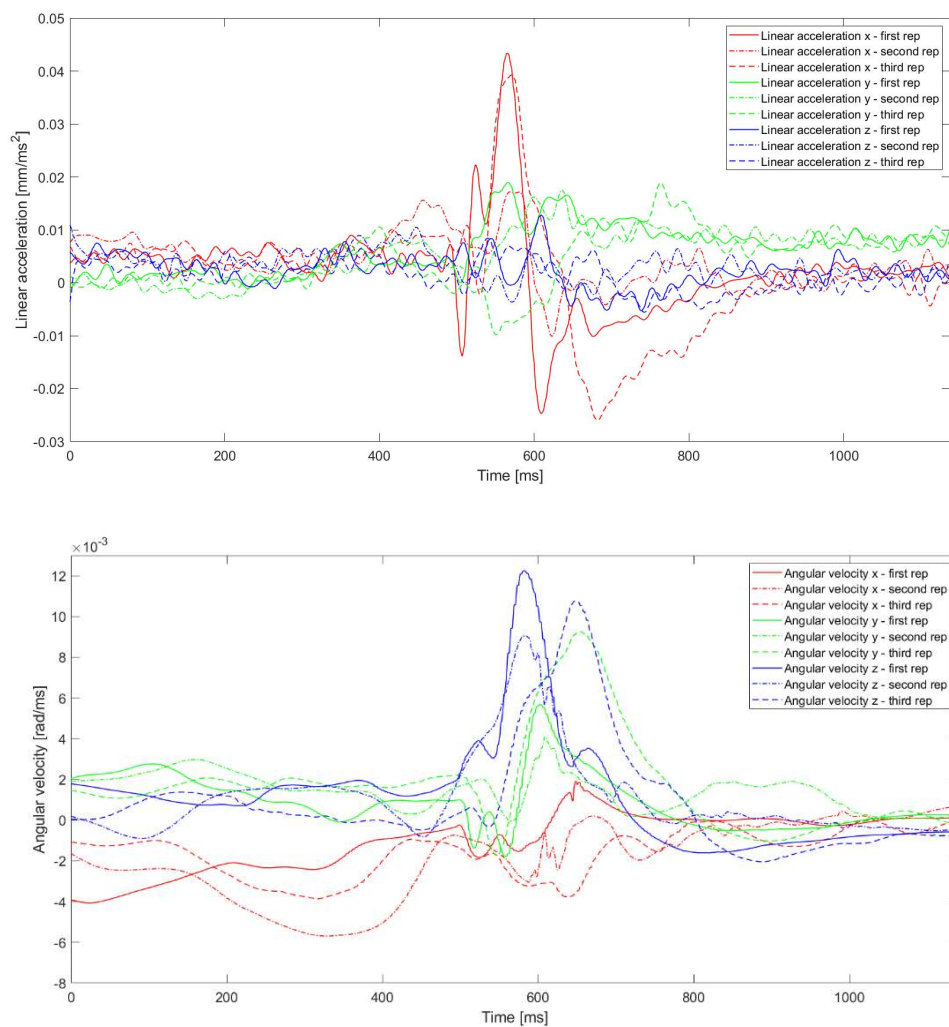
Figure 3.2 - *Linear acceleration and angular velocity obtained by o-soto-gari technique for first child*
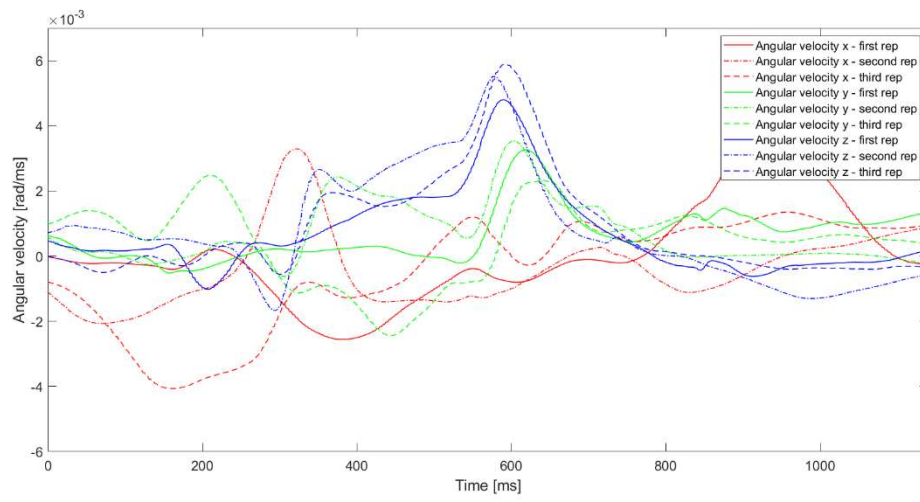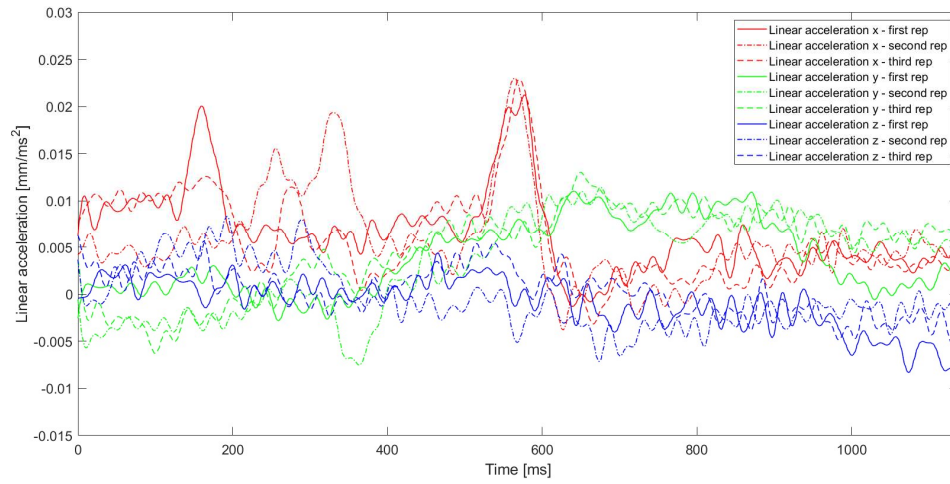
Figure 3.3 - *Linear acceleration and angular velocity obtained by o-uchi-gari technique for first child*
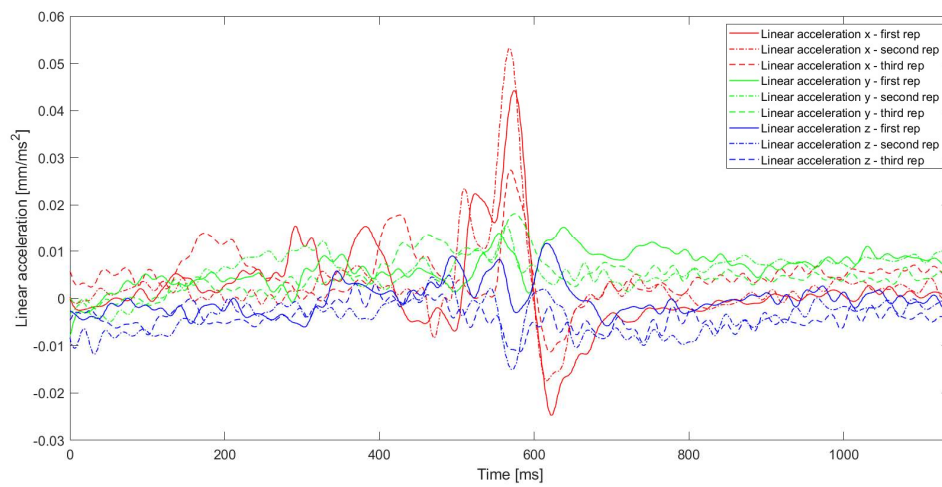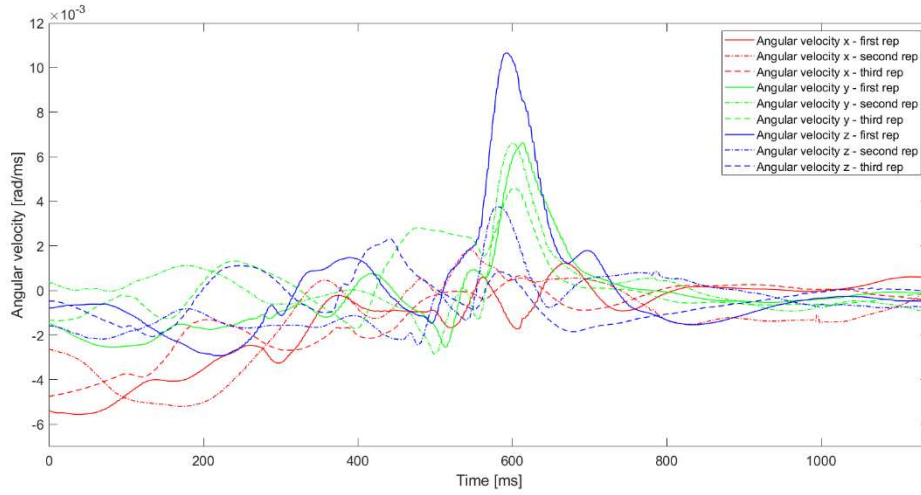
Figure 3.4 - *Linear acceleration and angular velocity obtained by ippon-seoi-nage technique for first child*
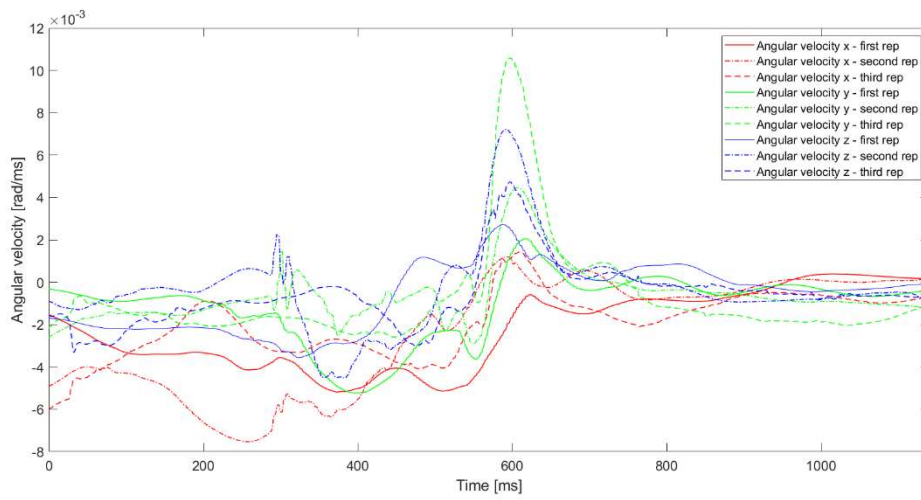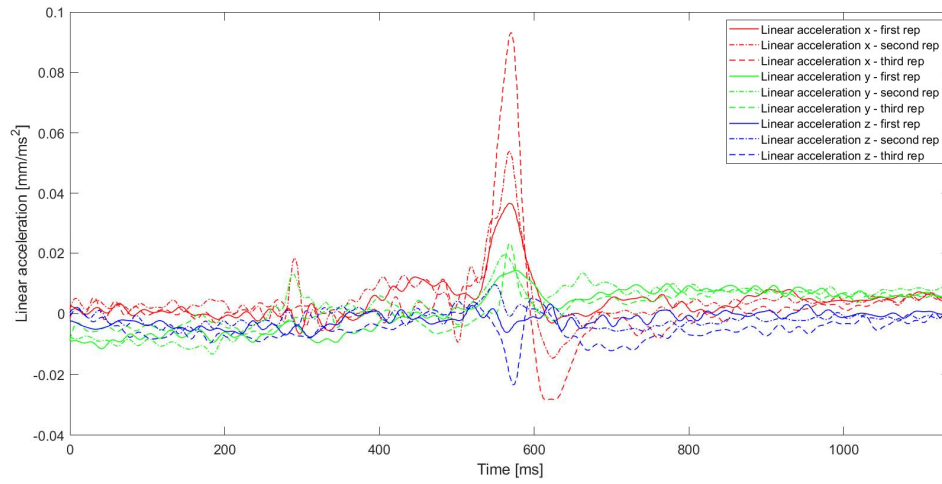
Figure 3.5 - *Linear acceleration and angular velocity obtained by tai-otoshi technique for first child*
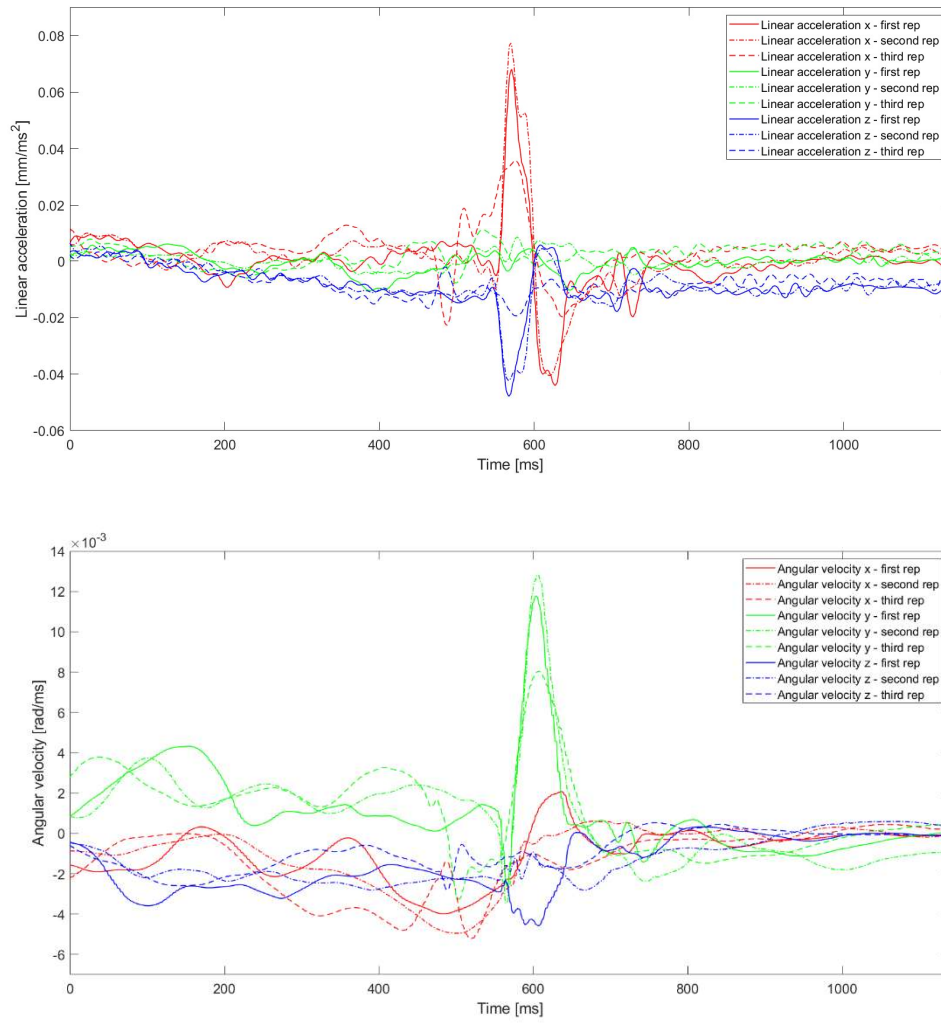
Figure 3.6 *- Linear acceleration and angular velocity obtained by o-soto-gari technique for second child*

All three repetitions of the same technique have the same duration and the same number of samples. Then, the average and the standard deviation of the three repetitions for each kinematics parameter for each technique have been calculated. The results are reported in the paragraph 4.1.

3.1.2 PIPER Head Model

The PIPER child model is very complex and consists of a great number of parts: in order to make the input file easy to manage, since the input data deck is very large. The model is split into subfiles and each subfile can again be split into sub – subfiles, called include files (figure 3.7). Each of them describes a portion of the body comprehending the description of the parts, material, contacts, constrained etc.

```
*INCLUDE
$#
main_Control.k
$
*INCLUDE
$#
main_Interfaces.k
$
*INCLUDE
$#
main_FleshSkin.k
$
*INCLUDE
$#
main_Neck.k
$
*INCLUDE
$#
NeckMuscles.k
$
*INCLUDE
$#
main_Head_Brain.k
$
*INCLUDE
$#
main_Head_Skull.k
$
*INCLUDE
$#
main_FleshSkin_HeadNeck.k
$
*INCLUDE
$#
main_Flesh_HeadNeck_InterfaceNodes.k
$
*INCLUDE
$#
main_LEx.k
$
*INCLUDE
$#
main_Trunk_UpperEx.k
$
*INCLUDE
$#
mesh_PIPER_Body.k
$
*INCLUDE
$#
main_Sensors.k
```

Figure 3.7 - *PIPER Model structure*

Based on the literature articles studied concerning sports impacts[33,37,42,45,47,48,50], it was established to cut the model at height of head, so that only files including the skull, the cerebrum, the cerebellum and the cerebrospinal fluid would be used for simulations, as shown in figure 3.8, 3.9 and 3.10. In the chapter 2.3.2, all the components of the brain and the properties of the various materials that make it up have been listed and accurately described.

```
*INCLUDE
$#
main_FleshSkin.k
$
*INCLUDE
$#
main_Head_Brain.k
$
*INCLUDE
$#
main_Head_Skull.k
$
*INCLUDE
$#
main_FleshSkin_HeadNeck.k
$
*INCLUDE
$#
main_Flesh_HeadNeck_InterfaceNodes.k
```

Figure 3.8 - *Head PIPER Model structure*
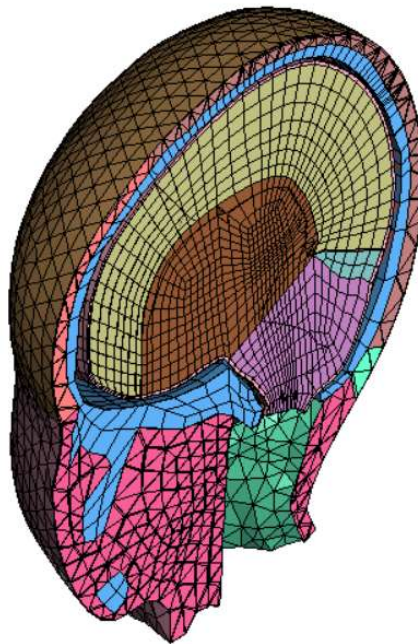
Figure 3.9 - *Isometric view of head PIPER Model*
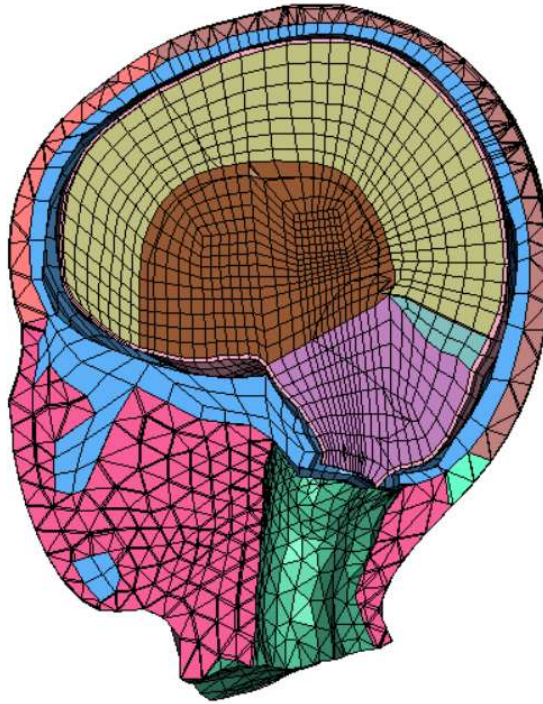
Figure 3.10 - *Right view of head PIPER Model*

Additionally, it is significant to specify consistent system of units, required for LS-DYNA. Subsequently, all quantities must be expressed according to the system of these units. In the Piper model the system used is:

- Mass [kg];
- Length [mm];
- Time [ms].

So, the other physical quantities will have these units:

- Force [kN];
- Stress [GPa];
- Density [kg/mm^3].

3.1.3 Simplified model

In order to be able to try different configurations faster and more efficiently and to understand how the Piper model works at the same time, the first step was to investigate and analyse some simplified geometries, setting the same parameters (like MAT, SECTION and PART) of the Piper model.

At the beginning the simplified model was made up only of a solid sphere (represented in blue in figure 3.11), which represented the skull, and then it was gradually complicated to represent in detail the head model: in fact, another solid sphere (represented in pink in figure 3.11), which represents the scalp and a spherical shell (represented in yellow in figure 3.11) which represents the skin were added.

To sum up, the complete assembly is composed of 3 parts, that have been represented in figure 3.11:
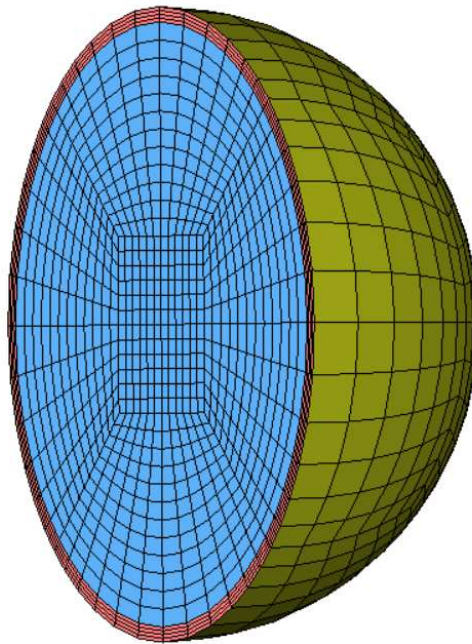
Figure 3.11 - Simplified Model
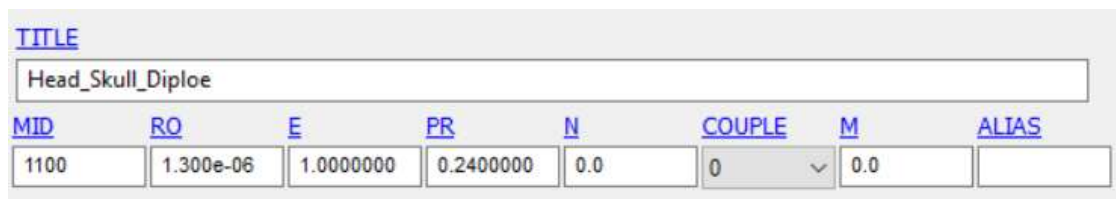
Different tests were performed: the motion was applied in different ways both on the part that represents the skull and on the part that represents the skin. Once certified that there were no problems of interpenetration between the parts, then the real child model was approached.

3.1.4 Final set up

To evaluate the best approach in the application of the field of acceleration and velocity, three configurations have been tested.

The motion was prescribed before on only a few nodes on the median part of the skull and then on all the nodes of the skull. In both cases, the trend of the kinematic quantities in some nodes of the skull was visualized. These trends have oscillations of a certain amplitude (numerical noise), so they cannot be considered appropriate. Moreover, with these two approaches, the order of magnitude obtained for Von Mises stress reach values much greater than those found in the literature and mentioned in the chapter 2.3.1.

Another approach was preferred to these two, which allows to simulate the reality in a consistent way. The skull can be considered as a rigid body. Therefore, the boundary conditions (field of acceleration and velocity) were applied to the skull made rigid. To make the skull rigid, it was enough to change the material of the skull and transform it into *MAT_020_RIGID*:

Figure 3.12 - *Definition of the keyword *MAT_020_RIGID**

An additional explanation should be made. The three configurations mentioned above were carried out both on the head model, presented in chapter 3.1.2, and on a model that included, beyond the head, also the neck. In both cases, the output quantities to be evaluated, widely discussed in chapter 4.2, presented almost equivalent results. This is the reason why the model consisting only of the elements of the head was chosen.

Since this material has been made rigid, the motion is given thanks to *BOUNDARY_PRESCRIBED_MOTION_RIGID_LOCAL.* Through this card, it was possible to prescribe the linear accelerations along x, y, z and the angular velocities around x, y, z, previously collected, on the head model, according to local accelerometer reference system modelled on the skull, as shown in figure 3.13.
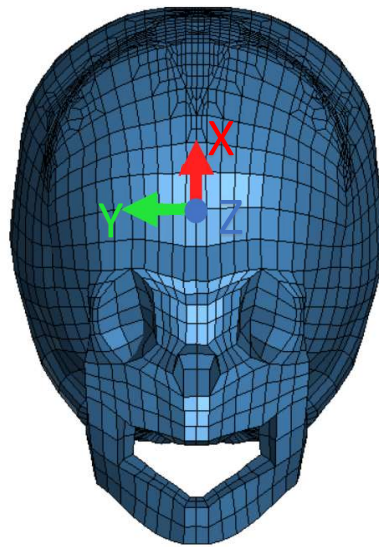
Figure 3.13 - *Reference system on skull*

In particular, the local coordinate system has been defined with three nodes of the skull. The first node has been defined in accordance with the fact that the sensor has been applied to the center of the forehead of the uke. The other two nodes have been defined so that the reference system adopted in the numerical simulation corresponds to experimental test. Indeed, the other two nodes have been chosen in order to belong to the skull and to be able to model the fact that the x-axis and the y-axis of the sensor follow the shape of the head.

3.2 Post Processing

Due to the high three-dimensionality of the techniques tested in this work of thesis and the limitations of the use of kinematic criteria[67], it has been decided to use one of the predictors of head injuries that are based on stress and deformation.

The output parameter used as a criterion for evaluating brain lesions is the Von Mises stress, which is among the most indicated in the literature[34], through the HyperView software.

The input signals used to drive the simulation last approximately a second, therefore indicate only the maximum values reached has not seemed an exhaustive approach.

Therefore, the evaluation was carried out in space to highlight the most stressed portions of the brain and in time to correlate these stresses with the linear acceleration and angular velocity to which the subject's head was exposed.

The desired outputs have to be requested in the pre-processing phase.

Therefore, the d3plot card is imposed every ms, in order to appreciate the evolution of the system over time according to the kinematic conditions imposed. The d3plot has been set to this value and not to a higher one in order to be able to choose, in retrospect, which temporal moments are more significant.

In addition, it is also possible to display contour maps, that provide a distribution of colors according to the quantity of interest. In order to visualize the most stressed elements of the brain in all its volume, it has been chosen to mask the elements under a limit value, chosen according to the simulation considered, as shown in figure 3.14:
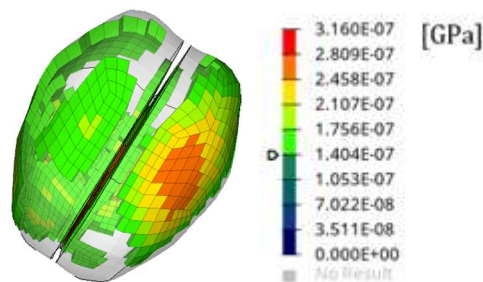
Figure 3.14 – Von Mises stress with Iso value = 140.4 Pa

4. Results

4.1 Variability of kinematic quantities between subjects, techniques and repetitions

The mean and the standard deviation of the linear accelerations along the 3 directions are represented on the same graph and the same approach is used for the angular velocities, as shown in figures 4.1, 4.2, 4.3, 4.4 and 4.5.
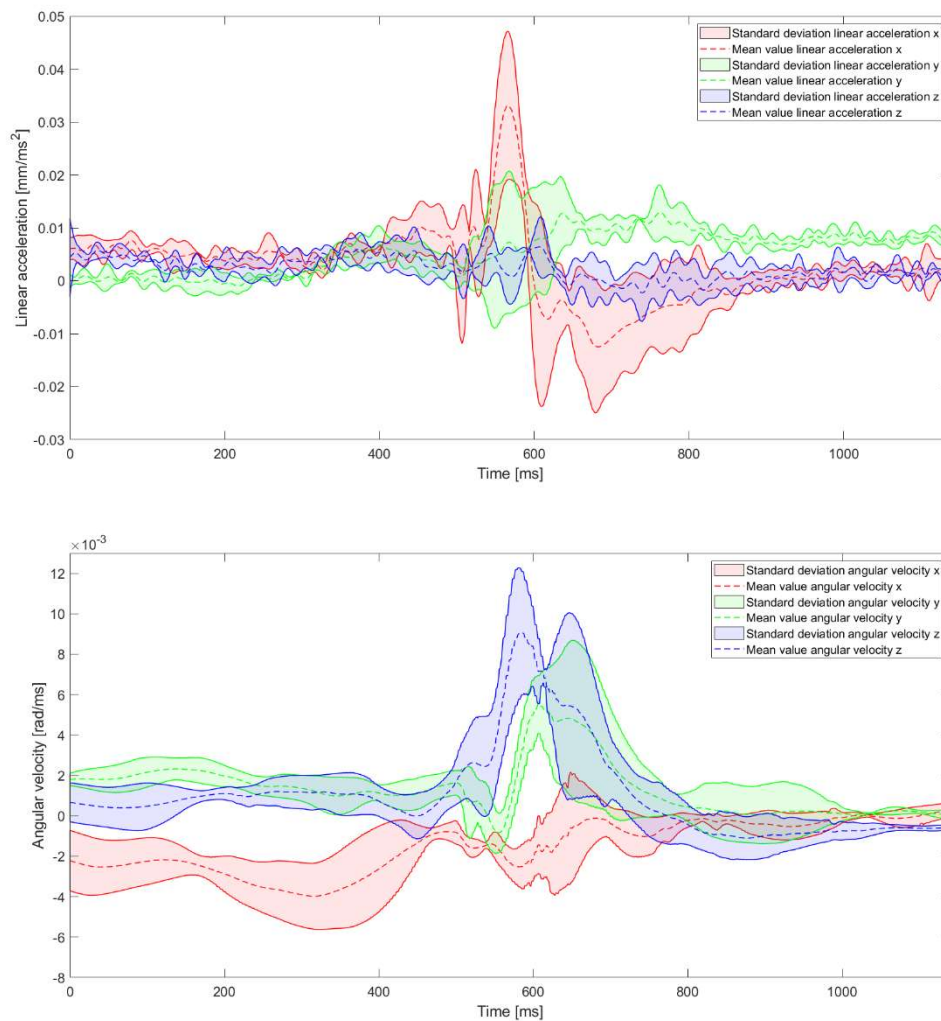
Figure 4.1 - Mean value and standard deviation of linear acceleration and angular velocity obtained by o-soto-gari technique for first child
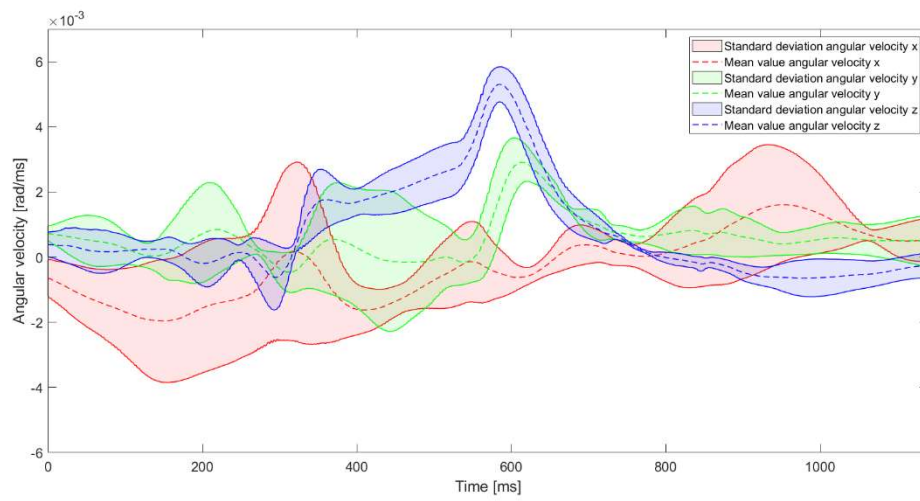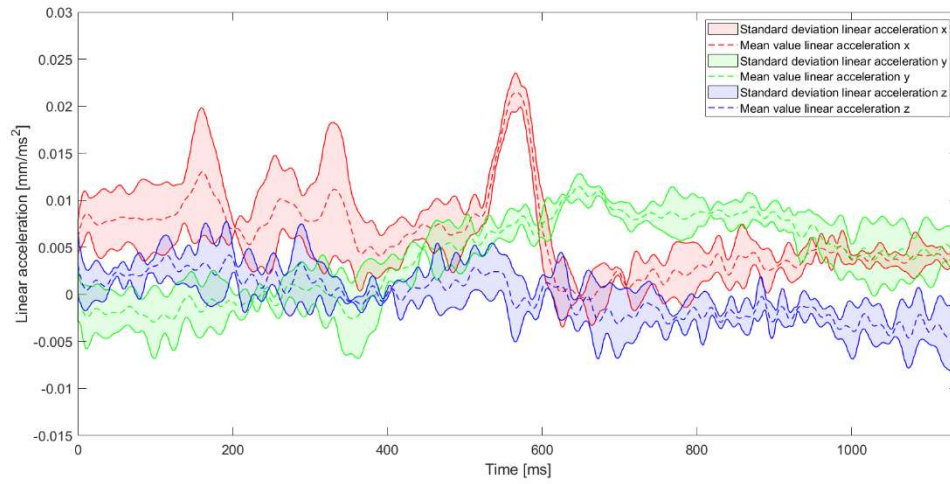
Figure 4.2 - Mean value and standard deviation of linear acceleration and angular velocity obtained by o-uchi-gari technique for first child
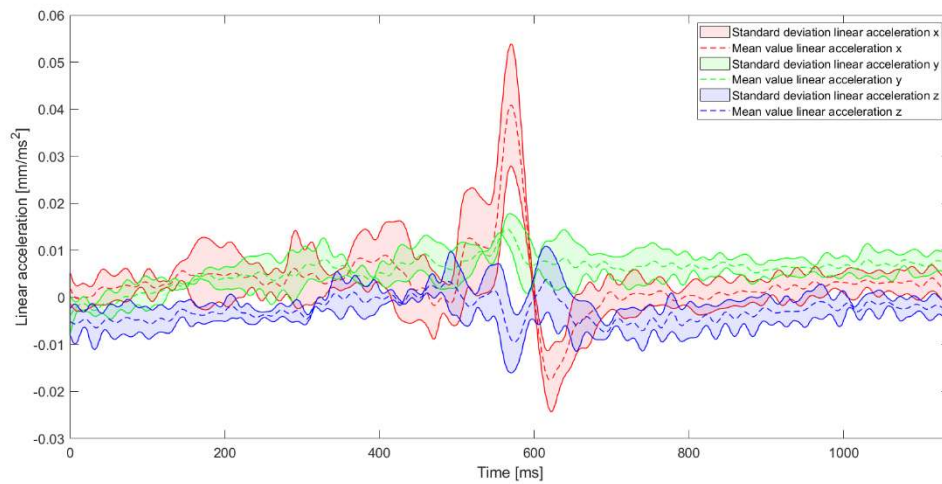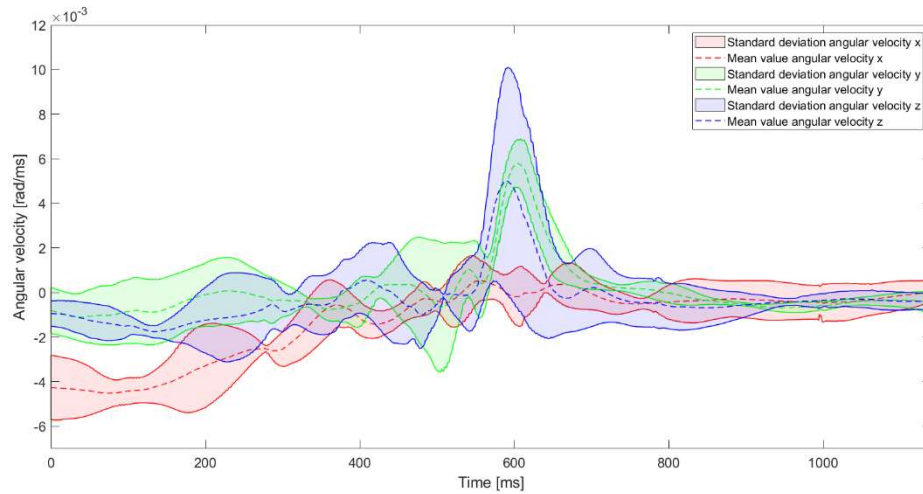
Figure 4.3 - Mean value and standard deviation of linear acceleration and angular velocity obtained by ippon-seoi-nage technique for first child
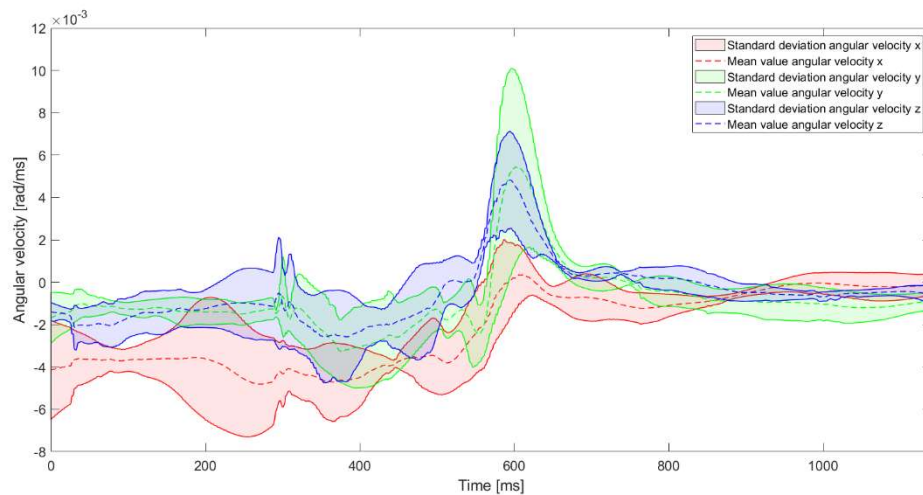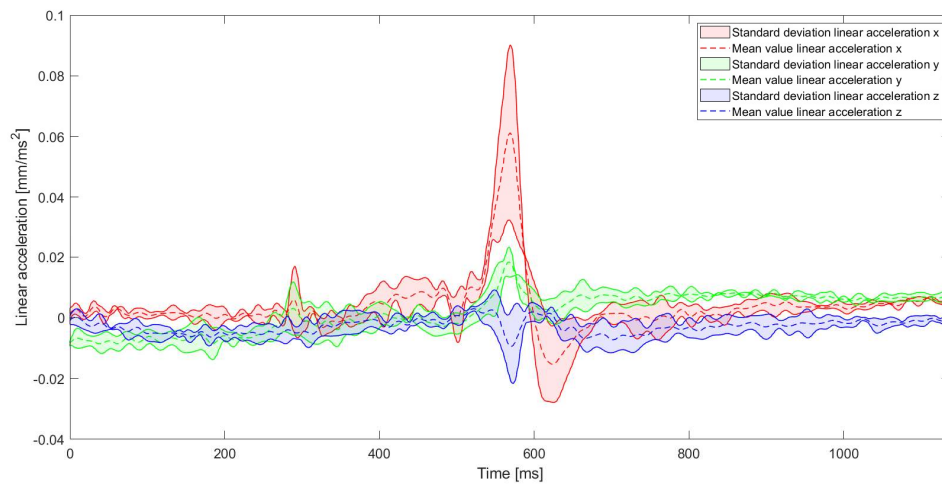
Figure 4.4 - Mean value and standard deviation of linear acceleration and angular velocity obtained by tai-otoshi technique for first child
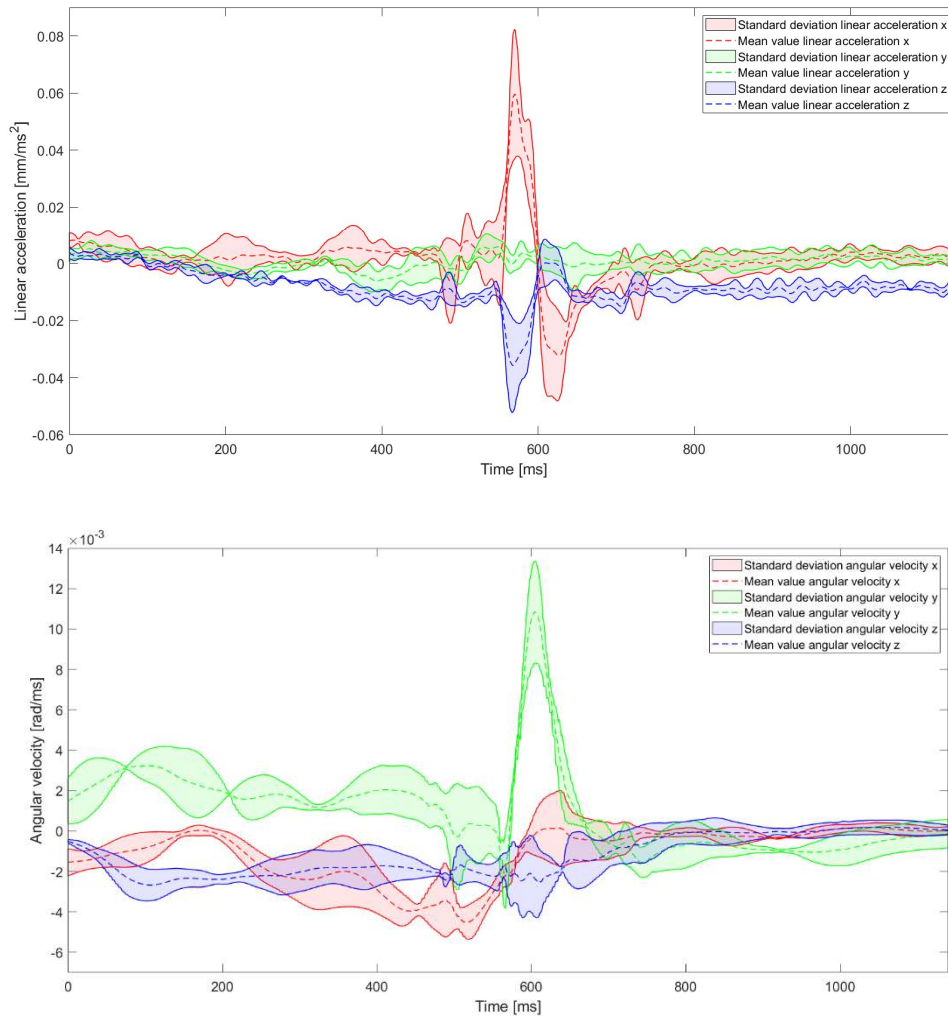
Figure 4.5 - Mean value and standard deviation of linear acceleration and angular velocity obtained by o-soto-gari technique for second child

Observing the illustrated trends, the standard deviation underlines a certain variability in the repetitions of the same technique. In particular, at the time when the kinematic quantities reach the highest values the standard deviation is considerable, as is evident in o-soto-gari, ippon-seoi-nage and tai-otoshi techniques (figures 4.1, 4.3, 4.4 and 4.5). It may seem necessary to consider this aspect, since the acceleration and velocity peaks seem to be located at the time window in which the highest concentrations of Von Mises are reached. On the other hand, the technique that has a smaller standard deviation, and therefore a smaller dispersion, is the o-uchi-gari (figure 4.2).

Not only the standard deviation, but also the mean can be an indicative parameter. Paying attention to the same technique practiced by two different children (figure 4.1 and 4.2): for the second child, the maximum mean value of the linear acceleration along x (which can be

considered as the predominant kinematic acceleration parameter) assumes a value that is approximately twice as much than the first child.

In addition, the predominant angular velocity for the first child is around the z axis, for the second child around the y axis.

This variability, in terms of shape and magnitude, can be attributed to the inexperience of the child in practicing the technique and to the greater attention in planning the movement to be performed to fall correctly avoiding trauma.

4.2 Von Mises evolution in time and space

4.2.1 O-soto-gari technique performed by two children

At first, two different children were considered performing the same technique, o-soto-gari, three times (see Appendix A, for a detailed analysis about o-soto-gari performed by first child).

For both children, the mean value $\pm$ standard deviation trend of the signals has been reported between 400 and 800 ms. For all repetitions, the highest stress values are located temporally in the time window, represented in yellow in the figures 4.6 and 4.7, at which the kinematic parameters have reached their peaks. The main Von Mises stresses, obtained in the study of first child (figure 4.6), are reached in the following time intervals: 549 ms - 599 ms (equal to 50 ms, indicated in magenta, referring to the first repetition), 574 ms - 652 ms (equal to 78 ms, indicated in orange, referring to the second repetition), 553 ms - 592 ms (equal to 39 ms, indicated in green, referring to the third repetition). The first and third repetition have a similar duration and are overlapping, while the second repetition has a longer duration and the Von Mises peak is reached later than the other two repetitions.
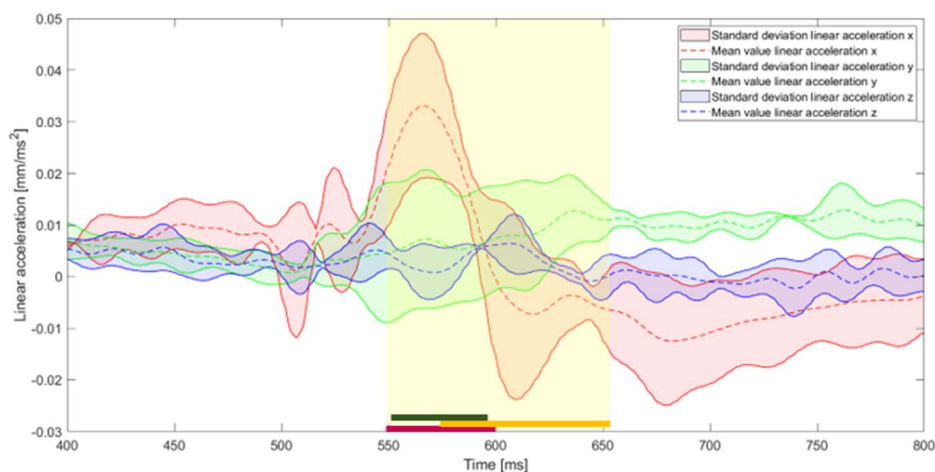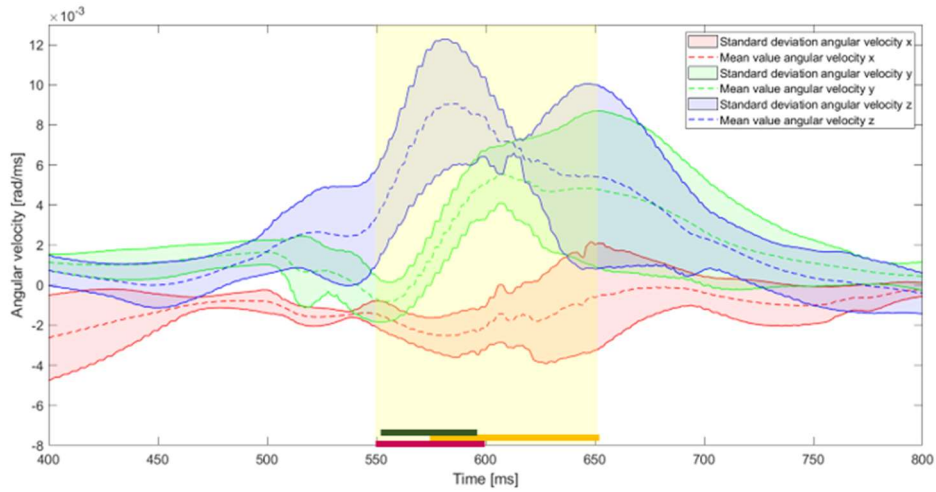
Figure 4.6 - *Time interval at which higher brain Von Mises stress values are reached during o-soto-gari technique for first child*

For the second child, the time interval at Von Mises Stress reaches higher values are between 573 ms – 601 ms (T=23ms), 571 ms – 606 ms (T=35 ms), 490 – 521 (T=31 ms) respectively for the first, second and third repetition executed by the second child. In this case, the duration of the intervals is approximately the same. The first and second repetition time interval are overlapping, while the second repetition time interval is reached before than the other two repetitions.
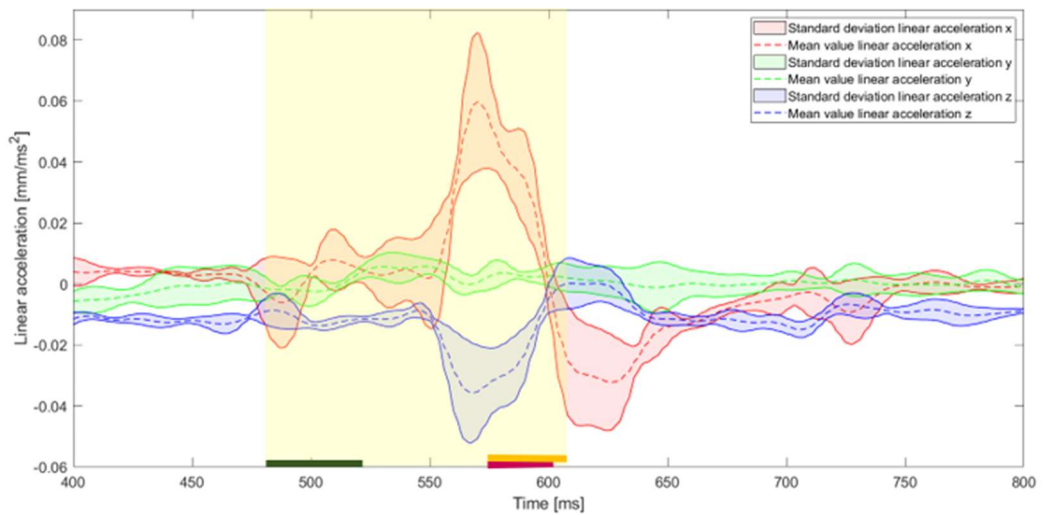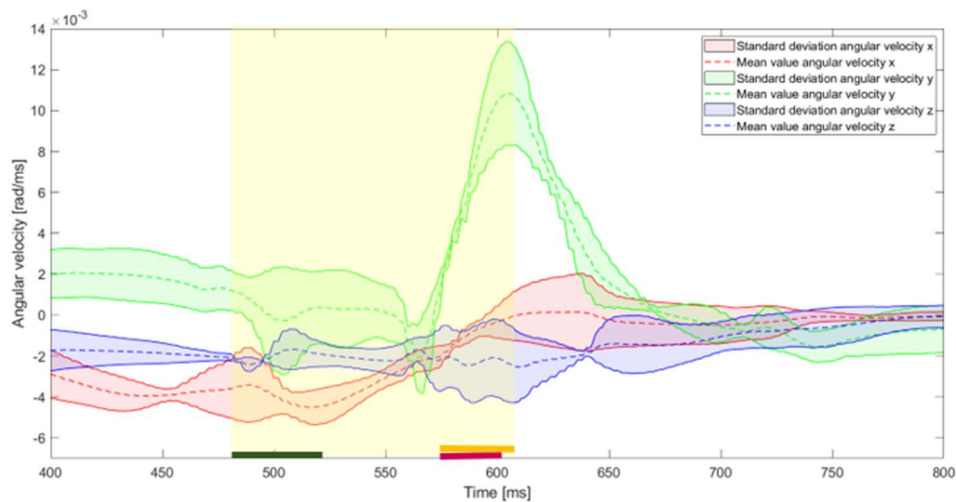
Figure 4.7 - *Time interval at which higher brain Von Mises stress values are reached during o-soto-gari technique for second child*

The motion conditions have an effect on the distribution of stress throughout the brain tissue. In order to visualize the areas of the brain most stressed in all its volume, the elements of the brain in which Von Mises Stress takes on values within a given range between two limit values were represented. The upper limit is the maximum value of Von Mises Stress reached for the repetition considered and the lower limit is a threshold value defined in order to mask the elements in which the stress of Von Mises Stress reaches lower values.

Considering respectively the first, second and third repetition executed by first child, table 4.1, 4.2 and 4.3 show Von Mises stress at the time in which the Von Mises peak was reached. Then, starting from this time, the trend of stress was also displayed while moving back and forth through time in a neighbourhood which was firstly fixed at a time step of 1ms, and then was increased to 3ms; respectively for the first, second and third repetition executed by first child.

It is shown a considerable volume, lower for the second repetition, where the Von Mises Stress values are ranging between 342.2 Pa – 770 Pa, 200 Pa – 450.8 Pa, 220.9 Pa – 497 Pa respectively for the first, second and third repetition executed by the first child.
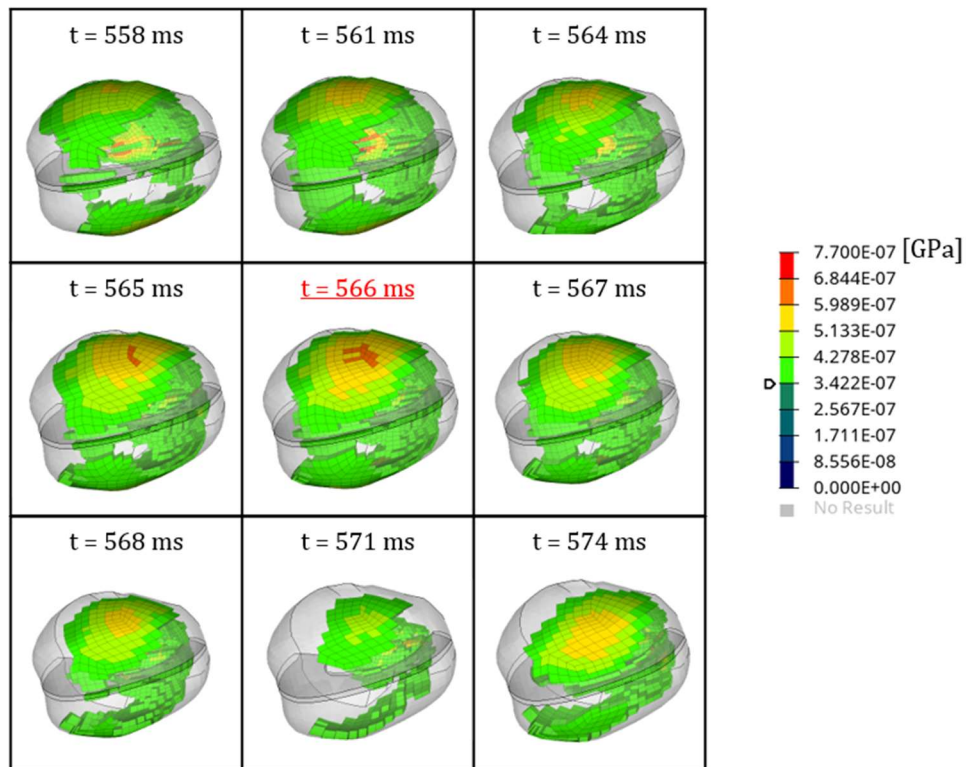
Table 4.1 - *Von Mises stress evolution with dt=1 ms and dt=3 ms (o-soto-gari, first repetition, first child)*
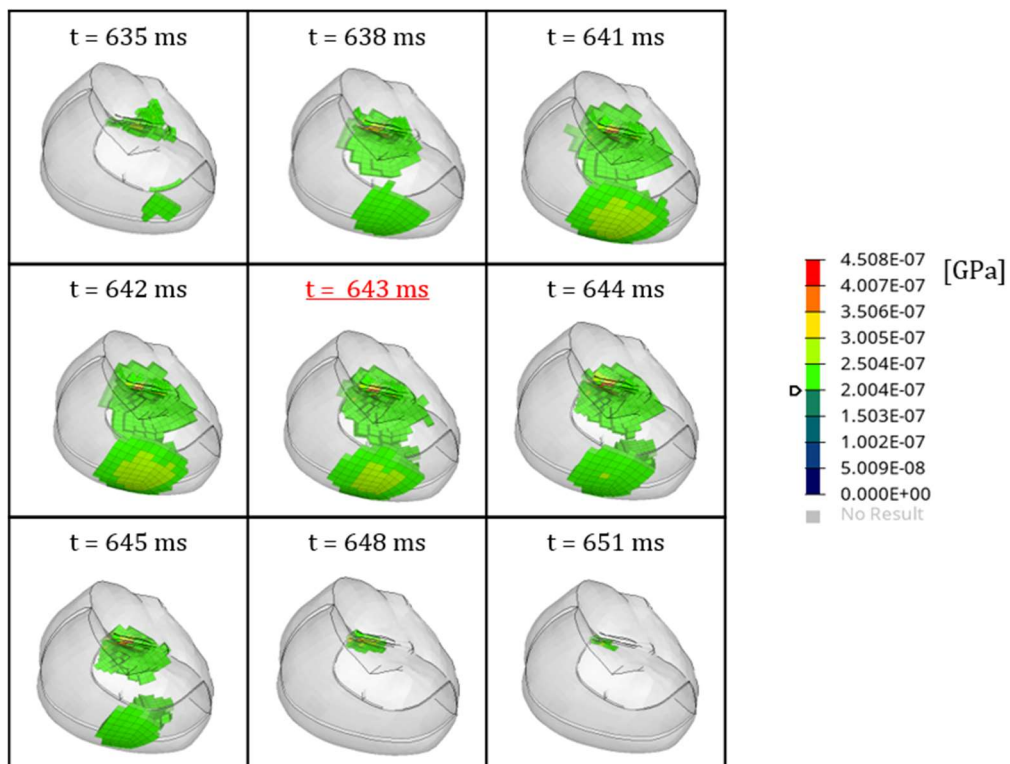
Table 4.2 - *Von Mises stress evolution with dt=1 ms and dt=3 ms (o-soto-gari, second repetition, first child)*
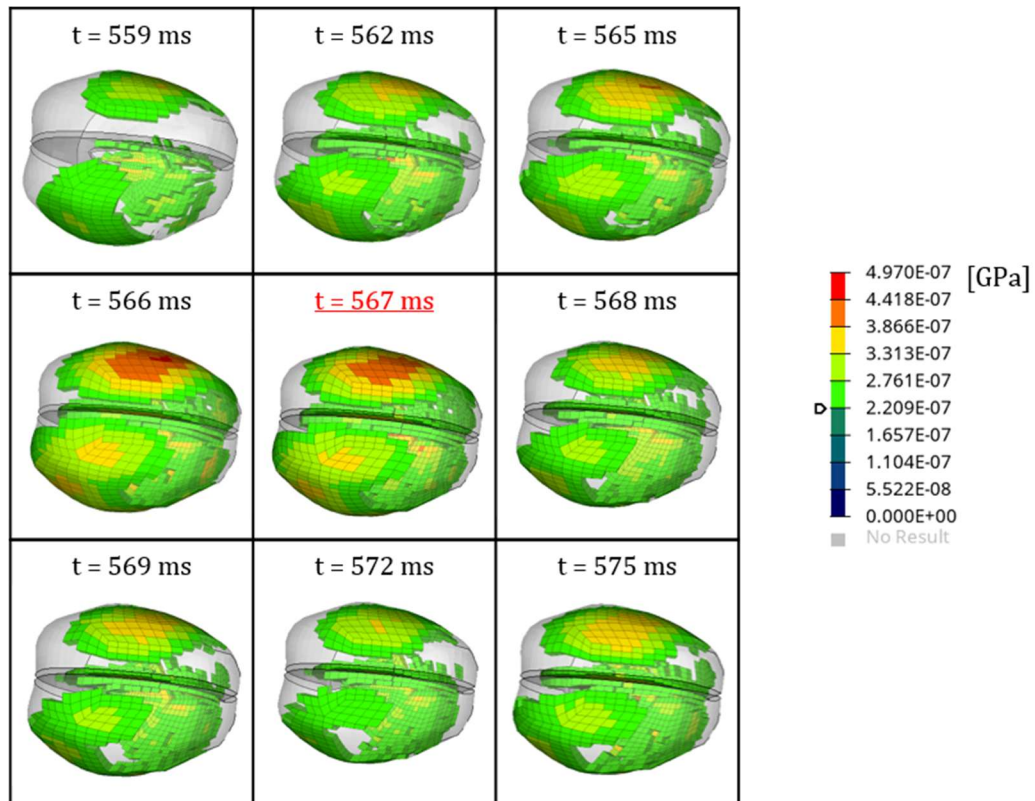
Table 4.3 - *Von Mises stress evolution with dt=1 ms and dt=3 ms (o-soto-gari, third repetition, first child)*

The same approach was followed for the second child. Tables 4.4, 4.5 and 4.6. show volume, where the Von Mises Stress values are ranging between 523.8 Pa – 1.178 kPa, 519.4 Pa – 1.169 kPa , 330.7 Pa – 744 Pa respectively to the first, second and third repetition.

t = 574 ms	t = 577 ms	t = 580 ms
t = 581 ms	t = 582 ms	t = 583 ms
t = 584 ms	t = 587 ms	t = 590 ms

	[GPa]
1.178E-06	
1.048E-06	
9.166E-07	
7.856E-07	
6.547E-07	
5.238E-07	
3.928E-07	
2.619E-07	
1.309E-07	
0.000E+00	
No Result	
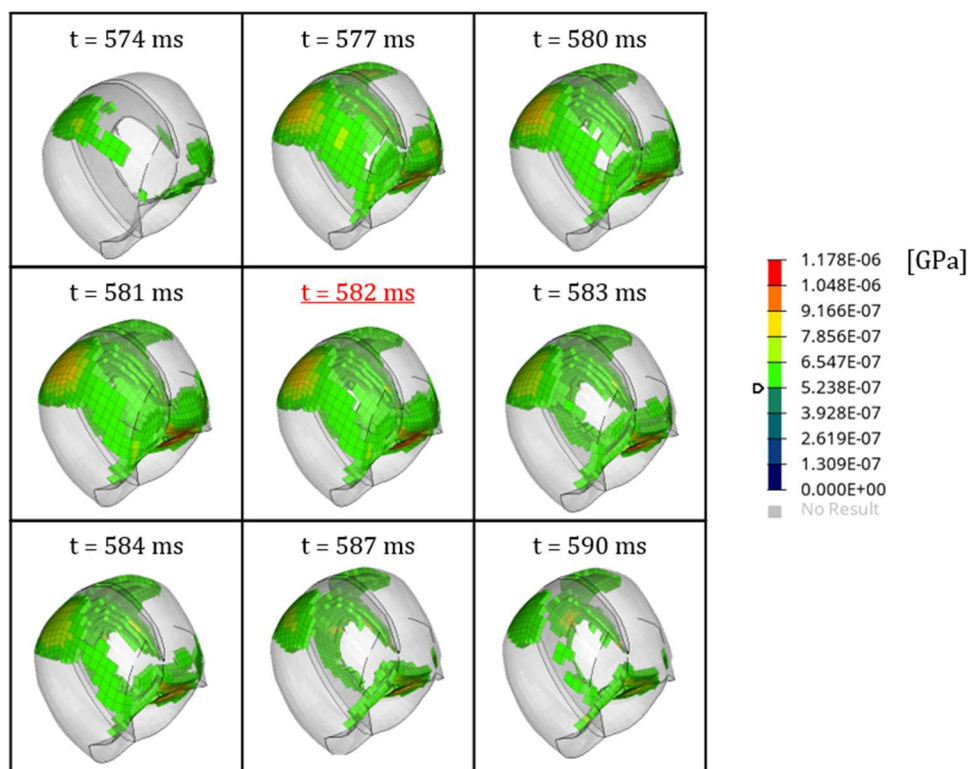
Table 4.4 - *Von Mises stress evolution with dt=1 ms and dt=3 ms (o-soto-gari, first repetition, second child)*

t = 572 ms	t = 573 ms	t = 578 ms
t = 579 ms	t = 580 ms	t = 581 ms
t = 582 ms	t = 585 ms	t = 588 ms

	[GPa]
1.169E-06	
1.039E-06	
9.090E-07	
7.791E-07	
6.493E-07	
5.194E-07	
3.896E-07	
2.597E-07	
1.299E-07	
0.000E+00	
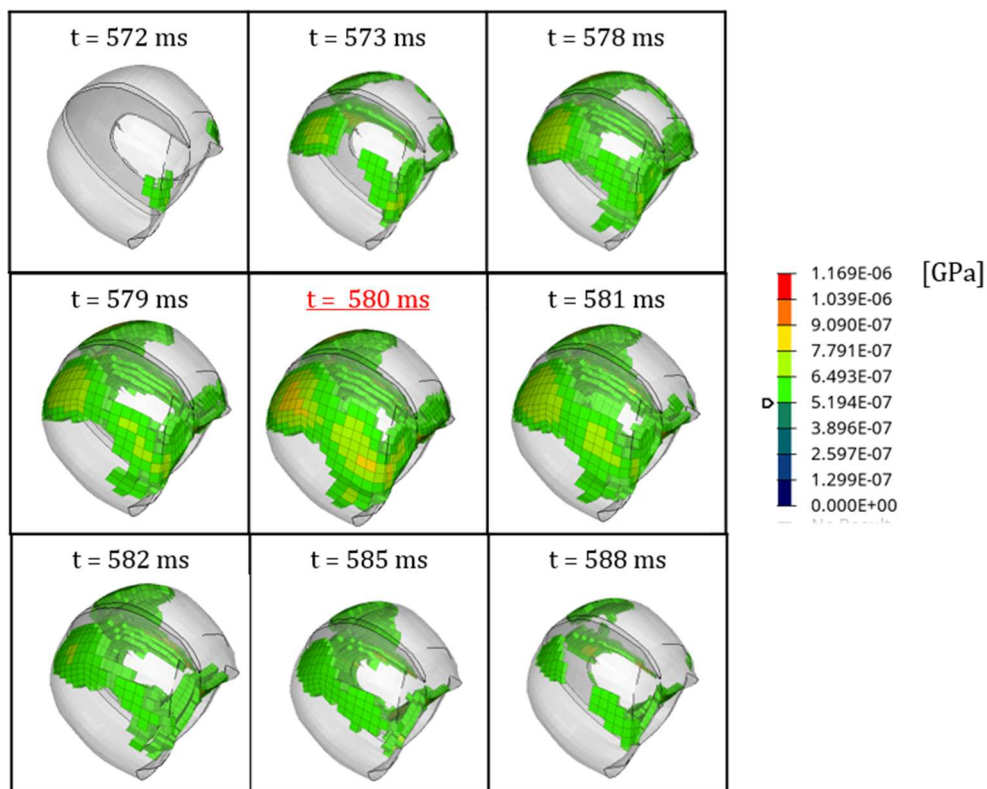
Table 4.5 - *Von Mises stress evolution with dt=1 ms and dt=3 ms (o-soto-gari, second repetition, second child)*

74

t = 497 ms	t = 500 ms	t = 503 ms
t = 504 ms	t = 505 ms	t = 506 ms
t = 507 ms	t = 510 ms	t = 513 ms
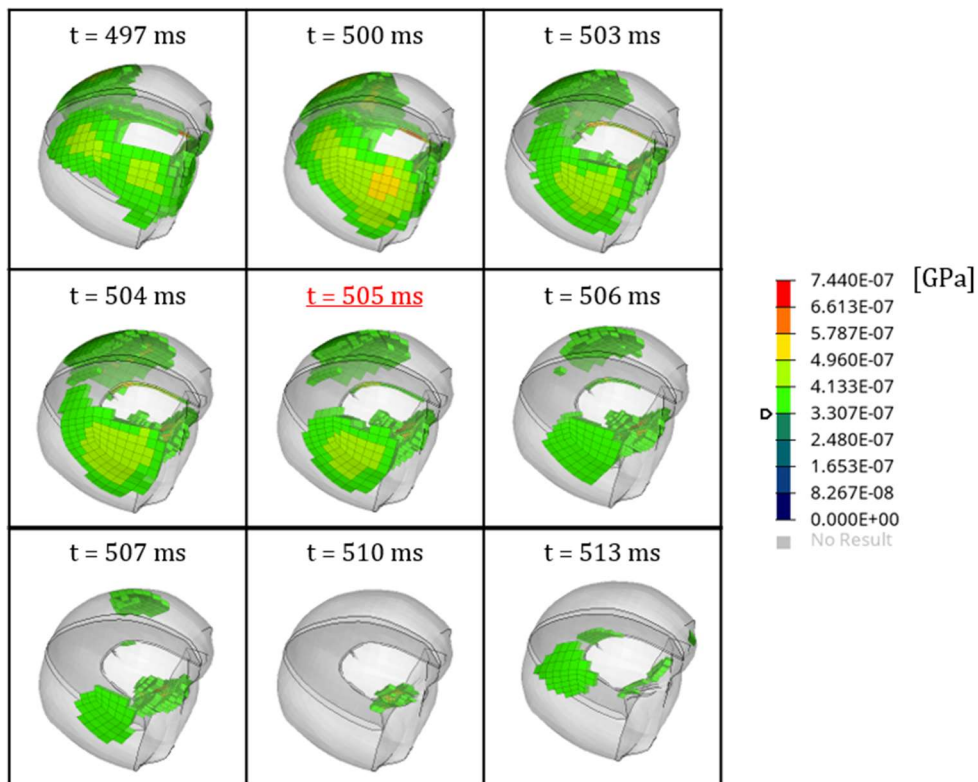
Table 4.6 *- Von Mises stress evolution with dt=1 ms and dt=3 ms (o-soto-gari, third repetition, second child)*

Regarding the colour scale, the red regions are under higher stress values. For both of children (table 4.7 and 4.8), at the time when the maximum value of Von Mises is reached, these regions are placed near the interfaces between different brain materials (i.e. between the cerebral cortex and the falx cerebri, between the cerebral cortex and the tentorium cerebelli). This consideration agrees with study suggesting that these areas would probably cause higher concentrations of rotational impact stress.[68] In addition, the 3D localization of maximum values is one of the tools used by Willinger for the evaluation of cerebral lesions.

75
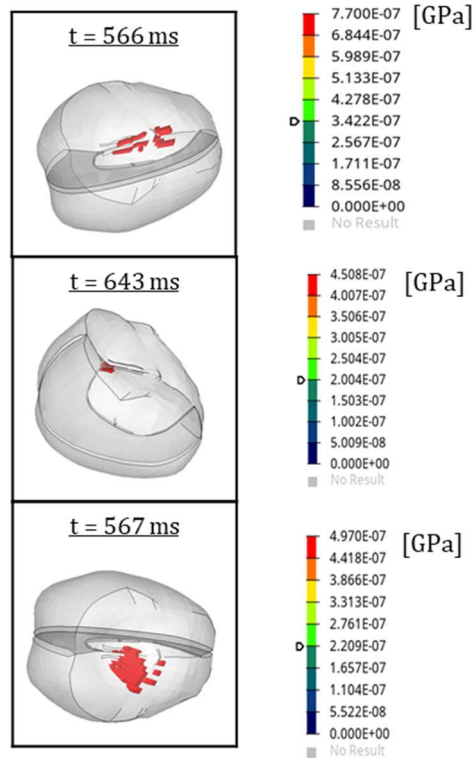
Table 4.7 - *Maximum Von Mises stress at peak time (o-soto-gari, all repetitions, first child)*
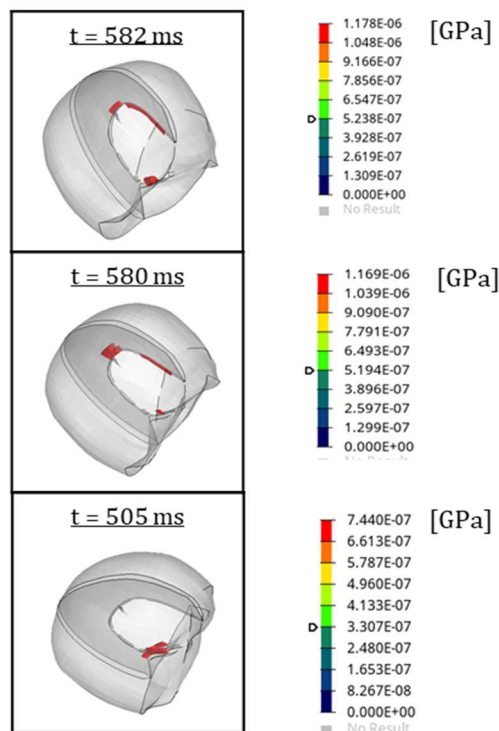
Table 4.8 - *Maximum Von Mises stress at peak time (o-soto-gari, all repetitions, second child)*

In conclusion, Von Mises stress reached during the execution of this technique by the first child is less than that achieved during the execution of the second child, that amount to the order of kPa. To parity of configuration of the model, such difference can be connected to the fact that the accelerations and the velocities given as input assume greater maximum values for the second child, as explained in chapter 3.1.1.

4.2.2 Four technique performed by one child

Four techniques (o-soto-gari, o-uchi-gari, ippon-seoi-nage and tai-otoshi), executed three times, are tested on the first child. The results concerning the first technique, o-soto-gari, for the first child have been reported in the previous paragraph (figure 4.6 and table 4.1, 4.2, 4.3, 4.7).

The tools used to represent the results are the same as those used in the previous paragraph.

For o-uchi-gari (figure 4.8), the mean value $\pm$ standard deviation trend of the signals has been reported between 250 and 700 ms. For ippon-seoi-nage and tai-otoshi (figure 4.9 and 4.10), the mean trend of the signals used to drive the model has been reported between 400 and 800 ms. For all repetitions, the highest stress values are located temporally in the time window, represented in yellow in the figures 4.8, 4.9 and 4.10, at which the kinematic parameters have reached their peaks.

Concering o-uchi-gari technique (figure 4.8), the time interval at Von Mises Stress reaches higher values are between 545 ms – 609 ms (T=64ms), 305 ms – 372 ms (T=67 ms), 559 ms – 669 ms (T=110 ms) respectively for the first, second and third repetition. In this case, the duration of the intervals for first and second is approximately the same, while the third is nearly twice as many. But, the first and third repetition time interval are overlapping for part of their intervals, while the second repetition time interval is reached before than the other two repetitions. It may be due to the fact that during that interval both the peak of linear acceleration along x and the peak of angular velocity around x were reached.
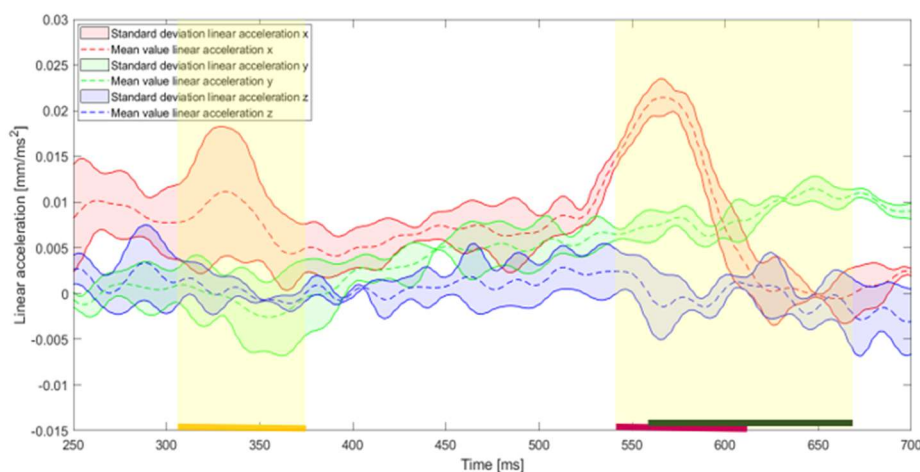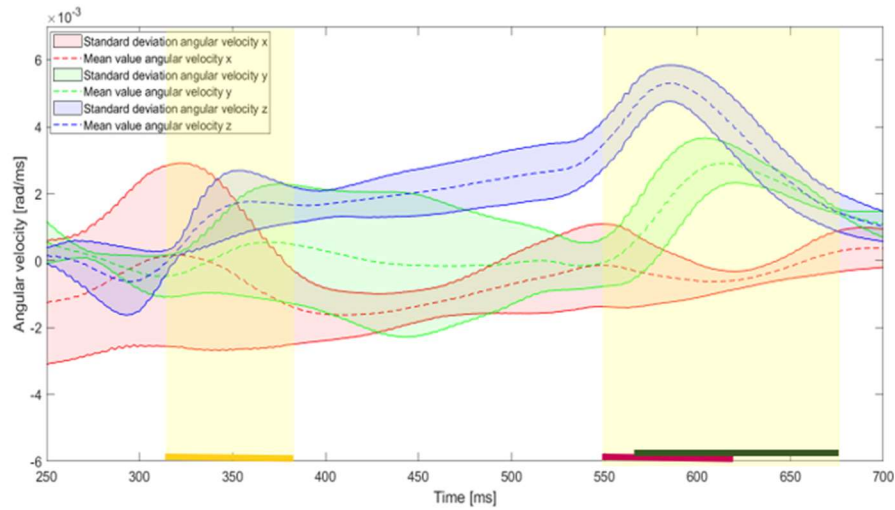
Figure 4.8 - Time interval at which higher brain Von Mises stress values are reached during o-uchi-gari technique for first child

Concering ippon-seoi-nage technique (figure 4.9), the time interval at Von Mises Stress reaches higher values are between 563 ms – 602 ms (T=39ms), 555 ms – 592 ms (T=37 ms), 559 ms – 600 ms (T=41 ms) respectively for the first, second and third repetition. In this case, the duration of the intervals for all repetitions is approximately the same and also time intervals are overlapping.
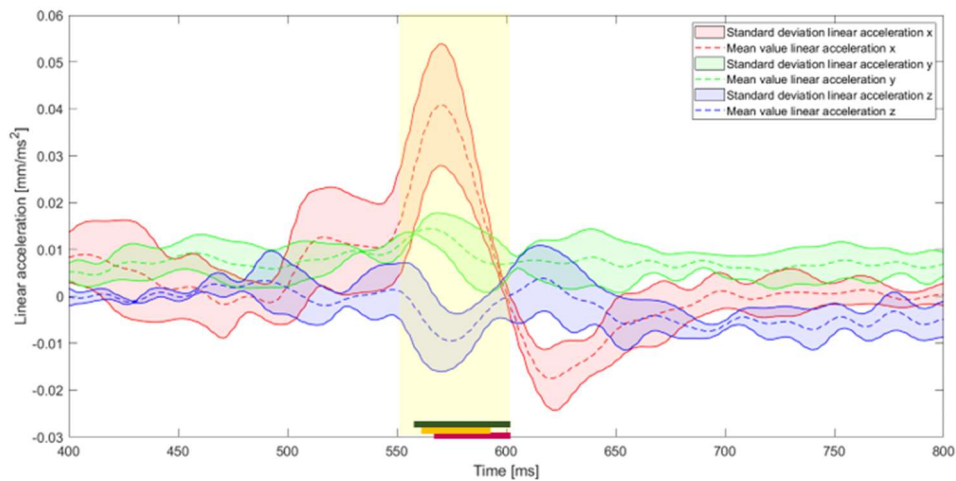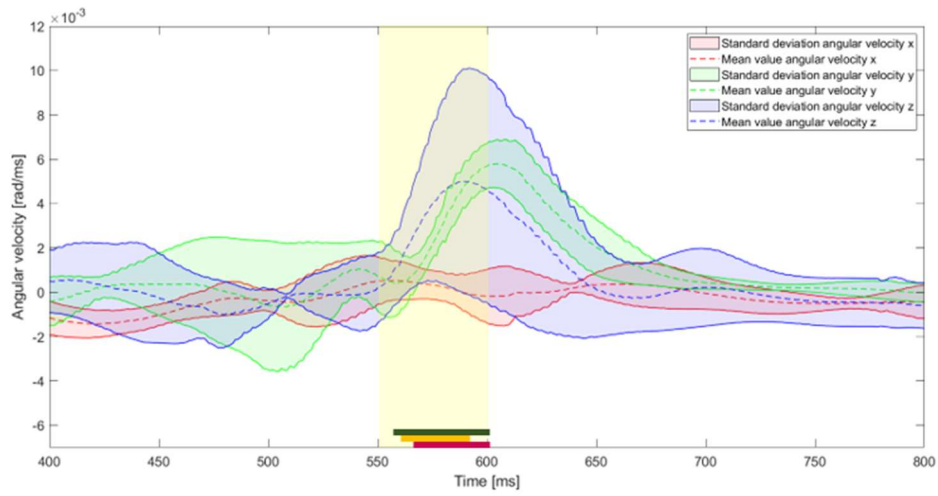
Figure 4.9 - Time interval at which higher brain Von Mises stress values are reached during ippon-seoi-nage technique for first child

Concerning tai-otoshi technique (figure 4.10), the time interval at Von Mises Stress reaches higher values are between 554 ms – 620 ms (T=66 ms), 567 ms – 591 ms (T=24 ms), 567 ms – 591 ms (T=24 ms) respectively for the first, second and third repetition. In this case, the duration of the interval for the first repetitions is larger than the second and the third, but all repetitions time intervals are overlapping.
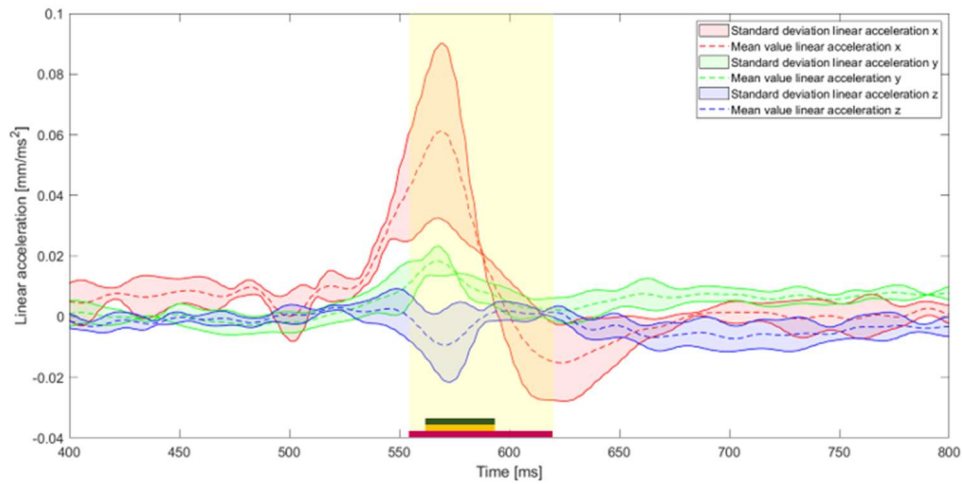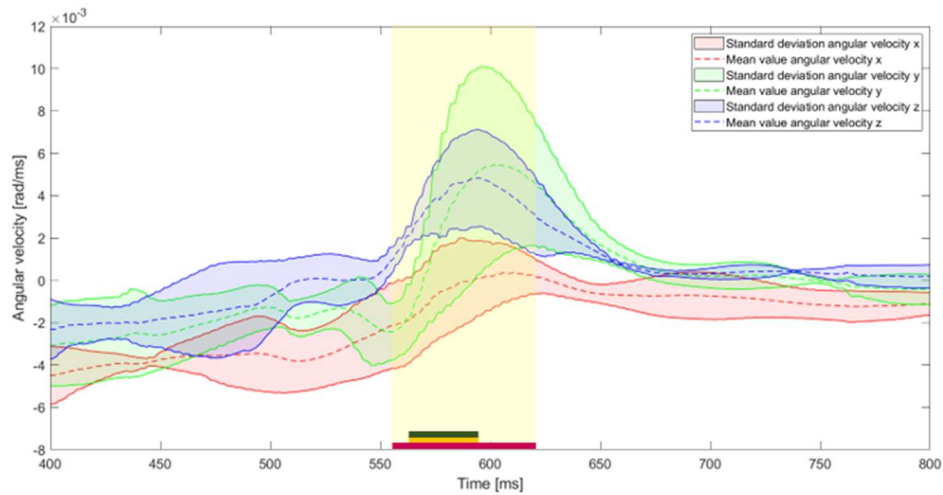
Figure 4.10 - *Time interval at which higher brain Von Mises stress values are reached during tai-otoshi technique for first child*

In view of this, the repetitions performed during o-uchi-gari technique find the maximum values of Von Mises in very different time intervals compared to the repetitions of other techniques (o-soto-gari, ippon-seoi-nage, tai-otoshi).

The results in terms of distribution of Von Mises Stress are pointed out below.
Concerning o-uchi-gari tecnique have been reported in table 4.9, 4.10 and 4.11 that shows the trend over time of Von Mises Stress around its maximum value, for each repetition. It is shown a considerable volume, where the Von Mises Stress values are ranging between 91.67 Pa – 165 Pa, 138.7 Pa – 249.7 Pa, 106.1 Pa –191 Pa respectively for the first, second and third repetition executed. Moreover, table 4.12 shows, at the time when the maximum value of Von Mises is reached, the most stressed area.

t = 562 ms	t = 565 ms	t = 568 ms
t = 569 ms	<u>t = 570 ms</u>	t = 571 ms
t = 572 ms	t = 575 ms	t = 578 ms

1.650E-07 [GPa]
1.467E-07
1.283E-07
1.100E-07
9.167E-08
7.333E-08
5.500E-08
3.667E-08
1.833E-08
0.000E+00
No Result
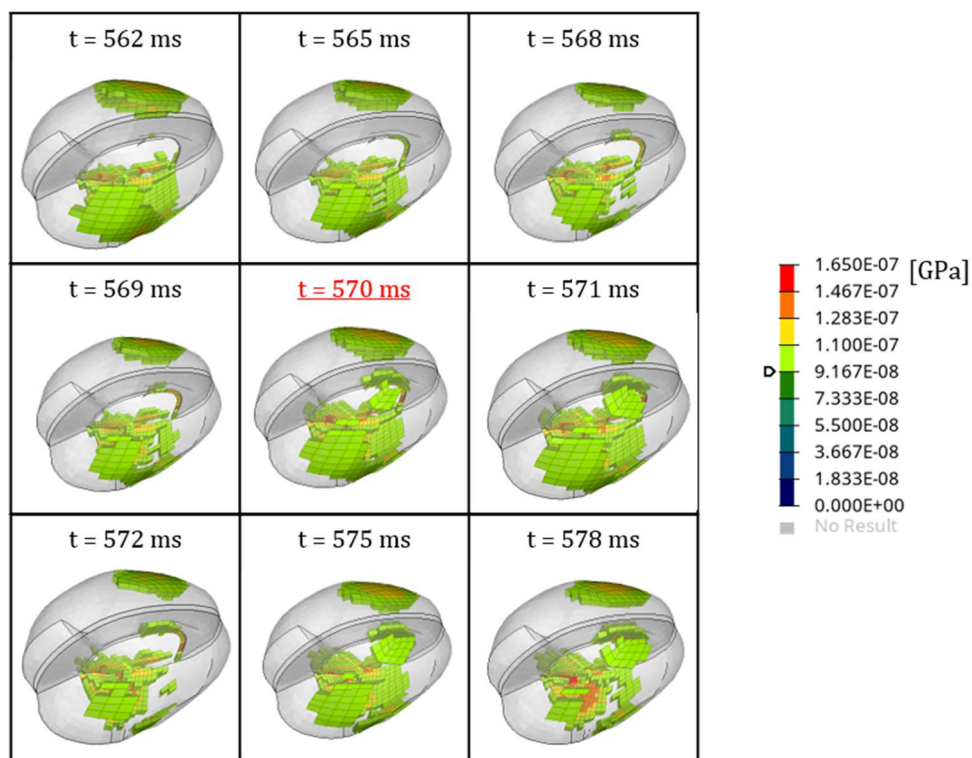
Table 4.9 - *Von Mises stress evolution with dt=1 ms and dt=3 ms (o-uchi-gari, first repetition, first child)*

t = 322 ms	t = 325 ms	t = 328 ms
t = 329 ms	<u>t = 330 ms</u>	t = 331 ms
t = 332 ms	t = 335 ms	t = 338 ms

2.497E-07 [GPa]
2.220E-07
1.942E-07
1.665E-07
1.387E-07
1.110E-07
8.323E-08
5.549E-08
2.774E-08
0.000E+00
No Result
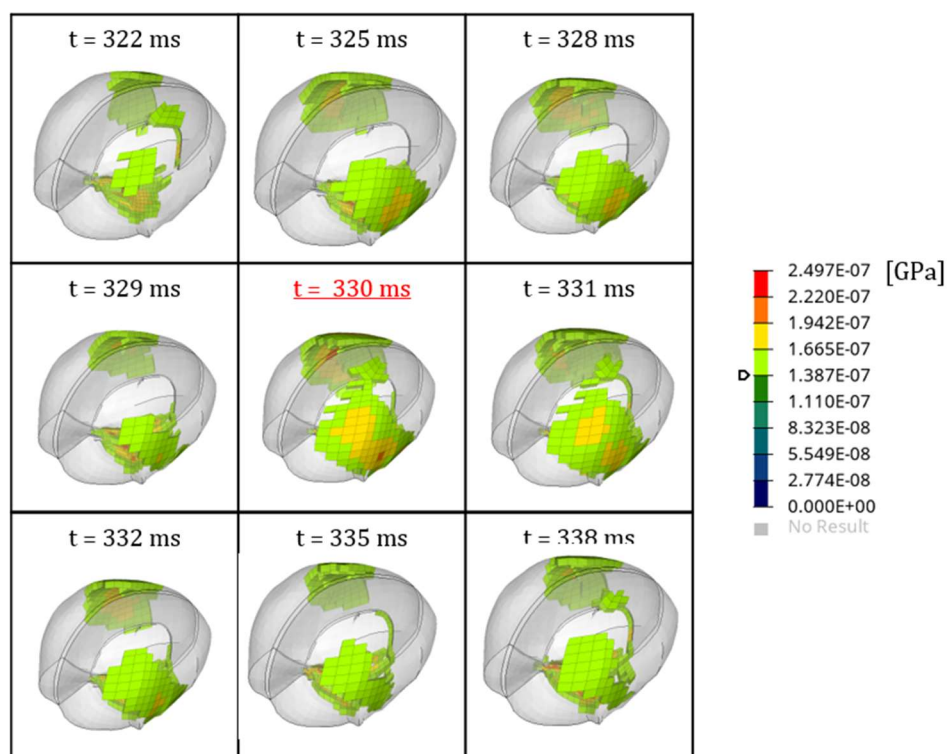
Table 4.10 - *Von Mises stress evolution with dt=1 ms and dt=3 ms (o-uchi-gari, second repetition, first child)*
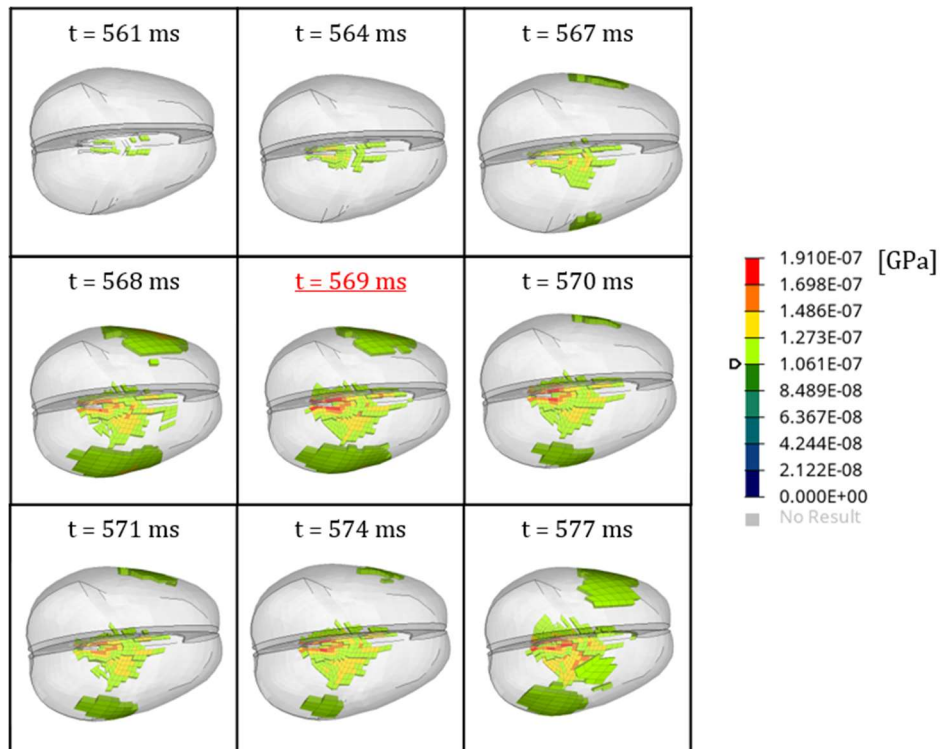
Table 4.11 - *Von Mises stress evolution with dt=1 ms and dt=3 ms (o-uchi-gari, third repetition, first child)*
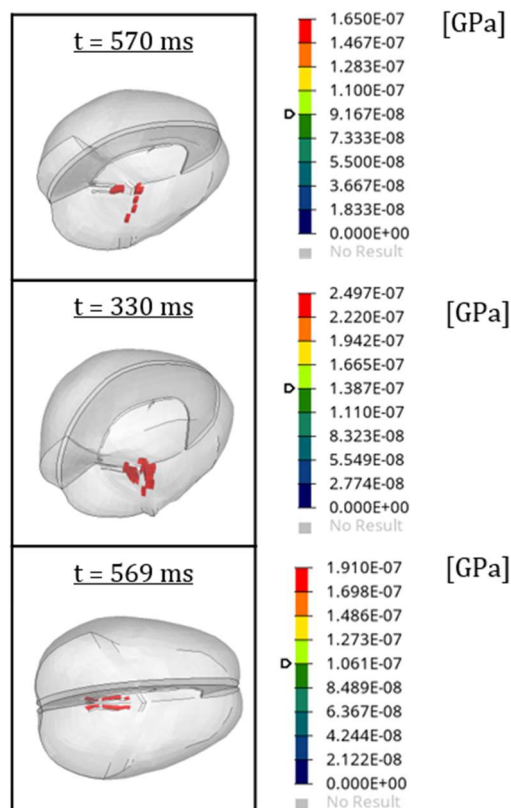
Table 4.12 - *Maximum Von Mises stress at peak time (o-uchi-gari, all repetitions, first child)*

The results concerning ippon-seoi-nage tecnique have been reported in table 4.13, 4.14 and 4.15, that show the trend over time of Von Mises Stress around its maximum value, for each repetition. It is shown the volume, where the Von Mises Stress values are ranging between 302.2 Pa – 680Pa, 289.3 Pa – 651 Pa, 112.4 Pa – 253 Pa respectively for the first, second and third repetition executed. Moreover, table 4.16 shows, at the time when the maximum value of Von Mises is reached, the most stressed area.
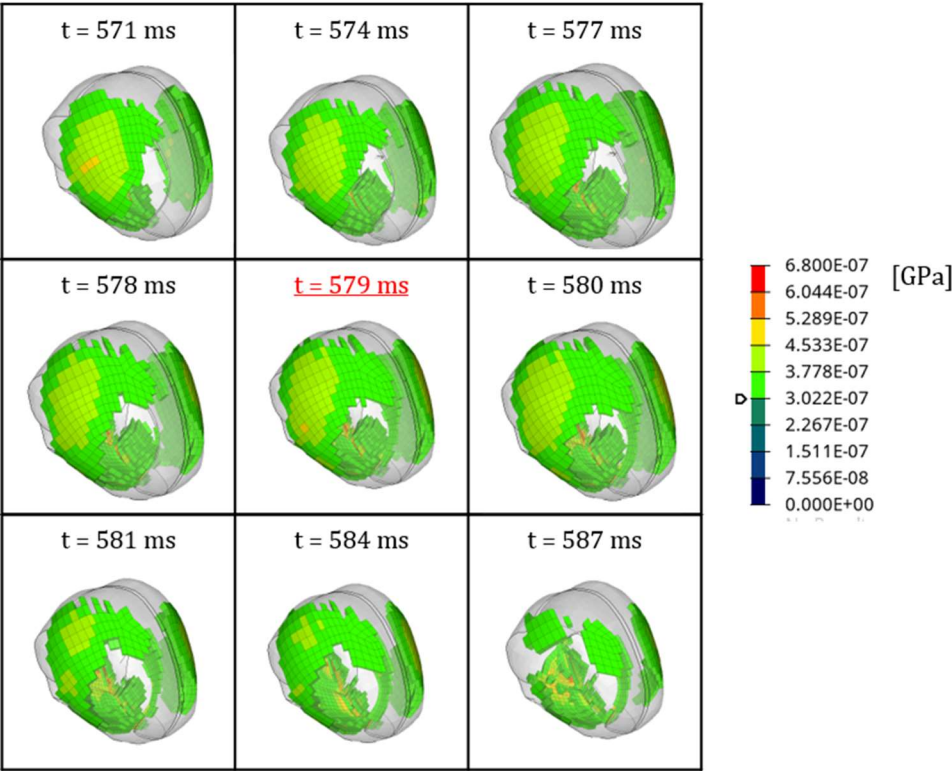
Table 4.13 - *Von Mises stress evolution with dt=1 ms and dt=3 ms (ippon-seoi-nage, first repetition, first child)*
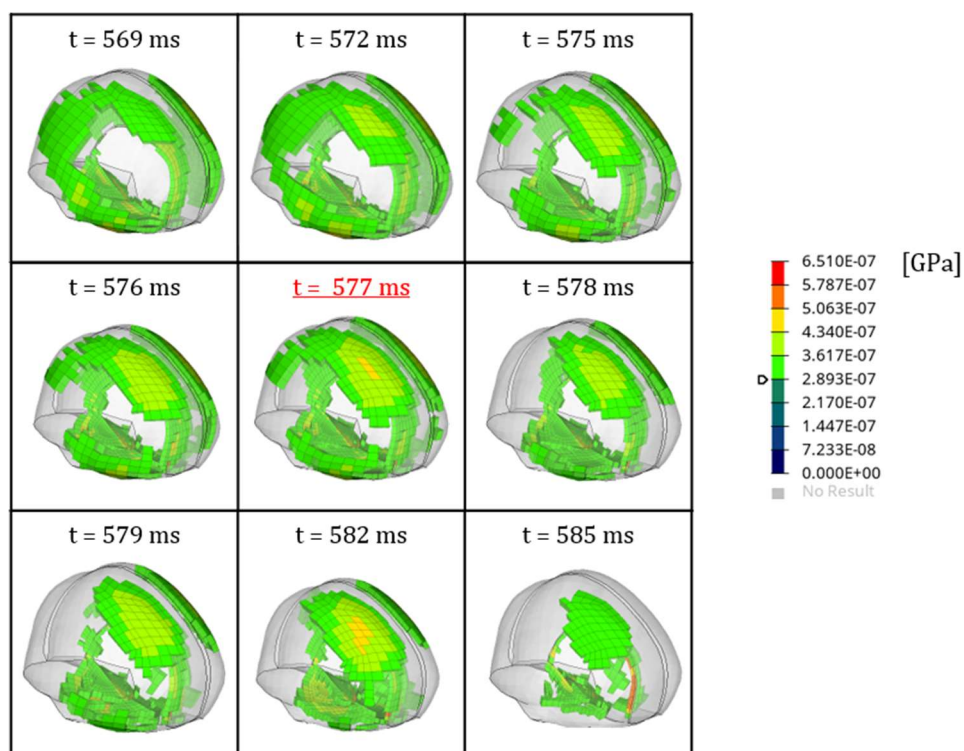
Table 4.14 - Von Mises stress evolution with dt=1 ms and dt=3 ms (ippon-seoi-nage, second repetition, first child)
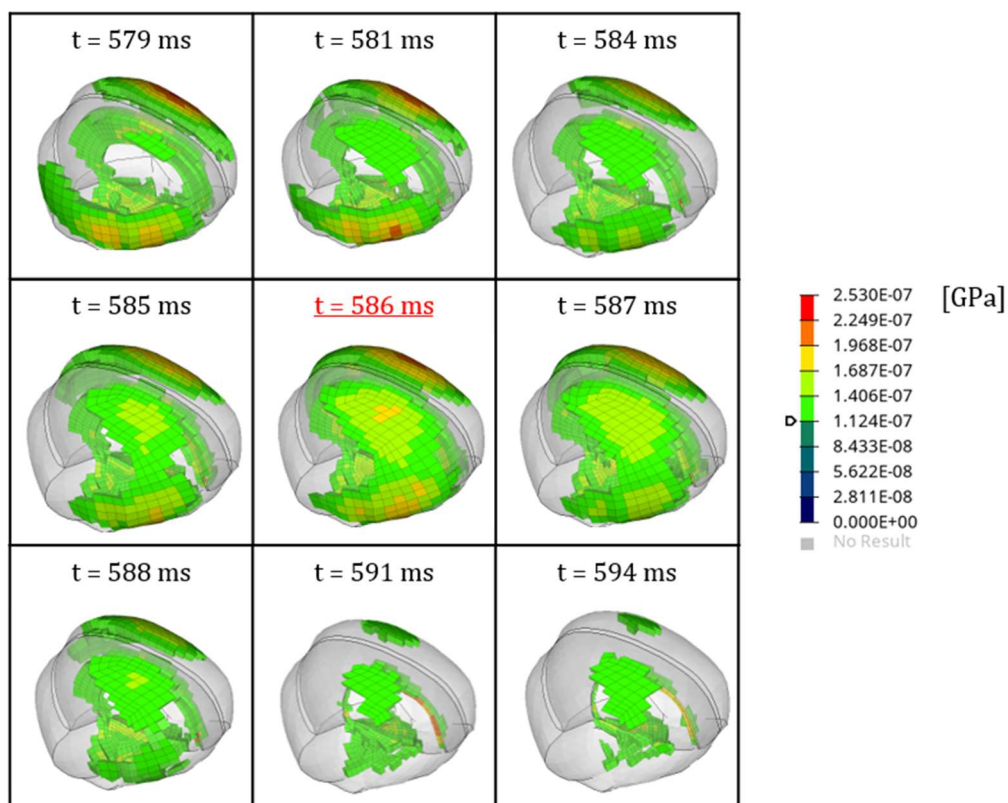
Table 4.15 - Von Mises stress evolution with dt=1 ms and dt=3 ms (ippon-seoi-nage,third repetition, first child)
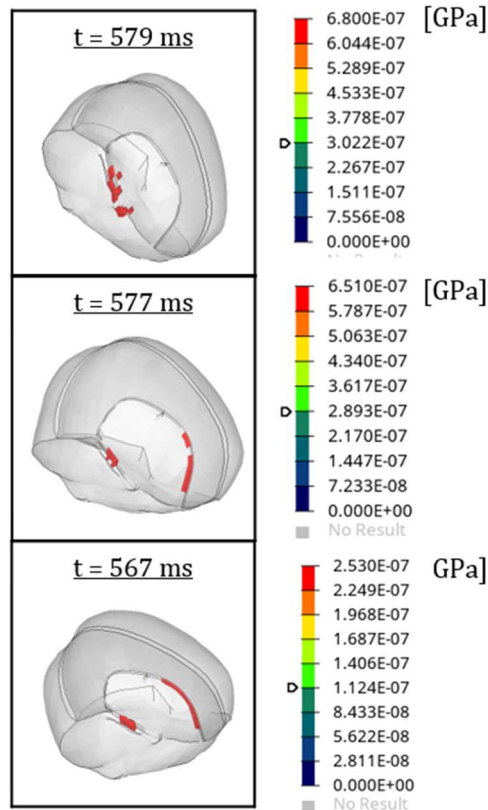
Table 4.16 - Maximum Von Mises stress at peak time (ippon-seoi-nage, all repetitions, first child)

The results concerning tai-otoshi tecnique have been reported in table 4.17, 4.18 and 4.19, that show the trend over time of Von Mises Stress around its maximum value, for each repetition. It is shown the volume, where the Von Mises Stress values are ranging between 140.4 Pa – 316 Pa, 513.8 Pa – 1.156 kPa, 520 Pa – 1.171 kPa respectively for the first, second and third repetition executed. Moreover, table 4.20 shows, at the time when the maximum value of Von Mises is reached, the most stressed area.
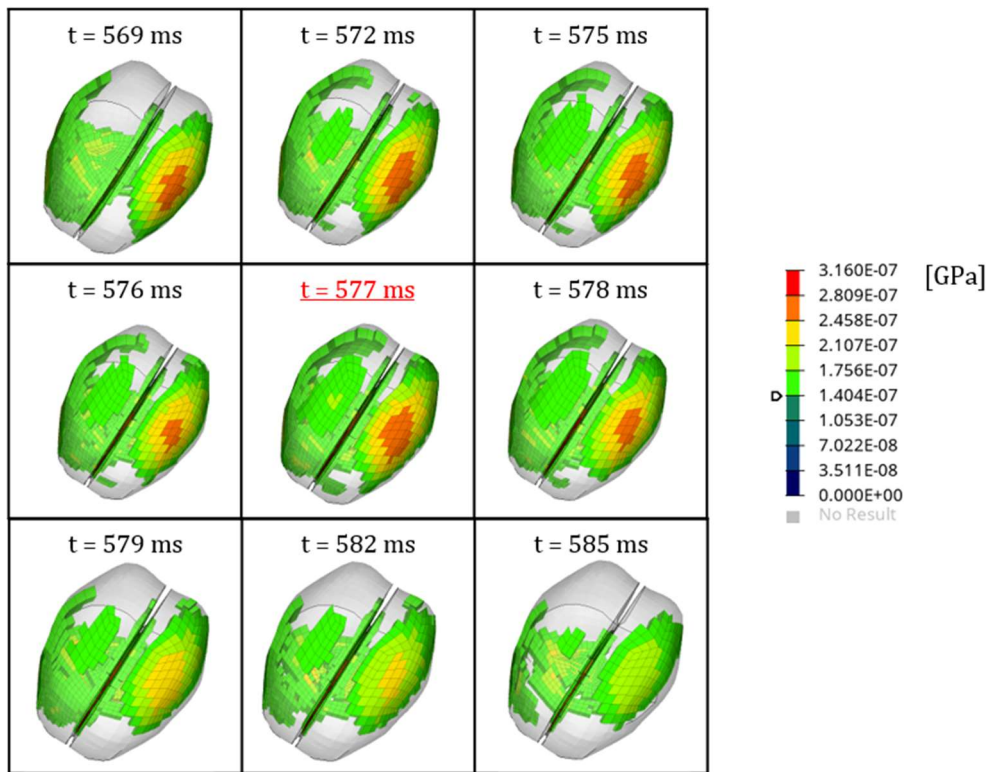
Table 4.17 - *Von Mises stress evolution with dt=1 ms and dt=3 ms (tai-otoshi, first repetition, first child)*
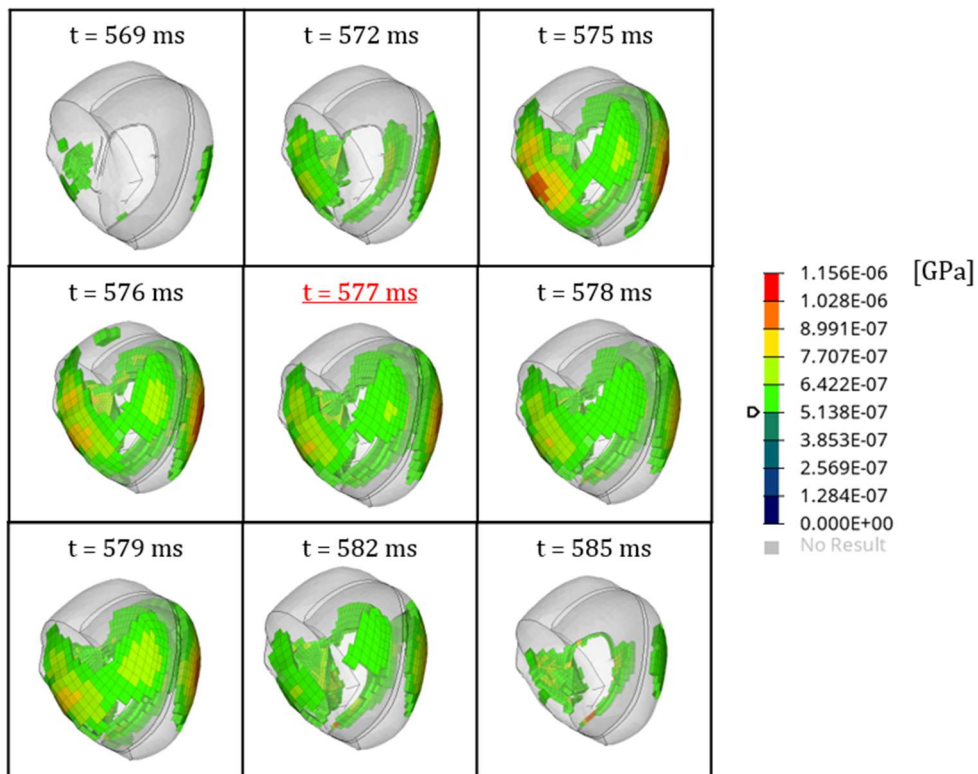
Table 4.18- *Von Mises stress evolution with dt=1 ms and dt=3 ms (tai-otoshi, second repetition, first child)*
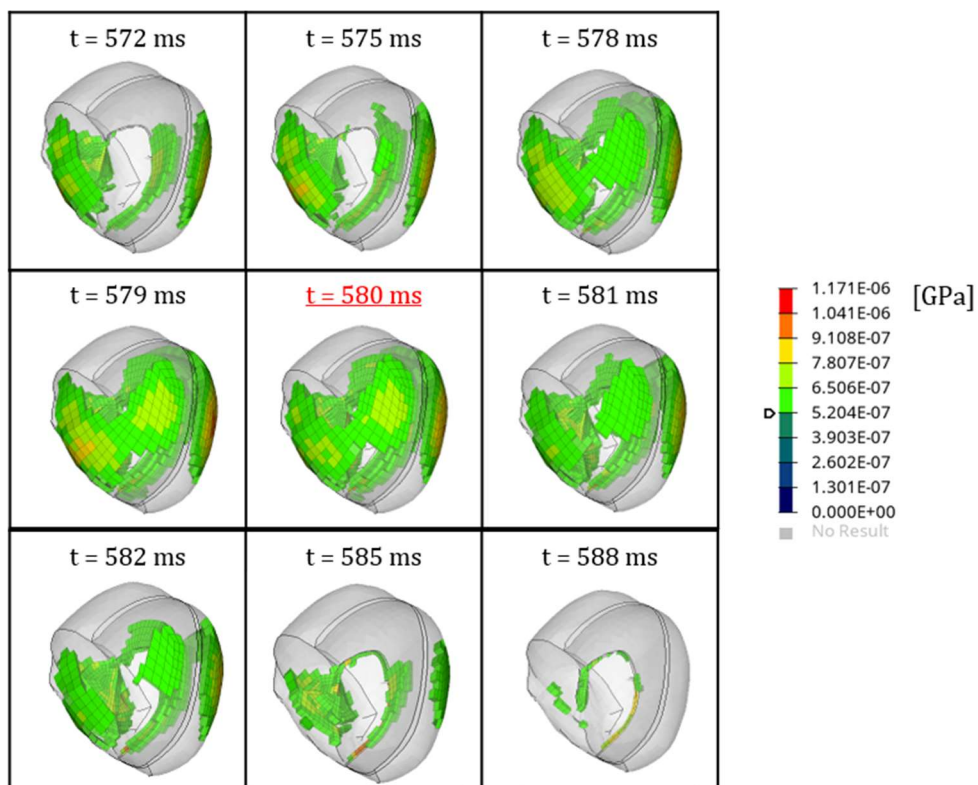
Table 4.19 - *Von Mises stress evolution with dt=1 ms and dt=3 ms (tai-otoshi, third repetition, first child)*
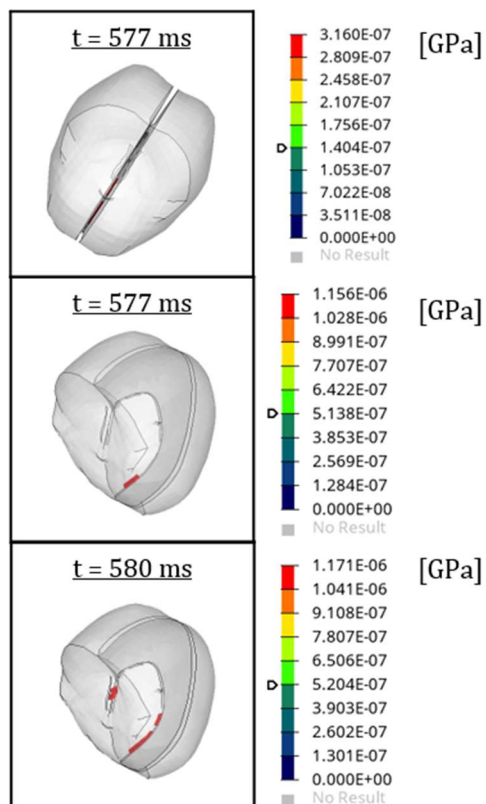
Table 4.20 - *Maximum Von Mises stress at peak time (tai-otoshi, all repetitions, first child)*

As o-soto-gari technique, also in the other three techniques (o-uchi-gari, ippon-seoi-nage, tai-otoshi) the most stressed region was placed near the interfaces between different brain materials (table 4.7, 4.12, 4.16 and 4.20).

For all repetitions of the o-soto-gari technique and for all repetitions of the tai-otoshi technique, it can be noted that there is a higher concentration of Von Mises Stress on the left side of the brain. This could be justified by the execution of the movement itself.

To summarize, the maximum stress values reached during the execution of each technique are reported (table 4.21).

		Maximum Value Von Mises Stress [Pa]	Mean [Pa]	Standard Deviation [Pa]
O-soto-gari	First Repetition	770	572,6	172,5
	Second Repetition	450,8		
	Third Repetition	497		
O-uchi-gari	First Repetition	165	201,9	43,4
	Second Repetition	249,7		
	Third Repetition	191		
Ippon-seoi-nage	First Repetition	680	528	238,6
	Second Repetition	651		
	Third Repetition	253		
Tai-otoshi	First Repetition	316	881	489,4
	Second Repetition	1156		
	Third Repetition	1171		

Table 4.21 - Maximum Von Mises stress for all techiniques

The o-uchi-gari technique is the one with the lowest Von Mises peaks, this can be related to the fact that both linear accelerations and angular velocities take much lower values than the other techniques.

It is evident that there are considerable differences in the maximum values of Von Mises between repetitions of the same technique, which can be traced back to the fact that it was a child with little experience to perform the technique. So, it is difficult to establish the most dangerous technique for this child.

In any case, it seems that the higher Von Mises values were reached when higher accelerations and velocity were prescribed.

Fernandes[32], in an exhaustive review on head injury predictors in sports trauma, reported injury thresholds of Von Mises stress, that typically range from 14.8 to 33 kPa (table 3.28). He also emphasizes other values: Marjoux for a moderate and severe neurological injury,

obtained von Mises stress values of 27 kPa and 39 kPa, respectively; more recently, Deck and Willinger updated these tolerance limits to 28 kPa and 53 kPa, respectively.

Brain injury	von Mises stress (kPa)
Brain injury	12
	14.8
Severe brain injury	11–16.5
	27
Concussion	22
	20
	40
Long duration concussion	20
Short duration concussion	10
Severe neurological injury	46
50% Moderate neurological injury	18
50% Severe neurological injury	38
50% Mild DAI	26
50% Severe DAI	33
50% Probability of concussion	8.4 in corpus callosum
Severe and irreversible TBI	14.8 ± 4.5

Table 4.22 - Stress thresholds[32]

These thresholds are considerably higher than the values determined in simulations of this work of thesis: the highest Von Mises Stress was 1.178 kPa, performed by second child during the execution of the first repetition of o-soto-gari.

5. Conclusion

The aim of this thesis was to evaluate the traumatic brain injury on the brain of children during technique usually used in Judo practice, with the use of human body modelling.

A literature review was carried out to understand the methods applied for studying traumatic brain injury in children and during sporting activities in quantitative manner.

Children are often treated as small adults, but with head injuries the same hypothesis is inappropriate, because children brain have been different from adults one in the relative volumes of grey and white matter, in the development of the neural pathways and in mechanical properties.

Literature also pointed out different way to conduct experimental test and physical reconstructions test were reported. In this regard, linear and rotational accelerations and velocities can be achieved using inertial sensor (gyroscopic rate sensor and accelerometers). Head Impact Telemetry (HIT), head-mounted sensors, sensorized helmet, instrumented mouthguard have been used in a lot of studies.

Then, injury criteria based on measures head kinematics widely employed in sporting brain injury research were presented in literature. However, in order to determine stress and strain in brain tissue, the finite element modelling (FEM), is probably a more complete and appropriate approach. Recently, there is a tendency among researchers to use head injury predictors that are based on the head tissue level response, rather than on its kinematics. The most common metrics used for calculating risk are Von Mises Stress, maximum principal strain (MPS), the cumulative strain damage measure (CSDM) and Pressure.

In children, FE modelling is developing topic and limited, even if children are at higher risk for concussion, prolonged recovery, and repeat concussive injury when compared to adults. In addition to the Scaled University College Dublin Brain Trauma Model, other head model are recently proposed: Roth proposed a 3-year-old subject model, Giordano and Kleiven have proposed a scalable model for ages 1.5–6 (Piper), Koncan introduced a FE model of a 6-year-old child for use in sporting impact research of young children.

For this study, six degree-of-freedom kinematic data, specifically linear accelerations along the x, y, z axis and angular velocities around the x, y, z axis of the head measured with an inertial sensor applied to the forehead from a previous laboratory study of Judo impacts were used. The data of two children have been used for the current study: for the first child, the data gained from all 4 techniques (o-soto-gari, o-uchi-gari, ippon-seoi-nage and tai-otoshi) have been considered. For the second child, the data gained from the first technique

(o-soto-gari) have been considered, because of its higher possibility of reaching dangerous levels.

Using the LS - PrePost software, the children were modeled with the head PIPER model (6 years old) and the experimental data were prescribed, on the head model, according to local accelerometer reference system modeled on the skull.

The output parameter used as a criterion for evaluating brain lesions is Von Mises stress, which is among the most indicated in the literature, through the HyperView software. The evaluation was carried out both in space, to highlight the most stressed portions of the brain, and in time to correlate these stresses with the linear acceleration and angular velocity to which the subject's head was exposed.

The mean value $\pm$ standard deviation trend of the data gained from sensors have been reported. A variability, in terms of shape and magnitude, can be noticed. It could be attributed to the inexperience of the child in practicing the technique and to the greater attention in planning the movement to be performed to fall correctly avoiding trauma.

Secondly, Von Mises Stress was analysed. Two different children were considered performing the same technique, o-soto-gari, three times. Von Mises stress reached during the execution of this technique by the first child is less than that achieved during the execution of the second child, that amount to the order of kPa. Then, four techniques (o-soto-gari, o-uchi-gari, ippon-seoi-nage and tai-otoshi), executed three times, are tested on the first child. For o-soto-gari technique and for tai - otoshi technique, it can be noted that there is a higher concentration of Von Mises Stress on the left side of the brain. The o-uchi-gari is the one with the lowest Von Mises peaks. In addition, it is evident that there are considerable differences in the maximum values of Von Mises between repetitions of the same technique, so it is difficult to establish the most dangerous technique for this child. In any case, the higher Von Mises values were reached when higher accelerations and velocity were prescribed.

However, for all techniques, the highest stress values are located temporally in the time window at which the kinematic parameters have reached their peaks. At the time when the maximum value of Von Mises is reached, regions that are placed near the interfaces between different brain materials (i.e. between the cerebral cortex and the falx cerebri, between the cerebral cortex and the tentorium cerebelli). The thresholds reported in literature are considerably higher than the values determined in simulations of this work of thesis: the

highest Von Mises Stress was 1.178 kPa, performed by second child during the execution of the first repetition of o-soto-gari.

Further analysis may be necessary to demonstrate and validate the results obtained, analyzing all the techniques also for the second child and using other head injury criteria reported in the literature.
In addition, an idea could be to consider not only the head model, but to use a more complete model, i.e. with more body parts.

Appendix

O-soto-gari was the technique analysed in great detail, for its diffusion and dangerousness, and because it is the one that allowed the choice of parameters to be considered to carry out the study.

The trend of the accelerations along the 3 axes and the 3 angular velocities around the 3 axes is shown in figure A.1. In addition the time windows, in which the peaks of Von Mises stress in the brain are recorded, are indicated: in blue is indicated the window in which the maximum values of Von Mises are reached, in pink are indicated, instead, the time windows in which lower values of Von Mises are reached. For each window, in addition to the time interval, the maximum Von Mises value reached for that interval is also indicated.
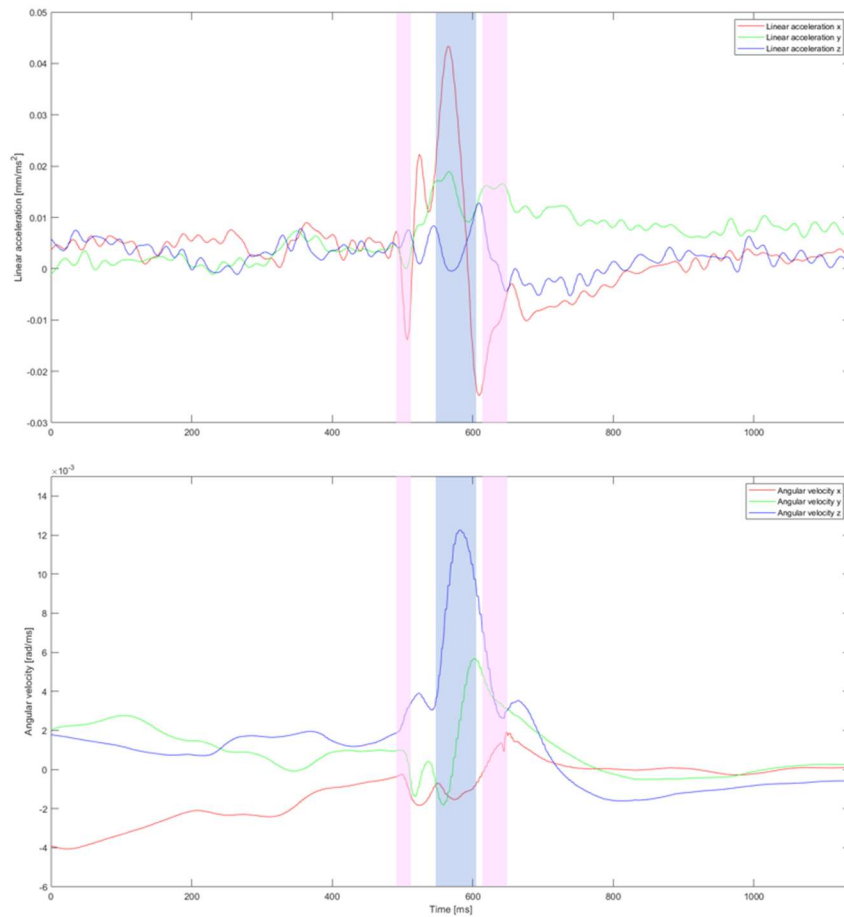
Figure A.1 - *Time intervals at which higher brain Von Mises stress values are reached during o-soto-gari technique, first repetition*

The maximum Von Mises Stress values is 406 Pa, 770 Pa, 534 Pa respectively for the first, second and third time windows. The time interval at Von Mises Stress reaches higher values are between 513 ms – 518 ms, 549 ms – 599 ms, 602 ms – 631 ms respectively for the first,

second and third time windows. The results concerning Von Mises evolution have been reported in table A.1, A.2 and A.3 that show the trend over time of Von Mises Stress with a time step of 1 ms, respectively for the first, second and third time windows. The stress scale is reported only the first time.
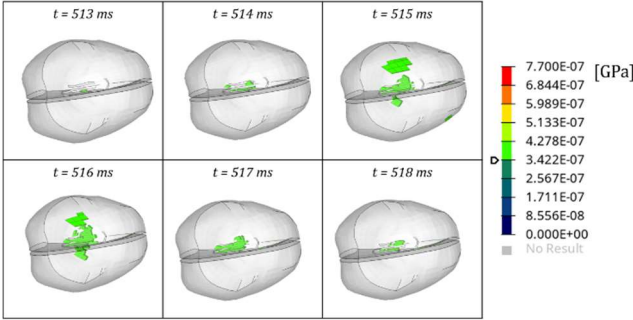
Table A.1 - *Von Mises stress evolution with dt=1 (first time interval, first repetition)*

t = 589 ms	t = 590 ms	t = 591 ms	t = 592 ms	t = 593 ms
t = 594 ms	t = 595 ms	t = 596 ms	t = 597 ms	t = 598 ms
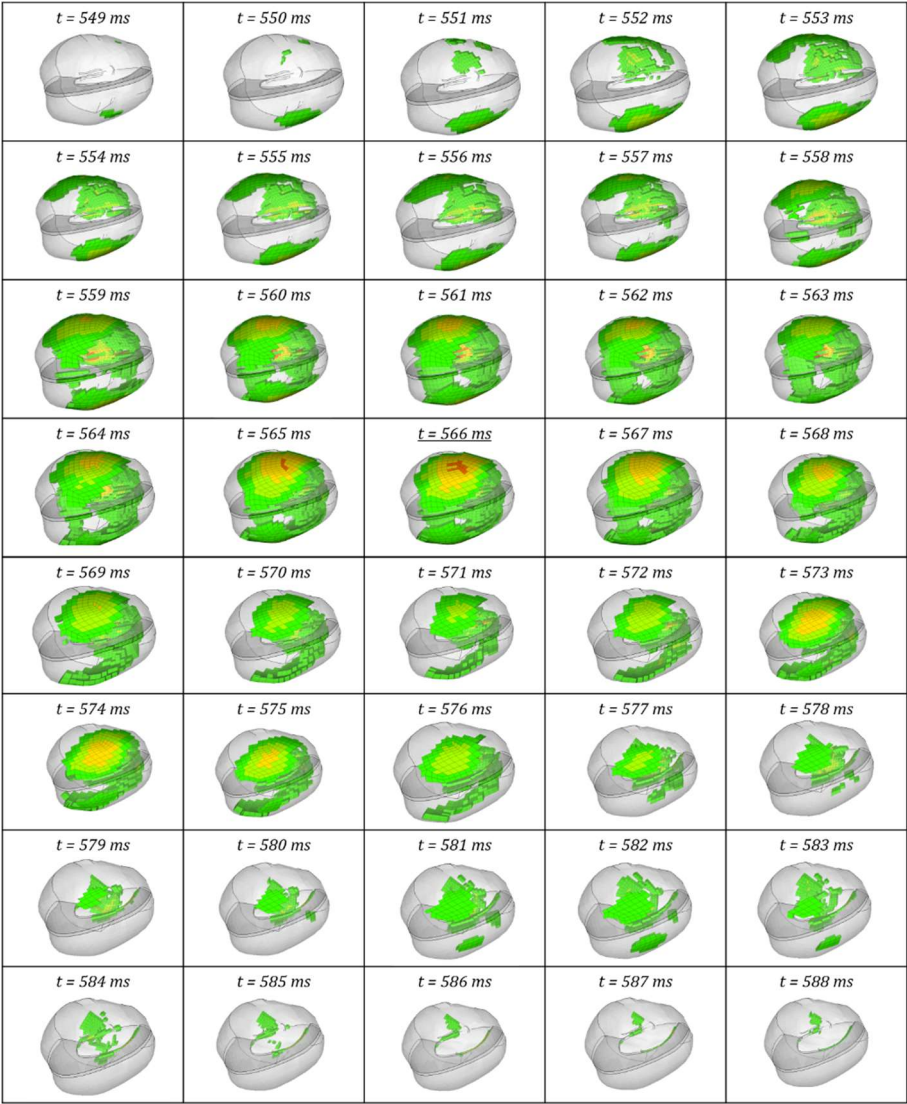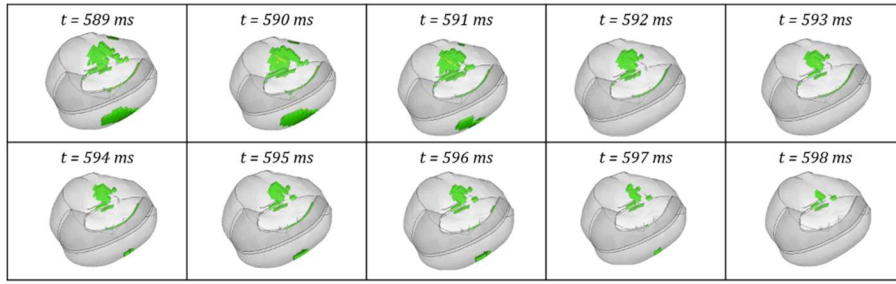
Table A.2 - *Von Mises stress evolution with dt=1 (second time interval, first repetition)*

t = 602 ms	t = 603 ms	t = 604 ms	t = 605 ms	t = 606 ms
t = 607 ms	t = 608 ms	t = 609 ms	t = 610 ms	t = 611 ms
t = 612 ms	t = 613 ms	t = 614 ms	t = 615 ms	t = 616 ms
t = 617 ms	t = 618 ms	t = 619 ms	t = 620 ms	t = 621 ms
t = 622 ms	t = 623 ms	t = 624 ms	t = 625 ms	t = 626 ms
t = 627 ms	t = 628 ms	t = 629 ms	t = 630 ms	t = 631 ms
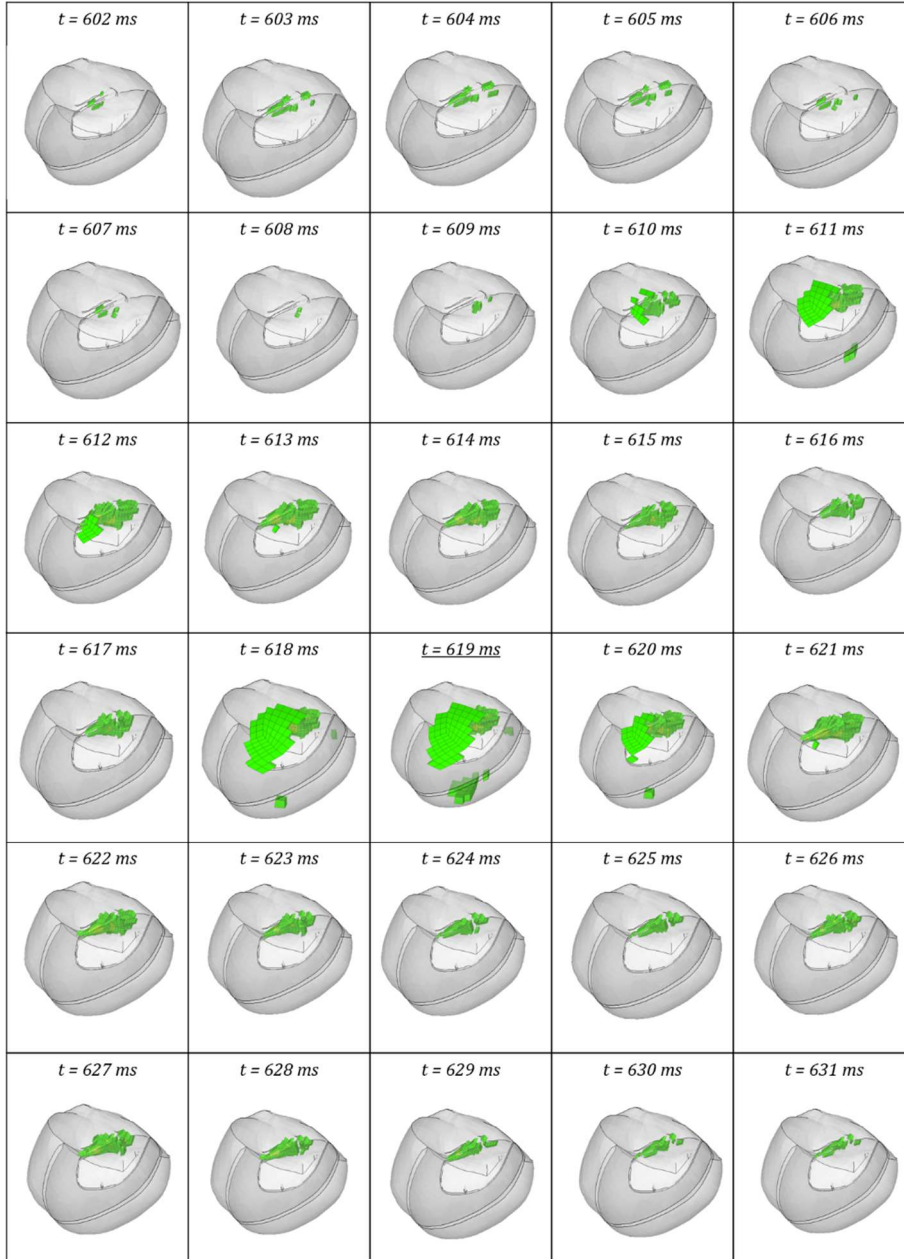
Table A.3 - *Von Mises stress evolution with dt=1 (third time interval, first repetition)*

Subsequently, the maximum value of the scale was set to 45 kPa, considered in the literature as the threshold for brain damage in children. The color transition between blue and green represents an approximate Von Mises Stress of 450 Pa. As can be seen from the colored plot in figure A.4, the values are far from the maximum value.
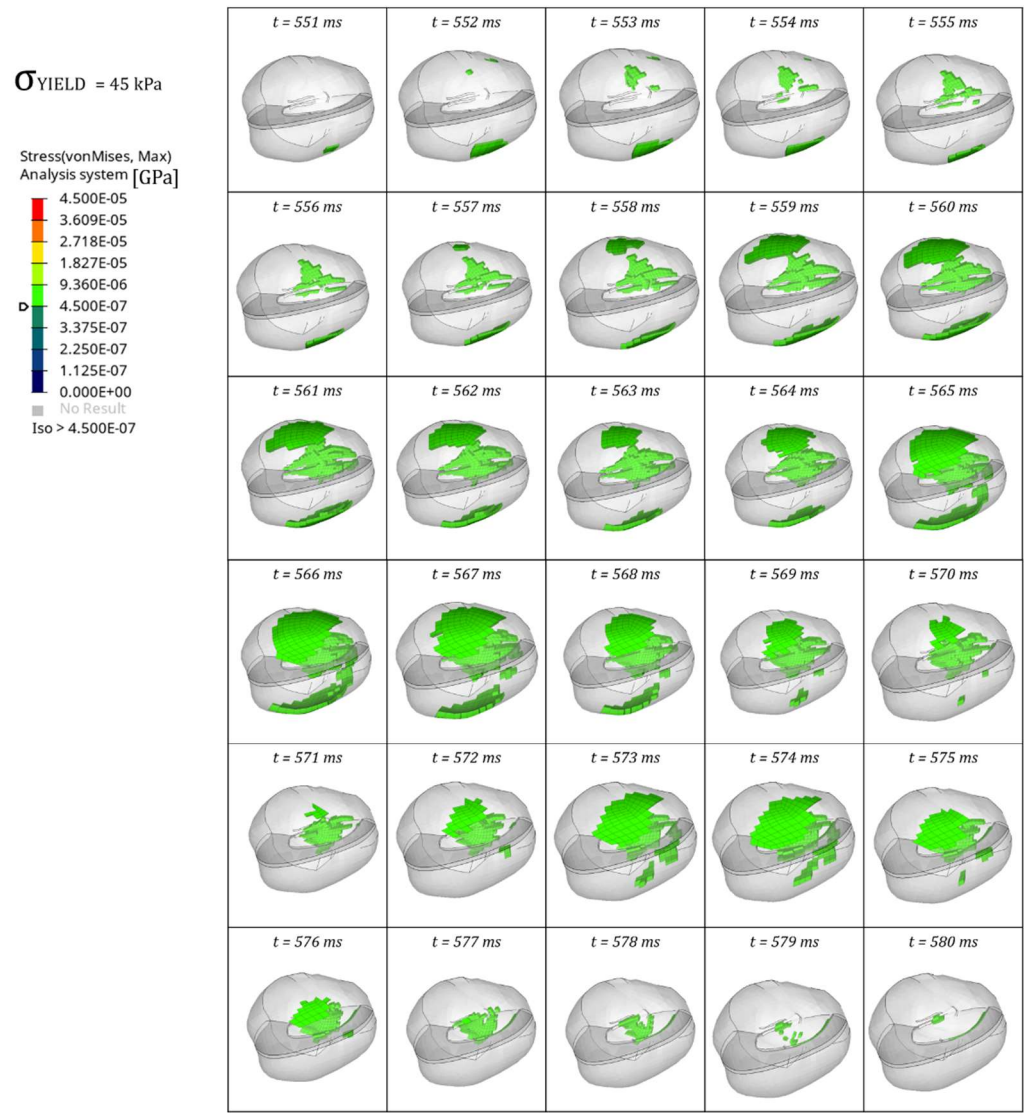
Table A.4 - *Von Mises stress evolution based on maximum literature value (first repetition)*

The same approach was taken for the second repetition. The trend of the accelerations along the 3 axes and the 3 angular velocities around the 3 axes and the time windows, in which the peaks of Von Mises stress in the brain are recorded, are shown in figure A.2.
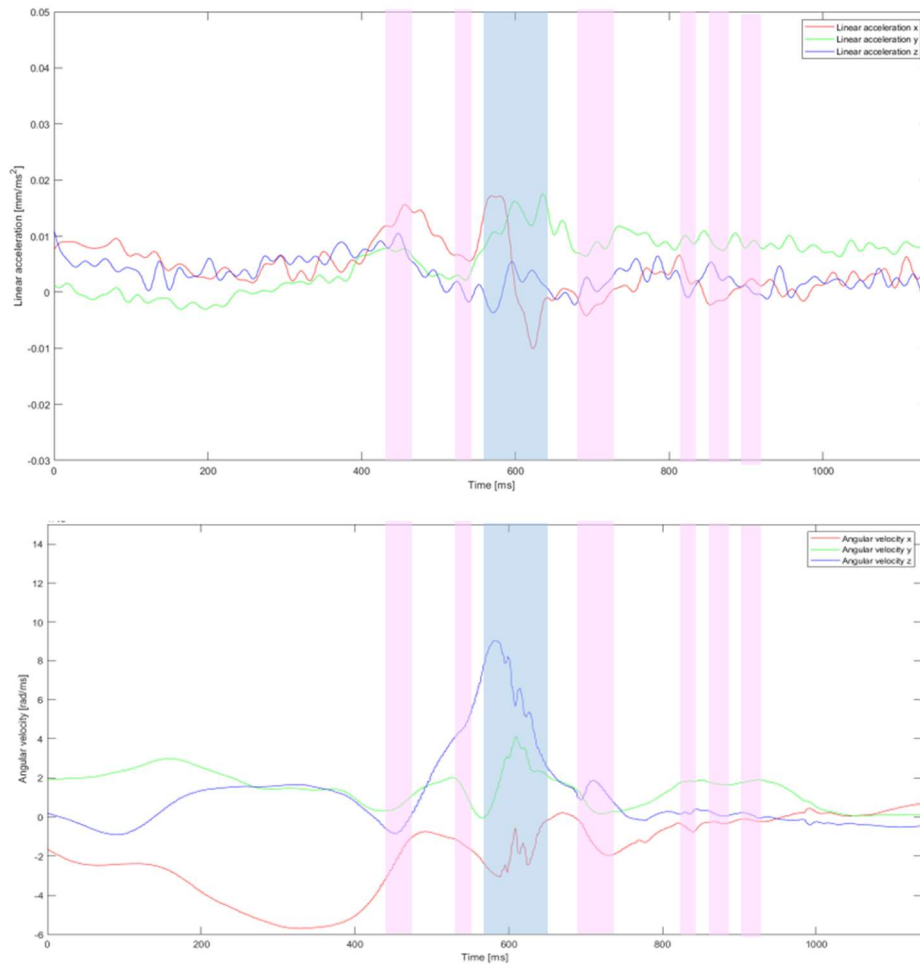
Figure A.2 *- Time intervals at which higher brain Von Mises stress values are reached during o-soto-gari technique, second repetition*

The maximum Von Mises Stress values is 368 Pa, 239 Pa, 451 Pa, 397 Pa, 287 Pa, 277 Pa, 383 Pa for each time windows.

The time interval at Von Mises Stress reaches higher values are between 453 ms – 491 ms, 542 ms – 556 ms, 574 ms – 652 ms, 699 ms – 733 ms , 812 ms – 831 ms, 848 ms – 864 ms, 880 ms – 908 ms for each time windows.

The results concerning Von Mises evolution have been reported in tables A.5, A.6, A.7, A.8, A.9, A.10 and A.11 that show the trend over time of Von Mises Stress with a time step of 1 ms, for each time windows. The stress scale is reported only the first time.
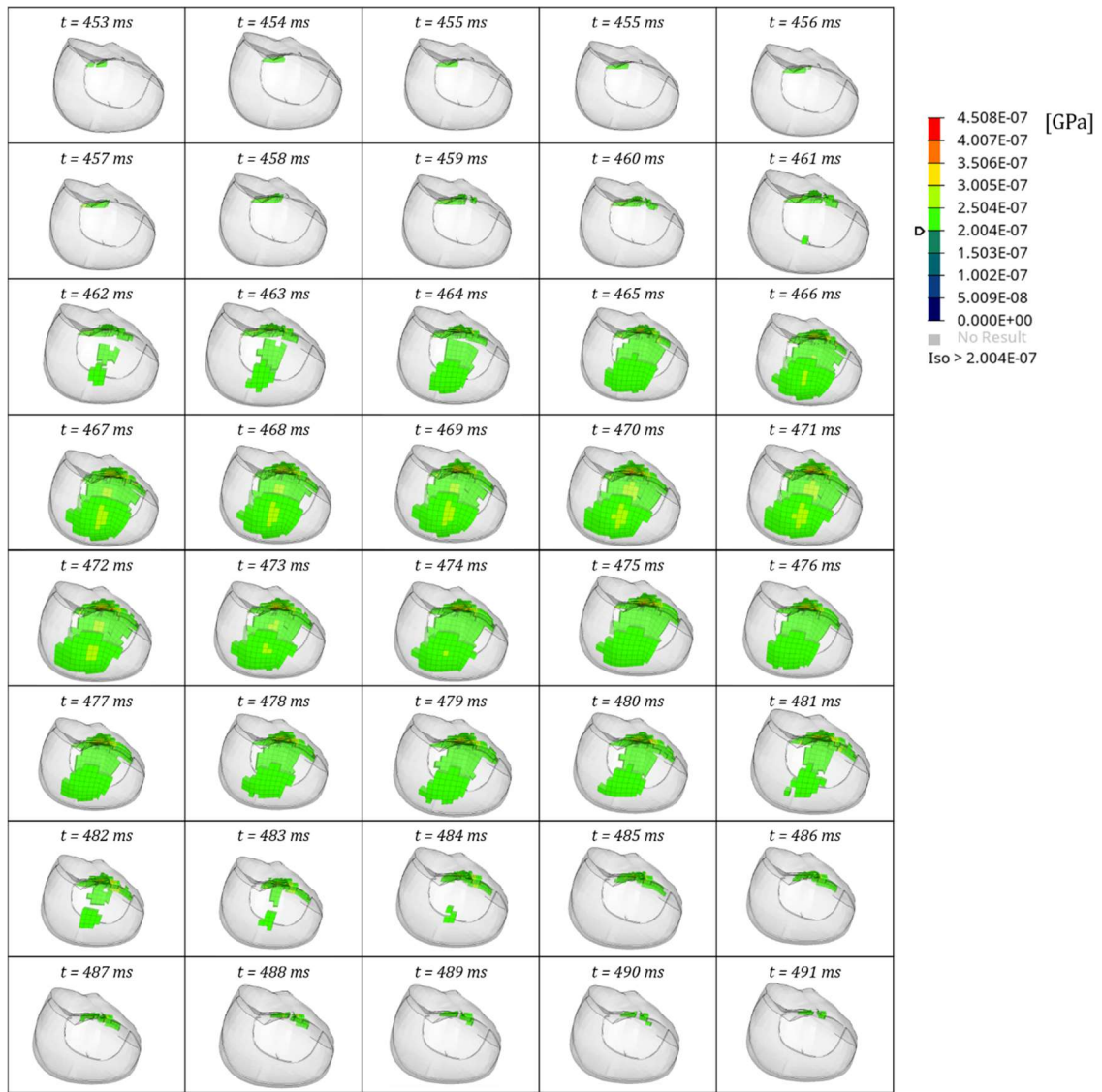
Table A.5 - Von Mises stress evolution with dt=1 (first time interval, second repetition)
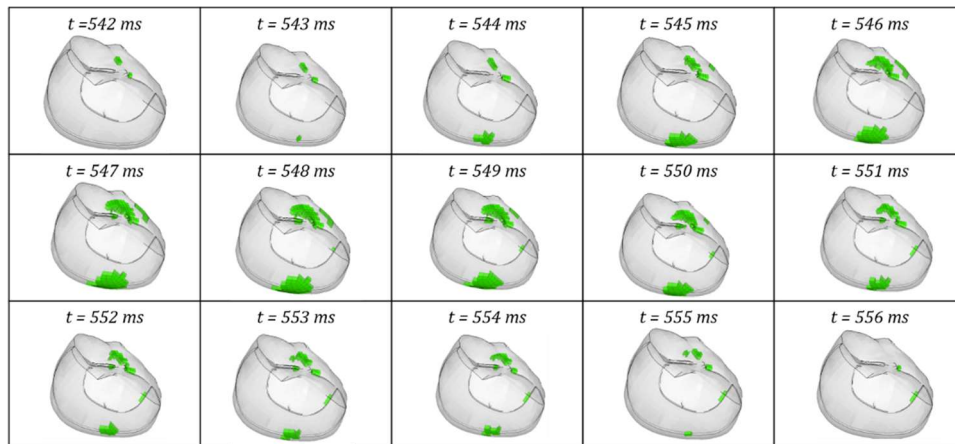
Table A.6 - Von Mises stress evolution with dt=1 (second time interval, second repetition)

t = 574 ms	t = 575 ms	t = 576 ms	t = 577 ms	t = 578 ms
t = 579 ms	t = 580 ms	t = 581 ms	t = 582 ms	t = 583 ms
t = 584 ms	t = 585 ms	t = 586 ms	t = 587 ms	t = 588 ms
t = 589 ms	t = 590 ms	t = 591 ms	t = 592 ms	t = 593 ms
t =594 ms	t = 595 ms	t = 596 ms	t = 597 ms	t = 598 ms
t = 599 ms	t = 600 ms	t = 601 ms	t = 602 ms	t = 603 ms
t = 604 ms	t = 605 ms	t = 606 ms	t = 607 ms	t = 608 ms
t = 609 ms	t = 610 ms	t = 611 ms	t = 612 ms	t = 613 ms
t =614 ms	t = 615 ms	t = 616 ms	t = 617 ms	t = 618 ms
t = 619 ms	t = 620 ms	t = 621 ms	t = 622 ms	t = 623 ms
t = 624 ms	t = 625 ms	t = 626 ms	t = 627 ms	t = 628 ms
t = 629 ms	t = 630 ms	t = 631 ms	t = 632 ms	t = 633 ms

t =634 ms	t = 635 ms	t = 636 ms	t = 637 ms	t = 638 ms
t = 639 ms	t = 640 ms	t = 641 ms	t = 642 ms	t = 643 ms
t = 644 ms	t = 645 ms	t = 646 ms	t = 647 ms	t = 648 ms
t = 649 ms	t = 650 ms	t = 651 ms	t = 652 ms	

Table A.7 *- Von Mises stress evolution with dt=1 (third time interval, second repetition)*

t =699 ms	t = 700 ms	t = 701 ms	t = 702 ms	t = 703 ms
t = 704 ms	t = 705 ms	t = 706 ms	t = 707 ms	t = 708 ms
t = 709 ms	t = 710 ms	t = 711 ms	t = 712 ms	t = 713 ms
t = 714 ms	t = 715 ms	t = 716 ms	t = 717 ms	t = 718 ms
t =719 ms	t = 720 ms	t = 721 ms	t = 722 ms	t = 723 ms
t = 724 ms	t = 725 ms	t = 726 ms	t = 727 ms	t = 728 ms
t = 729 ms	t = 730 ms	t = 731 ms	t = 732 ms	t = 733 ms

Table A.8 *- Von Mises stress evolution with dt=1 (fourth time interval, second repetition)*

101

t =812 ms	t = 813 ms	t = 814 ms	t = 815 ms	t = 816 ms
t = 817 ms	t = 818 ms	t = 819 ms	t = 820 ms	t = 821 ms
t = 822 ms	t = 823 ms	t = 824 ms	t = 825 ms	t = 826 ms
t = 827 ms	t = 828 ms	t = 829 ms	t = 830 ms	t = 831 ms

Table A.9 - *Von Mises stress evolution with dt=1 (fifth time interval, second repetition)*

|				
t =848 ms	t = 849 ms	t = 850 ms	t = 851 ms	t = 852 ms
t = 853 ms	t = 854 ms	t = 855 ms	t = 856 ms	t = 857 ms
t = 858 ms	t = 859 ms	t = 860 ms	t = 861 ms	t = 862 ms
t = 863 ms	t = 864 ms			

Table A.10 - *Von Mises stress evolution with dt=1 (sixth time interval, second repetition)*

Table A.11 - *Von Mises stress evolution with dt=1 (seventh time interval, second repetition)*

In this case, it is not visible with the color scale set to display the evolution of Von Mises according to the maximum value found in the literature.

The same approach was taken for the third repetition. The trend of the accelerations along the 3 axes and the 3 angular velocities around the 3 axes and the time windows, in which the peaks of Von Mises stress in the brain are recorded, are shown in figure A.3.
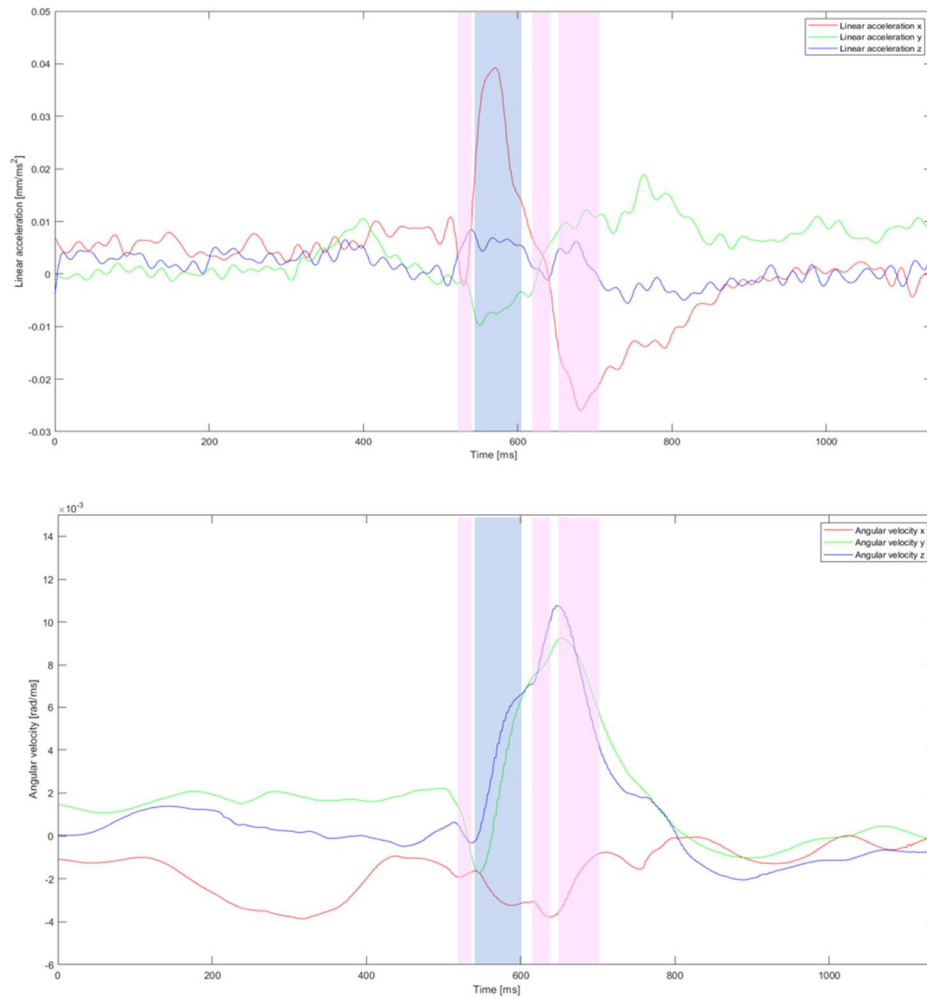
Figure A.3 - Time intervals at which higher brain Von Mises stress values are reached during o-soto-gari technique, third repetition

The maximum Von Mises Stress values is 355 Pa, 497 Pa, 335 Pa, 385 Pa for each time windows.

The time interval at Von Mises Stress reaches higher values are between 529 ms – 543 ma, 553 ms – 592 ms, 626 – 645 ms, 662 – 701 for each time windows.
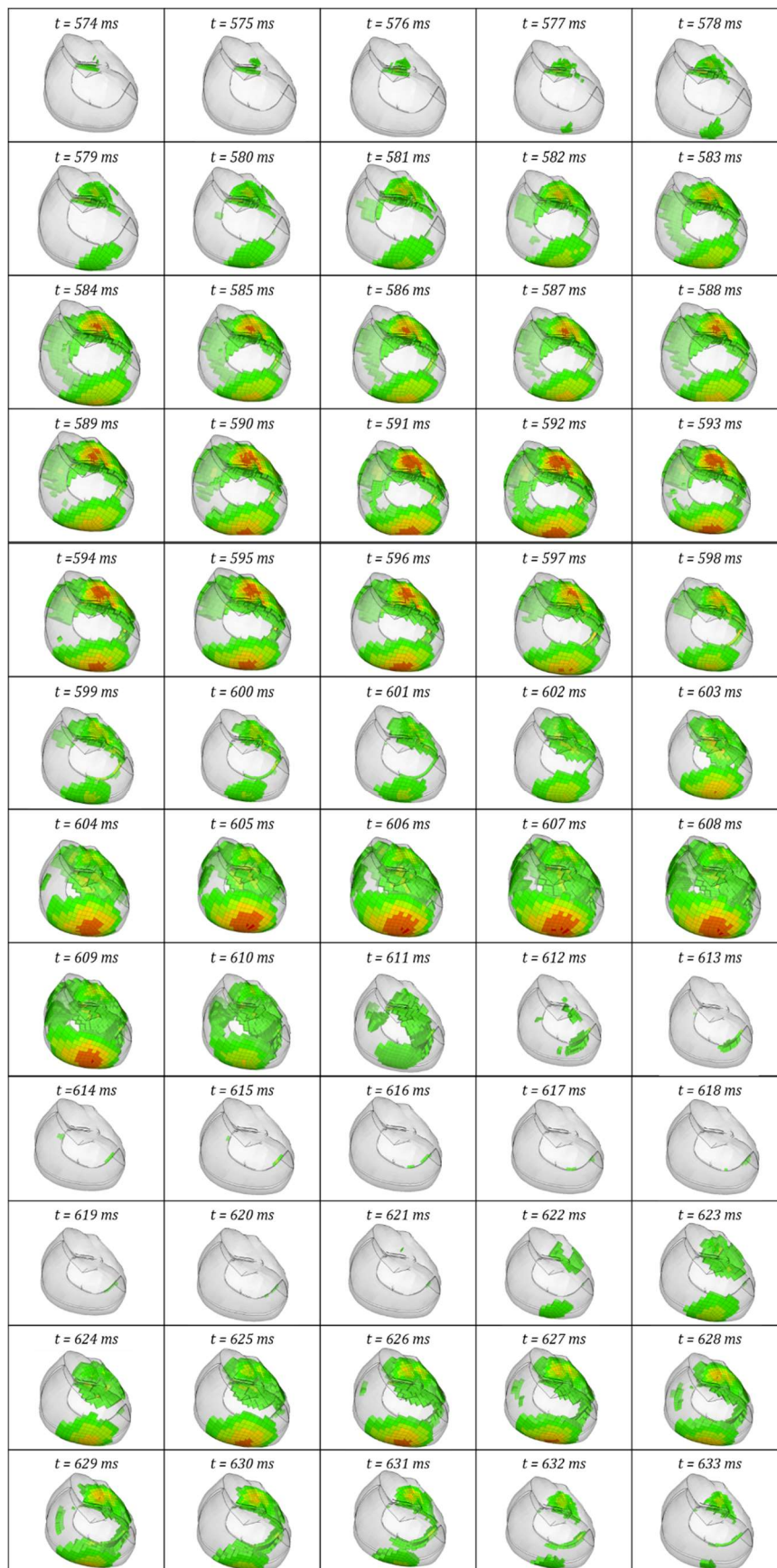
The results concerning Von Mises evolution have been reported in table A.13, A.14, A.15 and A.16 that show the trend over time of Von Mises Stress with a time step of 1 ms, for each time windows. The stress scale is reported only the first time.
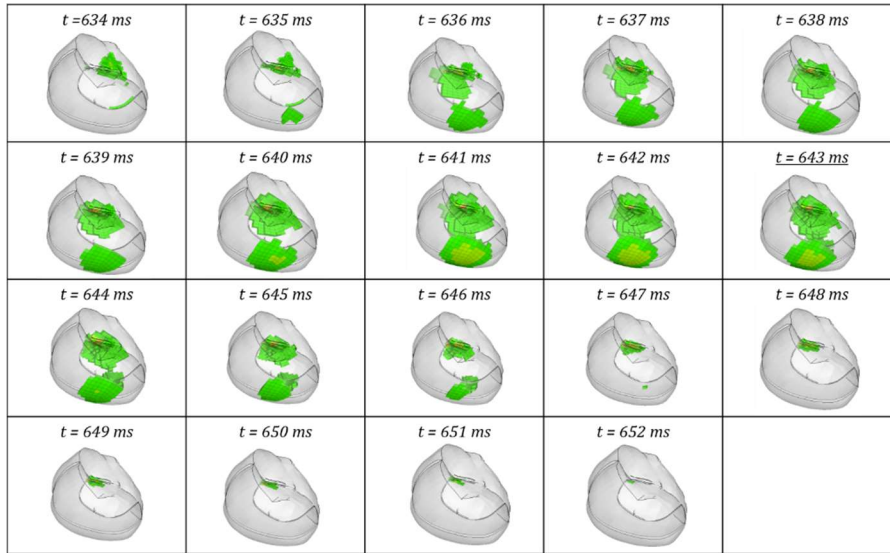
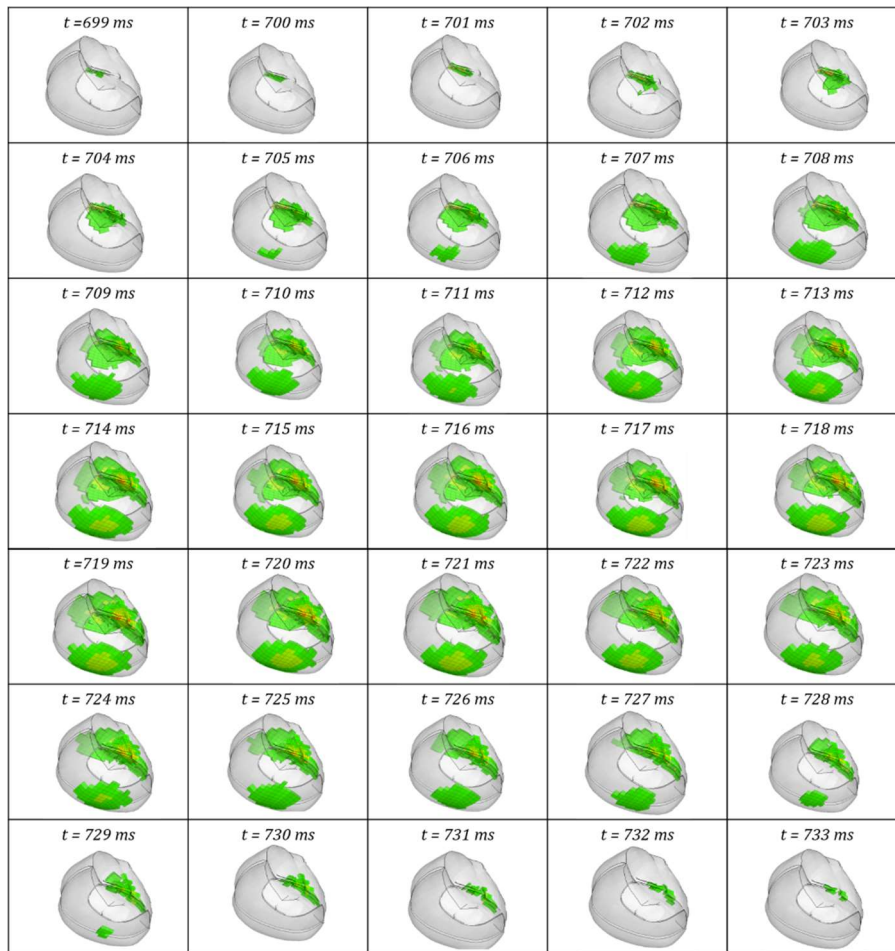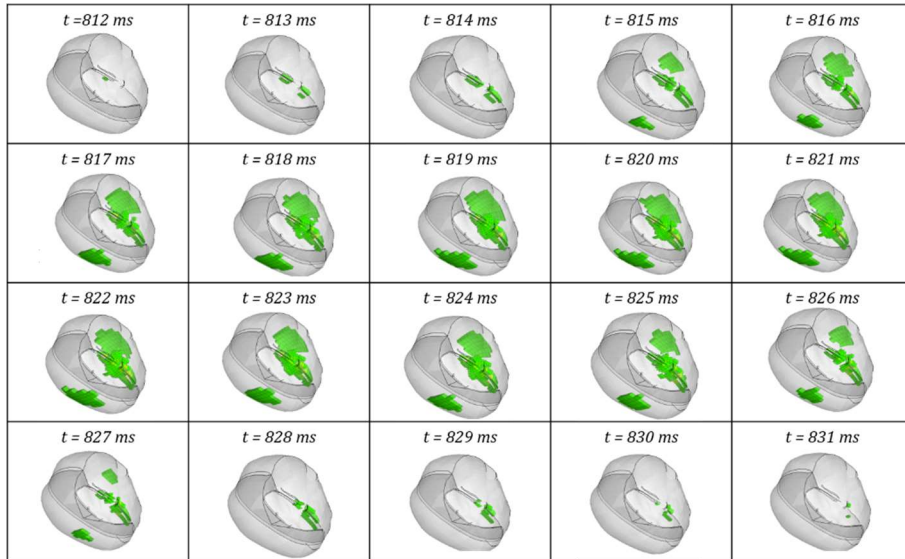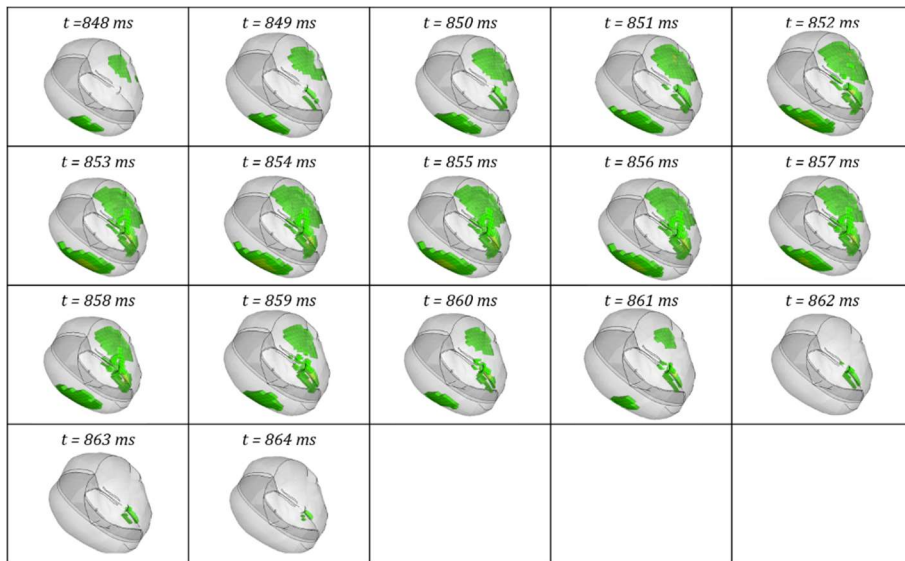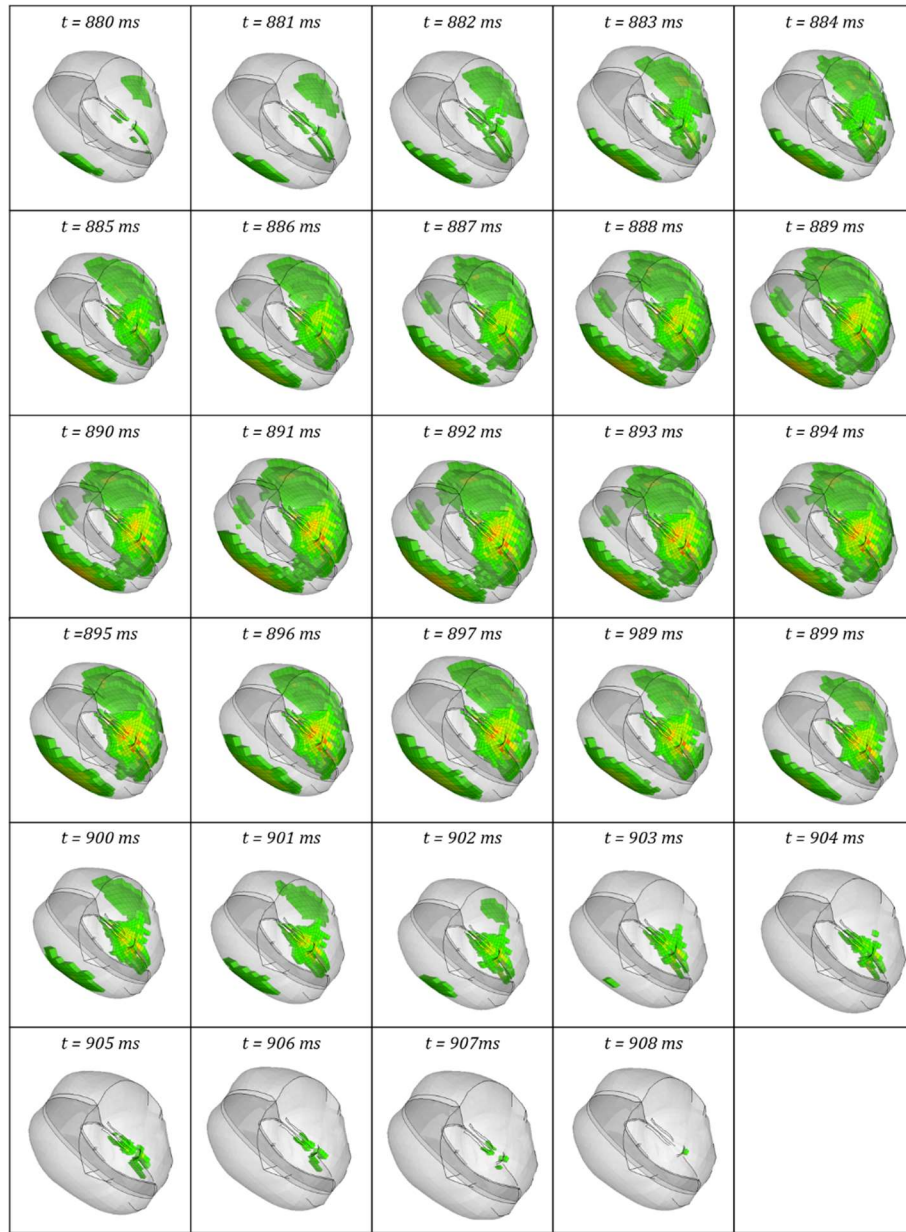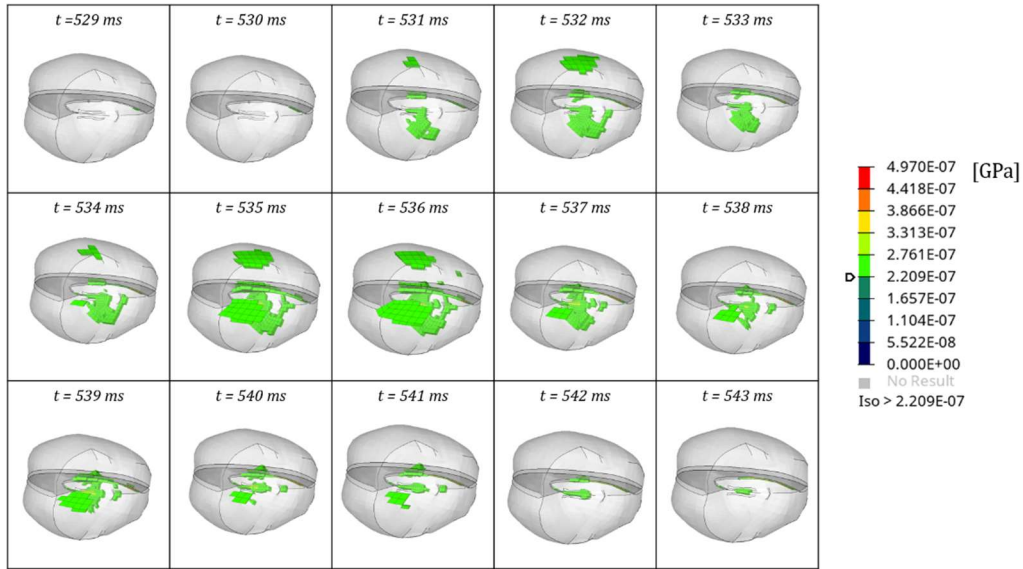**Table A.12** - Von Mises stress evolution with dt=1 (first time interval, third repetition)
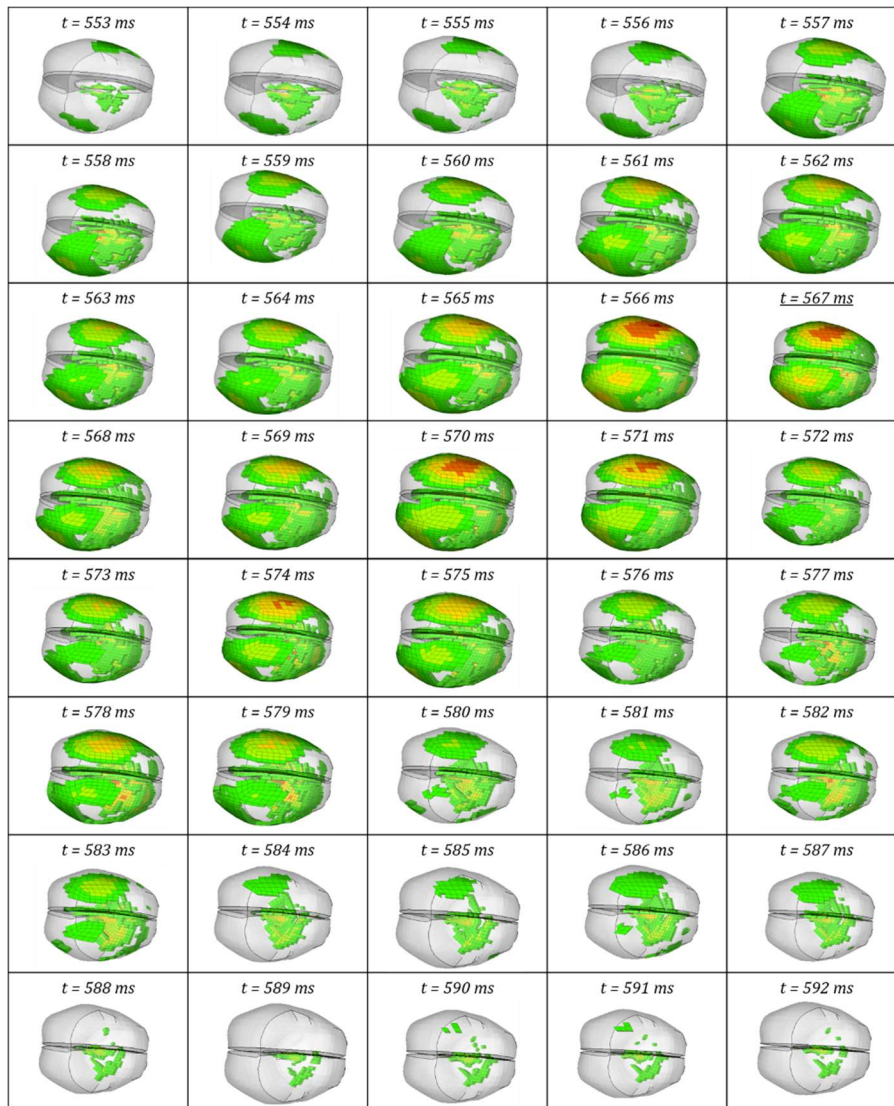
Table A.13 - Von Mises stress evolution with dt=1 (second time interval, third repetition)

t = 626 ms	t = 627 ms	t = 628 ms	t = 629 ms	t = 630 ms
t = 631 ms	t = 632 ms	t = 633 ms	t = 634 ms	t = 635 ms
t = 636 ms	t = 637 ms	t = 638 ms	t = 639 ms	t = 640 ms
t = 641 ms	t = 642 ms	t = 643 ms	t = 644 ms	t = 645 ms
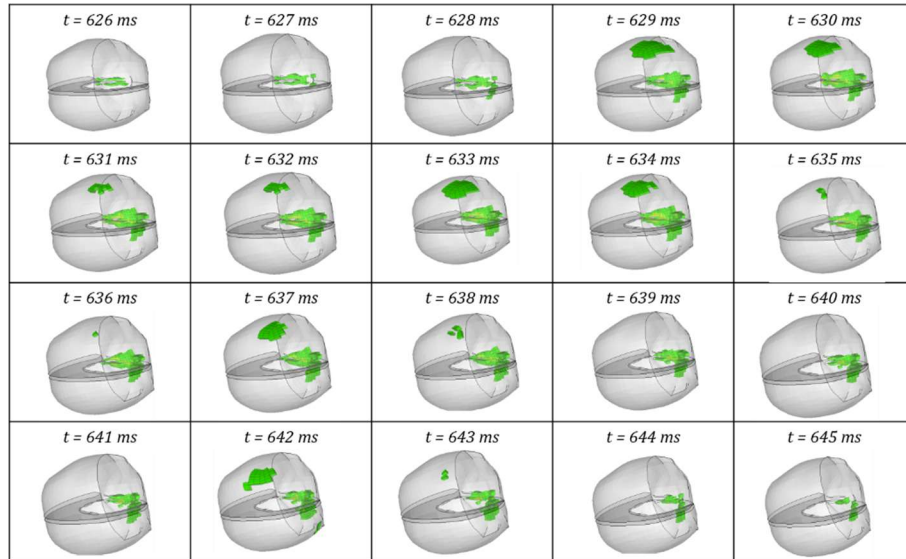
Table A.14 - *Von Mises stress evolution with dt=1 (third time interval, third repetition)*

t = 662 ms	t = 663 ms	t = 664 ms	t = 665 ms	t = 666 ms
t = 667 ms	t = 668 ms	t = 669 ms	t = 670 ms	t = 671 ms
t = 672 ms	t = 673 ms	t = 674 ms	t = 675 ms	t = 676 ms
t = 677 ms	t = 678 ms	t = 679 ms	t = 680 ms	t = 681 ms
t = 682 ms	t = 683 ms	t = 684 ms	t = 685 ms	t = 686 ms
t = 687 ms	t = 688 ms	t = 689 ms	t = 690 ms	t = 691 ms
t = 692 ms	t = 693 ms	t = 694 ms	t = 695 ms	t = 696 ms
t = 697 ms	t = 698 ms	t = 699 ms	t = 700 ms	t = 701 ms
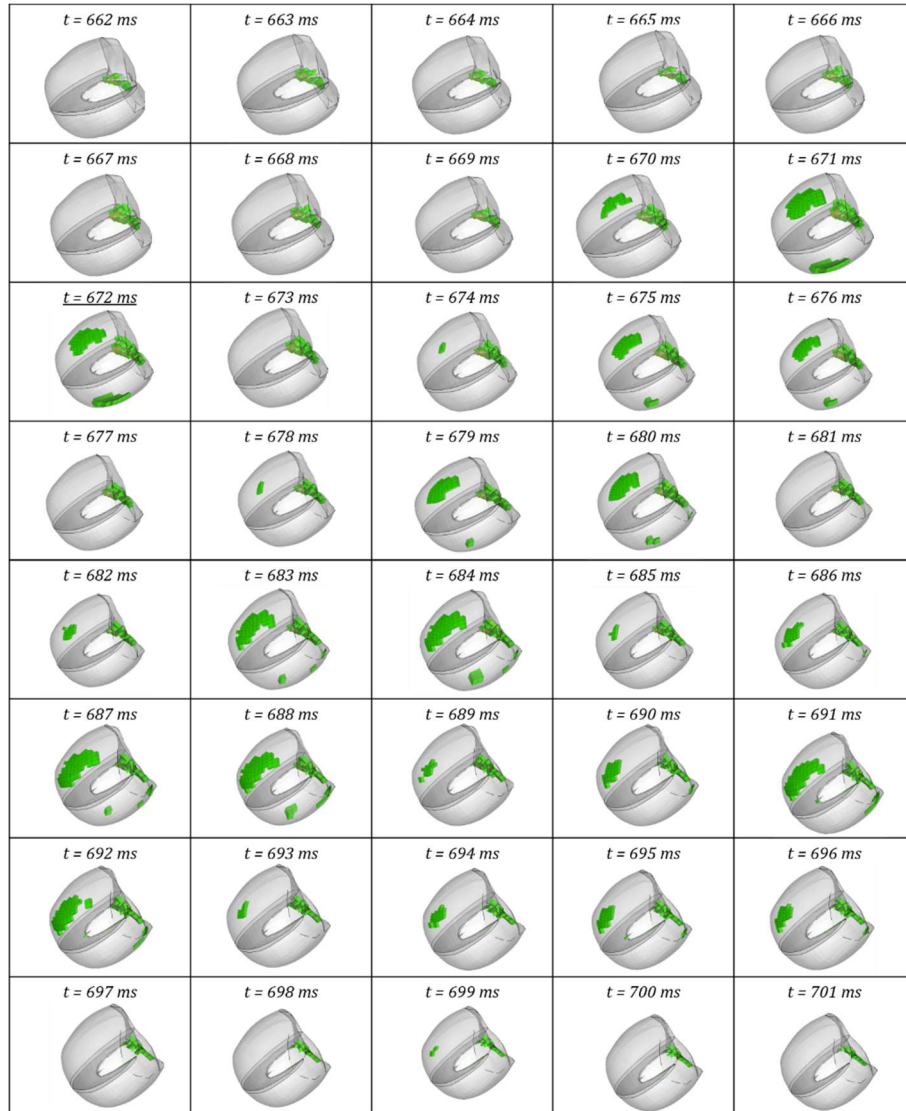
Table A.15 - *Von Mises stress evolution with dt=1 (fourth time interval, third repetition)*

106

Subsequently, the maximum value of the scale was set to 45 kPa (table A.17).

Stress(vonMises, Max)
Analysis system [GPa]
4.500E-05
3.609E-05
2.718E-05
1.827E-05
9.360E-06
4.500E-07
3.375E-07
2.250E-07
1.125E-07
0.000E+00
No Result
Iso > 4.500E-07

t = 566 ms   *t = 567 ms*   *t = 568 ms*

t = 569 ms   *t = 570 ms*   *t = 571 ms*
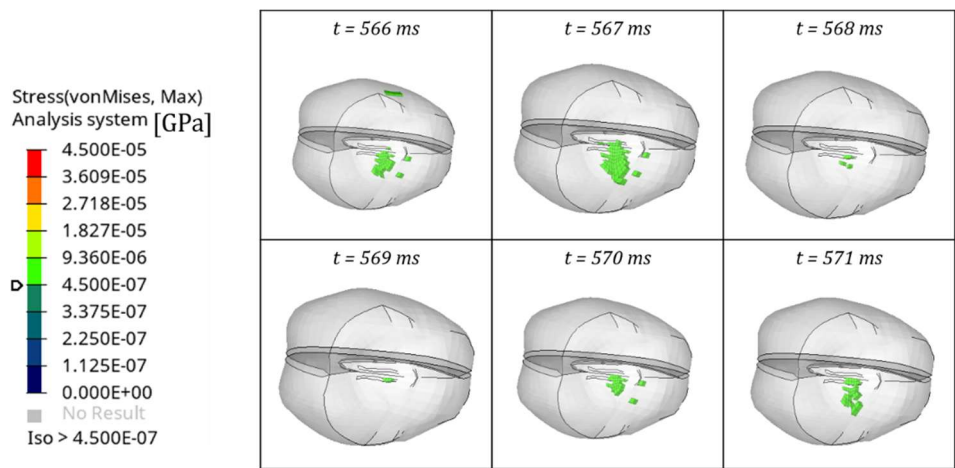
Table A.16 *- Von Mises stress evolution based on maximum literature value (third repetition)*

With this approach, it was possible to appreciate for all o-soto-gari repetition, how Von Mises stress reaches different values in different time windows, which, as shown in Figures A.1, A.2 and A.3, thicken when kinematic peaks are reached.

References

1.   Pocecco, E. *et al.* Injuries in judo: A systematic literature review including suggestions for prevention. *Br. J. Sports Med.* **47**, 1139–1143 (2013).

2.   Kamitani, T., Nimura, Y., Nagahiro, S., Miyazaki, S. & Tomatsu, T. Catastrophic head and neck injuries in judo players in Japan from 2003 to 2010. *Am. J. Sports Med.* **41**, 1915–1921 (2013).

3.   Koshida, S., Ishii, T., Matsuda, T. & Hashimoto, T. Biomechanics of the judo backward breakfall: Comparison between experienced and novice judokas. *Arch. Budo* **10**, 187–194 (2014).

4.   Ishii, T., Ae, M., Suzuki, Y. & Kobayashi, Y. Kinematic comparison of the seoi-nage judo technique between elite and college athletes. *Sport. Biomech.* **17**, 238–250 (2018).

5.   Abelson-Mitchell, N. Epidemiology and prevention of head injuries: Literature review. *J. Clin. Nurs.* **17**, 46–57 (2008).

6.   Healthcare, O. Head Injury. What is Head Injury? https://www.ohsu.edu/brain-institute/about-traumatic-brain-injury (2006).

7.   Dawodu ST. Traumatic Brain Injury: Definition, Epidemiology, Pathophysiology. https://emedicine.medscape.com/article/326510-overview (2003).

8.   McKee, A. C., Daneshvar, D. H., Alvarez, V. E. & Stein, T. D. The neuropathology of sport. *Acta Neuropathol.* **127**, 29–51 (2014).

9.   Jordan, B. D. The clinical spectrum of sport-related traumatic brain injury. *Nat. Rev. Neurol.* **9**, 222–230 (2013).

10. Viano, D., Von Holst, H. & Gordon, E. Serious brain injury from traffic-related causes: Priorities for primary prevention. *Accid. Anal. Prev.* **29**, 811–816 (1997).

11. Koncan, D., Gilchrist, M., Vassilyadi, M. & Hoshizaki, T. B. Simulated brain strains resulting from falls differ between concussive events of young children and adults. *Comput. Methods Biomech. Biomed. Engin.* **0**, 1–10 (2020).

12. Koncan, D. Finite Element Modelling of Sport Impacts –Brain Strains from Falls Resulting in Concussion in Young Children and Adults. (2018) doi:10.20381/ruor-22763.

13. Maxwell, W. L. International Journal of Developmental Neuroscience Traumatic brain injury in the neonate , child and adolescent human : An overview of pathology. **30**, 167–183 (2012).

14. Lenroot, R. K. & Giedd, J. N. Brain development in children and adolescents: Insights from anatomical magnetic resonance imaging. *Neurosci. Biobehav. Rev.* **30**, 718–729 (2006).

15. Post, A. *et al.* reconstruction. **19**, 502–510 (2017).

16. Gilchrist, M. D. Modelling and accident reconstruction of head impact injuries. *Key Eng. Mater.* **245–246**, 417–430 (2003).

17. Cobb, B. R. *et al.* Head impact exposure in youth football: Elementary school ages 9-12 years and the effect of practice structure. *Ann. Biomed. Eng.* **41**, 2463–2473 (2013).

18. Bussone, W. R. *et al.* Measurements of non-injurious head accelerations of a pediatric population. *SAE Tech. Pap.* **2**, 565–586 (2009).

19. Hanlon, E. M. & Bir, C. A. Real-time head acceleration measurement in girls' youth soccer. *Med. Sci. Sports Exerc.* **44**, 1102–1108 (2012).

20. King, D., Hume, P., Gissane, C. & Clark, T. Head impacts in a junior rugby league team measured with a wireless head impact sensor: An exploratory analysis. *J. Neurosurg. Pediatr.* **19**, 13–23 (2017).

21. King, D., Hume, P. A., Brughelli, M. & Gissane, C. Instrumented mouthguard acceleration analyses for head impacts in amateur rugby union players over a season of matches. *Am. J. Sports Med.* **43**, 614–624 (2015).

22. King, D., Hume, P., Gissane, C., Brughelli, M. & Clark, T. The Influence of Head Impact Threshold for Reporting Data in Contact and Collision Sports: Systematic Review and Original Data Analysis. *Sport. Med.* **46**, 151–169 (2016).

23. Le, R. K. *et al.* Differences in the Mechanism of Head Impacts Measured Between

Men's and Women's Intercollegiate Lacrosse Athletes. *Orthop. J. Sport. Med.* **6**, 1–7 (2018).

24. Young, T. J., Daniel, R. W., Rowson, S. & Duma, S. M. Head impact exposure in youth football: Elementary school ages 7-8 years and the effect of returning players. *Clin. J. Sport Med.* **24**, 416–421 (2014).

25. Post, A., Blaine Hoshizaki, T., Gilchrist, M. D. & Cusimano, M. D. Peak linear and rotational acceleration magnitude and duration effects on maximum principal strain in the corpus callosum for sport impacts. *J. Biomech.* **61**, 183–192 (2017).

26. Hoshizaki, T. B. *et al.* The development of a threshold curve for the understanding of concussion in sport. *Trauma (United Kingdom)* **19**, 196–206 (2017).

27. Mihalik, J. P., Bell, D. R., Ed, M., Marshall, S. W. & Ph, D. F Ootball P Layers : a N I Nvestigation of. *Neurosurgery* **61**, 1229–1235 (2007).

28. Crisco, J. J. *et al.* Frequency and Location of Head Impact Exposures in Individual Collegiate Football Players. *J. Appl. Biomech.* **28**, 174–183 (2012).

29. Cummiskey, B. *et al.* Reliability and accuracy of helmet-mounted and head-mounted devices used to measure head accelerations. *Proc. Inst. Mech. Eng. Part P J. Sport. Eng. Technol.* **231**, 144–153 (2017).

30. Koncan, D., Gilchrist, M., Vassilyadi, M. & Hoshizaki, T. B. A three-dimensional finite element model of a 6-year-old child for simulating brain response from physical reconstructions of head impacts. *Proc. Inst. Mech. Eng. Part P J. Sport. Eng. Technol.* **233**, 277–291 (2019).

31. Oeur, R. A., Gilchrist, M. D. & Hoshizaki, T. B. Interaction of impact parameters for simulated falls in sport using three different sized Hybrid III headforms. *Int. J. Crashworthiness* **24**, 326–335 (2019).

32. Fernandes, F. A. O. & Sousa, R. J. A. De. Head injury predictors in sports trauma - A state-of-the-art review. *Proc. Inst. Mech. Eng. Part H J. Eng. Med.* **229**, 592–608 (2015).

33. Post, A., Oeur, A., Walsh, E., Hoshizaki, B. & Gilchrist, M. D. A centric/non-centric impact protocol and finite element model methodology for the evaluation of American football helmets to evaluate risk of concussion. *Computer Methods in*

Biomechanics and Biomedical Engineering vol. 17 1785–1800 (2014).

34.   Roth, S., Vappou, J., Raul, J. S. & Willinger, R. Child head injury criteria investigation through numerical simulation of real world trauma. *Comput. Methods Programs Biomed.* **93**, 32–45 (2009).

35.   Burgos-Flórez, F. J. & Garzón-Alvarado, D. A. Stress and strain propagation on infant skull from impact loads during falls: a finite element analysis. *Int. Biomech.* **7**, 19–34 (2020).

36.   Van Den Bosch, H. L. A., Wismans, J. S. H. M. & Nijmeijer, H. *Crash helmet testing and design specifications*. vol. Ph.D. (2006).

37.   Post, A. *et al.* The biomechanics of concussion for ice hockey head impact events. *Comput. Methods Biomech. Biomed. Engin.* **22**, 631–643 (2019).

38.   Hernandez, F. *et al.* Six Degree-of-Freedom Measurements of Human Mild Traumatic Brain Injury. *Ann. Biomed. Eng.* **43**, 1918–1934 (2015).

39.   VIANO, D. C. & LOVSUND, P. Biomechanics of Brain and Spinal-Cord Injury: Analysis of Neuropathologic and Neurophysiology Experiments. *J. Crash Prev. Inj. Control* **1**, 35–43 (1999).

40.   Kimpara, H. & Iwamoto, M. Mild traumatic brain injury predictors based on angular accelerations during impacts. *Ann. Biomed. Eng.* **40**, 114–126 (2012).

41.   Patton, D. A., McIntosh, A. S. & Kleiven, S. The biomechanical determinants of concussion: Finite element simulations to investigate tissue-level predictors of injury during sporting impacts to the unprotected head. *J. Appl. Biomech.* **31**, 264–268 (2015).

42.   Bar-Kochba, E. *et al.* Finite Element Analysis of Head Impact in Contact Sports. *2012 SIMULIA Community Conf.* 1–10 (2012).

43.   Takhounts, E. G. *et al.* On the Development of the SIMon Finite Element Head Model. *SAE Tech. Pap.* **2003-Octob**, 107–133 (2003).

44.   Boroushak, N., Eslami, M., Kazemi, M., Daneshmandy, H. & Johnson, J. A. The dynamic response of the taekwondo roundhouse kick to head using computer simulation. *Ido Mov. Cult.* **18**, 54–60 (2018).

45.   Elkin, B. S., Gabler, L. F., Panzer, M. B. & Siegmund, G. P. Brain tissue strains vary with head impact location: A possible explanation for increased concussion risk in struck versus striking football players. *Clin. Biomech.* **64**, 49–57 (2019).

46.   Ito, D., Mizuno, K., Hitosugi, M., Murayama, H. & Koyama, K. Finite Element Analysis for Understanding Trauma Brain Injury in Judo. *IRCOBI Asia 2016* **28**, 1321–1322 (2016).

47.   Morse, J. D., Franck, J. A., Wilcox, B. J., Crisco, J. J. & Franck, C. An Experimental and Numerical Investigation of Head Dynamics Due to Stick Impacts in Girls' Lacrosse. *Ann. Biomed. Eng.* **42**, 2501–2511 (2014).

48.   Bartsch, A. J., Benzel, E. C., Miele, V. J., Morr, D. R. & Prakash, V. Boxing and mixed martial arts: Preliminary traumatic neuromechanical injury risk analyses from laboratory impact dosage data. Laboratory investigation. *J. Neurosurg.* **116**, 1070–1080 (2012).

49.   Post, A. *et al.* Brain tissue analysis of impacts to American football helmets. *Comput. Methods Biomech. Biomed. Engin.* **21**, 264–277 (2018).

50.   Viano, D. C. *et al.* Concussion in professional football: Brain responses by finite element analysis: Part 9. *Neurosurgery* **57**, 891–915 (2005).

51.   Report, M. W. Nonfatal traumatic brain injuries related to sports and recreation activities among persons aged ≤19 Years --- United States, 2001--2009. *Morb. Mortal. Wkly. Rep.* **60**, 1337–1342 (2011).

52.   Horgan, T. J. & Gilchrist, M. D. The creation of three-dimensional finite element models for simulating head impact biomechanics. *Int. J. Crashworthiness* **8**, 353–366 (2003).

53.   Giordano, C. & Kleiven, S. Development of a 3-year-old child FE head model, continuously scalable from 1.5-to 6-year-old. *2016 IRCOBI Conf. Proc. - Int. Res. Counc. Biomech. Inj.* 288–302 (2016).

54.   Davis, M. T. *et al.* The mechanical and morphological properties of 6 year-old cranial bone. *J. Biomech.* **45**, 2493–2498 (2012).

55.   Koshida, S., Ishii, T., Matsuda, T. & Hashimoto, T. Kinematics of judo breakfall for osoto-gari: Considerations for head injury prevention. *J. Sports Sci.* **35**, 1059–1065

(2017).

56.   Stephen Atkins, H. T. H. Reliability of a Portable Accelerometer for Measuring
        Workload during Mixed Martial Arts. *J. Athl. Enhanc.* **03**, (2014).

57.   Hitosugi, M. *et al.* Biomechanical analysis of acute subdural hematoma resulting
        from judo. *Biomed. Res.* **35**, 339–344 (2014).

58.   MURAYAMA, H., HITOSUGI, M., MOTOZAWA, Y., OGINO, M. & KOYAMA, K. Simple
        Strategy to Prevent Severe Head Trauma in Judo. *Neurol. Med. Chir. (Tokyo).* **53**,
        580–584 (2013).

59.   Murayama, H., Hitosugi, M., Motozawa, Y., Ogino, M. & Koyama, K. Rotational
        acceleration during head impact resulting from different judo throwing techniques.
        Neurol. Med. Chir. (Tokyo). **54**, 374–378 (2014).

60.   Patton, D. A. A Review of Instrumented Equipment to Investigate Head Impacts in
        Sport. *Appl. Bionics Biomech.* **2016**, (2016).

61.   Ishikawa, Y. *et al.* Effects of Different Throwing Techniques in Judo on Rotational
        Acceleration of Uke's Head. *Int. J. Sport Heal. Sci.* **16**, 173–179 (2018).

62.   Koshida, S., Ishii, T., Matsuda, T. & Hashimoto, T. Trunk biomechanics during
        breakfall for osoto-gari and its association with judo-related head injury risk in
        novice judokas. *36th Conf. Int. Soc. Biomech. Sport.* 146–149 (2018).

63.   Koncan, D., Oeur, R. A., Gilchrist, M. D. & Hoshizaki, T. B. Comparison of a 6-year-old
        child finite element model to a scaled adult model using simulated fall events for
        three levels of surface compliance. 1–5.

64.   Post, A. *et al.* A comparison in a youth population between those with and without a
        history of concussion using biomechanical reconstruction. *J. Neurosurg. Pediatr.* **19**,
        502–510 (2017).

65.   Vacca, L. Biomechanical Analysis of Judo-Related Head Injuries: A Pilot Study over
        Ages and Experience Levels. 157 (2019).

66.   Vacca, L., Rosso, V. & Gastaldi, L. Risk assessment in different Judo techniques for
        children and adolescent athletes. *Proc. Inst. Mech. Eng. Part H J. Eng. Med.* **234**, 686–
        696 (2020).

67.   Dawson, L. Impact Characteristics Describing Concussive Injury in Youth. (2016).

68.   OMMAYA, A. K. & GENNARELLI, T. A. Cerebral Concussion and Traumatic Unconsciousness. *Brain* **97**, 633–654 (1974).